ISSN Print 0970 - 3268
ISSN Online 2582 - 2020

The Journal of the Indian Association of Sedimentologists

The Indian Association of Sedimentologists

Volume 41 No. II July - Dec., 2024

*Field Photographs showing variety of ripple marks

Field Photographs showing variety of ripple marks: A– symmetrical ripples, B & C- symmetrical ripples with bifurcations, D-sinuous ripples and E- pointed crest and rounded trough ripples. *Courtesy Asha Saxena, M. K. Pandit, Nirmal Kant Verma*

ISSN Print 0970 – 3268
ISSN online 2582 - 2020

The journal of the Indian Association of Sedimentologists

DOI:
https://doi.org/10.51710/jias.v41iII

The Journal of the Indian Association of Sedimentologists (IAS) is both an international open access online and print journal and is leader in its field and publishes ground-breaking research from across the spectrum of sedimentology, sedimentary geology, sedimentary geochemistry, experimental and theoretical sediment transport, mass movement fluxes, modern and ancient sedimentary environments, sequence – cyclo – chrono – and chemostratigraphy, sediment – biological interaction, palaeosols, diagenesis, stable isotope geochemistry, environmental sedimentology, neo-tectonics, geo-hazards, stratigraphy, palynology, sedimentary mineral resources and hydrocarbons, and allied branches of sedimentary - stratigraphic research. It also publishes review articles, editorials, conference reports, tributes, announcements, advertisements, etc. It is currently distributed to universities and research laboratories in India and abroad. Access is open to complete electronic journal archive. Subscribers also have the option to buy the printed journal at subsidized cost.

Indian Association of Sedimentologists

TABLE OF CONTENTS

JOURNAL INDIAN ASSOCIATION OF SEDIMENTOLOGISTS ISSN NO 2582 – 2020
Vol. 41, Issue II, 2024, pp. 1 – 4
DOI: https://doi.org/10.51710/jias.v41iII.405

Editorial

Global Net-Zero Carbon Emission by 2070: a distant dream

The UN Climate Change Conference (COP29) concluded on 24 November 2024 with a new finance goal to help countries to protect their people and economies against climate disasters, and share in the vast benefits of the clean energy boom. With a central focus on climate finance, COP29 brought together nearly 200 countries in Baku (Azerbaijan) and reached an agreement to provide 300 billion USD finance to developing countries annually by 2035 and secure efforts of all actors to work together to scale up finance to developing countries, from public and private sources, to the amount of USD 1.3 trillion per year by 2035. "This new finance goal is an insurance policy for humanity, amid worsening climate impacts hitting every country," said Simon Stiell, Executive Secretary of UN Climate Change. Stiell also acknowledged, "The agreement reached in Baku did not meet all Parties' expectations, and substantially more work is still needed next year on several crucial issues". World leaders at COP29 were joined by civil society, sub-nationals, business, Indigenous Peoples, youth, philanthropy, and international organizations. More than 55,000 people attended COP29 to share ideas, solutions, and build partnerships and coalitions. COP29 marked a significant milestone as dedicated spaces were created to ensure the meaningful participation of children within the Youth-led Climate Forum for the first time. Four children, including the youngest (just 10 year old), took on roles as moderators and speakers, engaging directly with Parties and observer organizations. Their participation highlighted the importance of inclusivity and intergenerational collaboration in driving climate action.

The COP29 Summit concluded with an extension of one day with mixed reactions by the developed countries and the United Nations displaying a sense of achievement, who hail the deal as "start of a new era of climate finance" and "insurance policy for humanity," respectively. Contrarily, the reaction by the negotiators from developing countries including India, expressed dissatisfaction on the outcome of the summit, yet with a sense of satisfaction for managing to reiterate their long-time held principle stand on the course of climate action. The main issue of dissatisfaction among the developing countries is allocation of funds required for energy transition to combat the climate change and achieve net zero carbon emission by 2070 through stage-wise shelving out the use of non-renewable energy resources (coal and petroleum). This action needs funding by the developed countries amounting to 1 trillion USD in a phased manner until 2035 for implementing new strategies by the developing countries. The developing countries including India feel that the Rich Countries fell drastically short of their commitments to support the developing countries. The COP29 Summit set a climate finance goal of "at least $300 billion annually by 2035" and launches the "Baku to Belém Roadmap (Brazil) to 1.3 Trillion." India out rightly rejected the package. Chandni Raina, an official representative of India, said, "*The amount does not address the needs and priorities of developing countries and is incompatible with the principle of Common but Differentiated Responsibilities (CBDR) and equity, regardless of the battle with the impact of climate* change*". "I regret to say that this document is nothing more than an optical illusion. This, in our opinion, will not address the enormity of the challenge we all face. Therefore, we oppose the adoption of this document*," Indian delegation representative Chandni Raina told the closing plenary session of the summit.

India's principle stand at the summit has drawn support from a host of developing countries, which claim the allocated fund is insufficient to meet the needs of the developing and under developed countries. At the summit, India also pointed out at unequal focus on mitigation by developed countries, ignoring the concepts of per capita contribution to carbon emission and the history of the developed countries' responsibility for climate action as the crux of the problem, however, this was ignored and the focus was shifted to mitigation alone.

IS ENERGY TRANSITION DRIVEN BY CLIMATE FINANCE?

India is committed to address the climate change issue and is heavily investing in renewable energy; still fossil fuel resources dominate its development path. Like India, Fossil fuel energy resources drive China's development. Both these countries together host 35.5% of the world population and are among the major countries contributing to carbon footprints including USA. Any forced fast transition to cleaner energy would affect billions who in these countries are dependent on fossil fuels as a key source of development and livelihood. According to conservative estimates, about 20 million people in India earn their livelihood from coal-related industries and allied associates. Although, South Africa and Indonesia have entered into an agreement on coal focussed Just Energy Transition Partnership (JETP), India and China

cannot afford to enter into this agreement with ever-increasing energy demand vis-a-vis their fast increasing population.

India's renewable energy capacity grew by 250 % between 2014 and 2021. The country now ranks fourth in renewable energy installed capacity in the world. By 2030, it hopes to achieve 500 GW of non-fossil-based electricity generation capacity. At the same time, India's reliance on coal continues to grow, with new mines opening and production increasing. India does not expect such reliance to end in the near future even until 2070. India is fast growing and yet developing economy, can't afford forced energy transition. Speaking about the outcomes of COP29 at a session, Leena Nandan, Secretary of Environment, Forest and Climate Change Ministry said the Cop29 conference, which was anticipated to focus on implementation, fell short of expectations. "*This was to be an enabling COP, a COP which was going to be focused on the means of implementation and, what are means of implementation other than funds and resources. In addition, here it was that we found semantics and not solutions. We found rhetoric and not results. And that has been the biggest disappointment*," she added, the sentiment was echoed across the Global South.

Fig. 1: Five Sub-divisions of Asia. Reference: United Nations Statistics Division – Standard Country and Area Codes Classifications. The UNSD notes "the assignment of countries or areas to specific groupings is for statistical convenience".

GLOBAL SOUTH SCENARIO

According to the United Nations Trade and Development (UNCTAD), the Global South broadly comprises Africa, Latin America and the Caribbean, Asia (excluding Israel, Japan, and South Korea), and Oceania (excluding Australia and New Zealand). Most of the Global South countries commonly have low standard of living, which includes having lower incomes, extreme poverty, high population growth rates, inadequate shelter, limited educational opportunities, and poor health systems, poor urban infrastructure and other related issues. The Global South consists of the world's developing and least developed countries. The Global South classification, as used by governmental and developmental organizations, was first introduced as a more open and value-free alternative to "Third World". These countries have also been described as being newly industrialized or in the process of industrialisation, many of them were former subjects of colonialism. These countries are poorer and heavily dependent primarily on their largely agrarian-based economic sectors. Behind, both China and India in the development process, sub-Saharan Africa's population had increased to 1.20 billion in 2022 and is forecast to rise to 2.17 billion by 2050 and 3.57 billion by 2100. The region's urbanisation, industrialisation and energy consumption per person is even lower than China and India, which is going to increase substantially in future.

SOUTH ASIA AND EAST ASIA ENERGY SCENARIO

South Asia has a peninsula-like shape bordered by the Indian Ocean to the south, the Bay of Bengal to the east, and the Arabian Sea to the west. The region includes the Indian subcontinent and surrounding countries. South Asia includes Sri Lanka, Bangladesh, India, Afghanistan, Pakistan, Bhutan, Nepal, Iran, and the Maldives. The region covers roughly 3,218,688 Km^2 area and has a population of more than 2.074 billion (¼ of the world), the most densely populated region in the world. The current population of **South Asia** is **2,074,434,296** as of Saturday, December 28, 2024, based on the latest United Nations estimates, which is equivalent to 25.29% of the total world population.

East Asia is a geographical region of Asia including China, Japan, Mongolia, North Korea, South Korea, and Taiwan and includes Hong Kong and Macau, special administrative regions of China. The economies of China, Japan, South Korea, and Taiwan are among the worlds'

largest and most prosperous. East Asia borders North Asia to the north, Southeast Asia to the south, South Asia to the southwest, Central Asia to the west and Pacific Ocean to the east.

East Asia is spread over 11,840,000 Km^2. The current population of East Asia is 1,654,175,130 as of Saturday, December 28, 2024 (20.29% of the world), based on the latest United Nations estimates. East Asia is second in ranks in Asia among sub-regions by Population.

Both, South and East Asia together constitute 45.68% of the total World population. India and China the two most populous countries in world together constitute 2.87 billion people and account for about 25.17% population of the world and 60% of Asian population. Both are developing countries whose economic development is non-renewable driven energy resources. China and India are the two most populous countries in the world, with India hosting to about 1.45 billion people and China hosting to 1.42 billion as of December 2024. In 2022, fossil fuels accounted for 82% of primary energy consumption in China and 88% in India, including 70% of total electricity generation in China and 77% in India. The population of both the countries were each similar to the total for countries in the Organisation for Economic Cooperation and Development (OECD) (1.38 billion). But total primary energy consumption in China (159 exajoules) and India (36 exajoules) was far lower than in the OECD (234 exajoules). Each person in China consumed only 66% of the energy as their counterparts in the OECD and India consumes just 15%. These are the over estimates about the consumption of energy services locally because both countries and especially China export a large proportion of their energy-intensive manufactured output to the OECD. Continued modernisation in China and India will lead to more and more consumption of energy.

In the OECD, growing production from renewables and especially gas has decreased consumption of coal and to a lesser extent oil. Although, this has enabled a reduction in greenhouse emissions but total energy consumption has continued to increase rapidly in China (average of 3.1% per year) and India (3.8% per year). Renewable resources and gas have served as supplements to other fossil fuels but not replacement, ensuring energy remains affordable and reliable in the backdrop of increasing demand. China and India's current trajectory for energy consumption has remained parallel to that of USA or Western Europe between the 1950s and 1970s, a period of rapid growth in economic output, living standards and energy use. In the Euro-Atlantic economies, rapid growth in total energy demand required more energy from all sources; consumption from fossil fuels continued to rise in absolute terms even as its share was reduced relatively. U.S. coal consumption continued to increase in absolute terms until around 2010 even though it was losing relative share of the energy mix to oil from around 1910 and gas from 1980. China and India appear to be moving along the same trajectory, increasing their use of indigenous coal even as they import more oil and gas, use more nuclear power, and invest in renewable generation from wind, solar and hydro. Eventually, China and India's energy consumption from fossil fuels is likely to reduce only when renewables will substitute for fossil fuels rather than just supplement them. However, given their current position in the historical development process, that point is likely to be distant in the future for China and likely more distant for India. Since 2018, China's solar generation capacity has increased by 26% per year, wind generation capacity by 18% per year, while thermal capacity has grown by just 4% per year. Similarly, India's solar generation capacity has grown by 25% per year; wind has grown by 5% per year, while coal has risen by 1% a year.

In practice, China and India, following the historical and current example of the OECD nations, have prioritised increasing access to energy services and ensuring energy remains affordable and reliable. China, USA and India use more fossil fuels than the rest of the world combined (Table 1). Together, these countries consume 54% of the world's fossil fuels, according to the Global Material Flow Database developed by the UN Environment Programme (2019). China generated 37% of global wind and solar electricity in 2023. Despite this growth, China relied on fossil fuels for 65% of its electricity in 2023, making it the world's largest emitter. Its per capita power sector emissions were more than double the global average. Most of the electricity in China comes from coal power, which accounted for 62% of electricity generation in 2021which contributes a big part of greenhouse gas emissions by China. China leads the world in coal consumption with an estimated 4.4 billion short tons in 2023. In terms of oil consumption, the country consumed over 14.3 million barrels per day and increased its natural gas consumption by 13% in 2022. In India, total energy consumption per capita reached 0.8 tonnes of oil equivalent (toe) in 2023, half the Asian average. Electricity consumption per capita reached 985 kWh in 2023. Total energy consumption continued to grow significantly (6.5%/year since 2020, of which 5% in 2023), reaching 1.14 giga-tonnes of oil equivalent (Gtoe) in 2023. Nearly 80% of total electricity generated (utility and captive) in India is from coal and it is the main source of the nation's greenhouse gas emissions.

China has more than 80 percent of the world's solar manufacturing capacity (2024). The scale of China's renewables sector output has driven down prices worldwide, and this is a key factor in

reducing the cost barrier to renewable systems for poorer countries.

Table 1. World Scenario: about 85 percent of our energy comes oil, natural gas, coal. China and U.S. Account for Nearly Half of Global Fossil Fuel Use (12 August 2024)

Country	Oil (Exajoules)	Coal
China	33	92
U.S.	36	8
India	11	22
Russia	7	4

UNACHIEVABLE DECARBONISATION TARGETS

The highly ambitious goal includes decarbonising energy to 50% and achieving 500 GW of fossil fuel-free generating capacity by 2030. Meeting 50% of India's energy needs from renewable sources by 2030 is an ambitious, may be distant future achievable target, given the current growth trends and government commitments. However, this will require addressing challenges related to grid integration, financing, and policy support. Petroleum is a major energy source in India after coal. Petroleum provides fuel for heat and lighting lubricants for machinery and raw materials for a number of manufacturing industries. In India by 2050, oil and natural gas will remain the largest energy sources.

25 countries and European Union committed a “no new coal” pledge at the COP29 climate summit not to build any new unabated coal-power plants, in a push to accelerate the process to phase out fossil fuel. The developing countries including India, China, and even USA opposed this pledge. India, China and Saudi Arabia have also opposed the attempts to stress a clear and identified pathway for reducing use of fossil fuels. A global pledge taken at the Glasgow Climate Summit in 2021 to cut emissions by phasing out coal has failed and its use has increased in the countries including China and India, the two most populous countries in the world, which are justified in the absence of any assistance committed by the developed countries to achieve energy transition. India is urging that developed countries have exploited the global carbon budget but failed to meet their commitment to climate finances, and are wrong fully demanding that developing countries restrict their fossil fuel use (Reference: Proceedings in the International Court of Justice). Policymakers from OECD countries use the U.N. conference process and other diplomatic forums to press China and India to speed up their transition from fossil fuels to zero-emission alternatives. However, such advice can sound at best impractical and at worst, an effort to force them to accept structurally lower living standards.

G. M Bhat
Department of Geology, University of Jammu, Jammu India
bhatgm@jugaa.com

JOURNAL INDIAN ASSOCIATION OF SEDIMENTOLOGISTS ISSN NO 2582 – 2020
Vol. 41, Issue II, 2024, pp. 5 – 12
DOI: https://doi.org/10.51710/jias.v41iII.348

Provenance of minerals in the Assi river sediments, Varanasi, Uttar Pradesh, India

Ranjan Pratap Singh[1], Anis[2], Vertika Shukla[2], D. K Soni[3], Anita[1], Aneet Kumar Yadav[1], Narendra Kumar[1*]

[1]Department of Environmental Science, Babasaheb Bhimrao Ambedkar University, Lucknow-226025
[2]Department of Geology, Babasaheb Bhimrao Ambedkar University, Lucknow-226025
[3]Central Pollution Control Board (CPCB), Lucknow-226010
*Email: narendrakumar_lko@yahoo.co.in

ABSTRACT

Grain size analysis and mineralogical characterization are important sedimentological tools to interpret the depositional environment, source, hydrodynamic conditions, and mode of transport of river sediments. Clays derived from chemical weathering are an important group of minerals found in various sedimentary environments such as rivers, estuaries, and ocean. In the present study, mineralogy of Assi river sediments was investigated with the help of Fourier Transform Infrared spectroscopy (FTIR), X-ray diffraction (XRD), and Scanning Electron Microscopy (SEM). Results revealed that the sediments are dominated by sand and mud. Further, the sediments were found to be abundant in quartz with subordinate amount of feldspars, kaolinite, illite, chlorite, and montmorillonite. Abundance of these minerals suggests that the Himalayan and Vindhyan sedimentary rocks are the primary source for the Assi river sediments.

Keywords: Assi river sediments, Provenance, Mineralogical characterization, Grain size

INTRODUCTION

Rivers play a vital role in distributing sediments. Irrigation, potable water, inexpensive transportation, and energy are all provided by river systems, which also provide livelihoods for a significant number of people across the world. In India, there are 12 major, 46 medium, 14 small and desert river basins make up about 45000 km long river system (Balagurunathan and Shanmugasundaram, 2015). Rivers are very important for the deposition of fertile soil on the plains, formation of deltas, home and industrial water supply, hydroelectric power generation, and inland fishing. Sediments are mainly the product of weathering and denudation of pre-existing rocks.

Understanding river systems in the context of various forcing mechanisms such as climatic condition, tectonics, eustacy and their linkages is crucial for fluvial geoscientists (Singh et al, 2007; Blum and Törnqvist, 2000). Erosional, transportation, and depositional processes of clastic sediments are essentially controlled by crustal deformation and climatic conditions. These clastic sediments are transported to the ocean through rivers from the continents and offering insights into Earth's geological history by recording the effects of climatic conditions, tectonics and sea level changes. A river derives its sediments from various sources distributed throughout its drainage basin and transports them in a wide range of grain size.

Grain size analysis of river sediments is an important tool for understanding the intrinsic properties and dynamic forces that operated during deposition. Moreover, grain size analysis also gives direction to investigate the depositional environment and energy flux of diverse agents that transported the sediments (Moiola and Weiser, 1968). Remarkable work has been carried out on grain size analysis for deducing source of sediment, transport mechanism, sedimentary processes and depositional environment (Folk and Ward, 1957; Friedman, 1961, 1967; Sahu, 1983; Ghosh and Chatterjee, 1994; Hartmann, 2007; Srivastava and Mankar, 2008; Tripathi and Hota, 2013; Kanhaiya and Singh, 2014; Kanhaiya et al., 2017; Ghaznavi et al., 2019).

The mineralogical analysis of sediments reflects the transportation history and sorting processes and provides valuable information for understanding provenance, tectonic setting and weathering signatures, paleoclimate and paleogeography (Verma and Armstrong-Altrin, 2013; Zou et al., 2016; Ramasamy et al., 2017; Armstrong-Altrin et al., 2015, 2022a, b). The framework grains of sediments commonly indicate the lithological characteristics of the source rocks and depositional environment (Dickinson, 1985; Garzanti et al., 2009). The original composition of clastic sediments may be affected by transportation history, sorting, redox condition as well as lithification, diagenesis, and metamorphism (Johnsson, 1993; Tawfik et al., 2018; Sopie et al., 2023).

The River Ganga is one of the most important dynamic components of the Indian subcontinent and appears among the world's major rivers. Major sediment sources of the River Ganga viz. Himalaya orogenic belt, the Indo-Gangetic plain and the northern Indian craton regions are

topographically and geologically distinct in nature (Singh et al, 2007). Various tributaries of River Ganga also play an important role in controlling total sediment load of the main river. Assi river is one of the tributaries of Ganga joining in the Holy city of Varanasi. Previous studies on Assi river are focussed on land use classification and watershed analysis (Srivastava et al., 2017), palaeo and present channel (Mishra et al., 2020), delineation of palaeo-course using remote sensing data (Mishra and Raju, 2022) and ground water quality assessment (Chaurasia et al., 2018; Singh et al., 2022). However, provenance study of Assi river sediments is still lacking. Therefore, this study was conducted along the course of Assi river, a tributary of River Ganga to characterize the nature and source of sediments based on the grain size characteristics and mineralogy.

GEOLOGICAL SETTING

The study area lies in the Varanasi district of Uttar Pradesh between the Latitude 25.28° N and Longitude 82.96° E. Sediment samples were collected from the Assi river from different locations (Fig. 1). Generally, sediments derived from Himalayan region are grey in colour comprising fine-grained silty sand with abundant mica. However, sediments derived from the craton are fine to coarse-grained sand with abundant potassium feldspars (Shukla and Raju, 2008). At Varanasi, the Ganga river carries a mixed sediment load derived from the Himalayan and peninsular regions including Vindhyan sedimentary rocks. The sediment fill of the Ganga basin is asymmetric decreasing in thickness from north to south. In the piedmont zone the alluvial fill is 3–8 km thick decreasing to about 0.5–1.0 km in the central part (Sastri et al.,1971; Shukla and Raju, 2008).

Varanasi City and its environs are located at an average height of about 76 m above the MSL (mean sea level) (Gupta and Mishra, 2022). The Varanasi City spreading over 100 km^2 area is part of the Indo-Gangetic Plain underlain by Quaternary alluvial sediments of Pleistocene to Holocene (Raju, 2012). The earliest phase of the geological history of the Indo-Gangetic Plain commenced with the formation of fore-deep concurrent with uplift of the Himalayan mountain system (Raju et al., 2011). In the Varanasi area, unconsolidated sediments form a sequence of clay, silt and sand of different grades. The presence of kankar carbonates is at times intercalated with clays and sands forming potential aquifers at various depths. Throughout the Central Ganga Plain the top few meters shows a distinctive fining upward succession terminating with clay-rich sediments (Shukla and Raju, 2008). OSL (Optically Stimulated Luminescence) dating techniques has been performed on an about 20 m thick fine-grained sedimentary sequence exposed on the eastern bank of River Ganga near Ramnagar dated between 59 ± 6 ka at the base to 7 ± 1 ka near the top (Raju et al., 2011). The sand, silt, and clays were originated from the alluvial deposits, and the precipitation of calcium carbonate from the groundwaters results in the formation of kankar (Raju et al., 2011). The Quaternary alluvial deposits are divided into older and recent alluviums (Shukla and Raju 2008; Raju et al., 2011).

Varanasi is the world's oldest city, situated between the Varuna river in the north and Assi river in the south (Fig. 1). The Assi river in Varanasi, Uttar Pradesh, India, is a small, local, ephemeral floodplain tributary of the River Ganga, with a length of about 8 km and catchment area of about 22 km^2 (Mishra et al., 2020). The Assi river originates from the Karmdeshwar Mahadev Kund in Kandwa village of Varanasi and Chitaipur, Karaundi, Newada, Sundarpur, Shukulpura, Naria, and Nagwa joins the Ganges (Das and Tamminga, 2012). The Ganges River flows in the eastern part of Varanasi; the Assi river joins the southern end while the Varuna River forms the northern boundary (Mishra and Raju, 2022). These rivers receive vast quantities of untreated sewage, agriculture runoff with fertilizers and pesticides from the catchment areas, which leads to degradation of water quality (Singh et al., 2022).

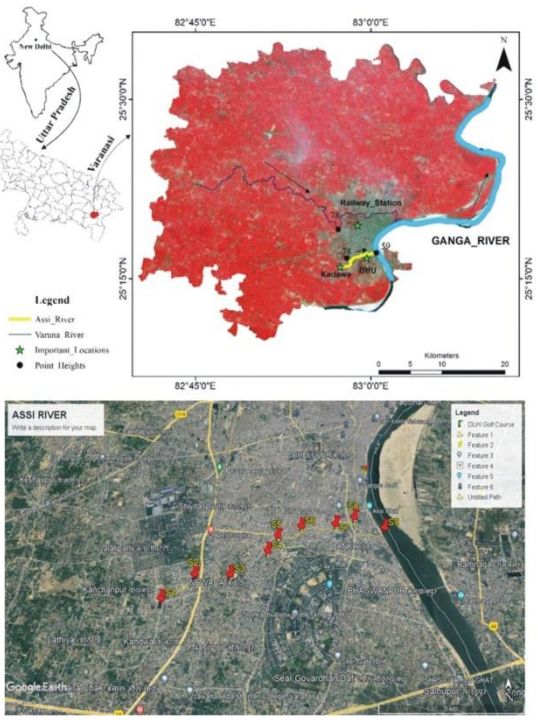

Fig. 1: Map showing sampling locations in the Assi River, Varanasi district, India

ANALYTICAL METHODS

A total of nine representative sediment samples were collected from different locations of Assi river. Sampling sites were carefully chosen to

avoid contamination and about 2 kg of sediment sample was collected with the help of a spatula and scraper. The collected samples were kept in the pre-cleaned zip-locked polyethylene bags for laboratory analysis. For the grain size analysis, standardized laboratory techniques were used following the methodology of Folk's (1980) scheme. Grain size of the bulk sediment samples was analysed using laser diffraction particle size analyser (CILAS 1190).

XRD (X-ray Diffraction) is a powerful technique for characterizing crystalline and polycrystalline materials. It gives information about structures, phases, texture, and other structural features, such as average grain size, crystallinity, strain, and crystal defects. X-ray diffraction (XRD) analysis is used to understand the source of sediments through identification of mineralogical composition of sediments to explain the causes and mechanisms of sedimentation (Kumar et al, 2018). The sediment samples were subjected to X-ray Diffraction for quantitative analysis of bulk mineralogy.

The IR technique is most powerful when used in conjunction with XRD (X-Ray diffraction) and other techniques. In earlier work, quantitative determination of quartz by infrared spectroscopy in soil, sediments, dust, other silicates and powdered coal was reported by Hlavay et al. (1978). Madejova (2003) applied infrared spectroscopy to identify various types of clay minerals from different angles. River sediments were analyzed for its vibration spectra with the aid of Fourier Transform Infrared Spectroscopy (FTIR, Nocolet 6700; Thermo-Scientific). Samples were mixed with KBr and pellets were prepared under a hydraulic press. Pellets were analyzed for vibration spectra of clay mineral by FTIR in the range 400–4000 cm^{-1}.

EDS analysis provides information about elemental composition of the particular particles in the sediments and allows determination of the relative mineral abundance (Rajkumar et al., 2012). The sediment samples were analyzed with the help of Scanning Electron Microscopy (SEM) attached to the Electron Diffraction Spectra (EDS) (JSM 6490 JEOL). The SEM was fitted with a Moran Scientific EDS analyzer that was employed to confirm mineral identification.

RESULTS AND DISCUSSION

Grain size Analysis

Grain size analysis is a reliable procedure to characterize the sediment and provide information on its depositional environment and transport mechanism (Folk and Ward, 1957). To identify the grain size distribution of the sediment samples (gravel, sand, and mud), sieving technique was used. The grain weight of the collected samples was calculated by Folk's (1980) method, using the measured grain weight and cumulative percentages of the grain weights obtained. The percentage values of gravel, sand, and mud were plotted on a ternary diagram for classification of sediments. A ternary diagram is a three-component system where each side corresponds to an individual binary system. However, in three dimensions the diagram is more complex with surfaces emerging rather than lines as in the binary system (Flemming, 2000). The ternary diagram representing the gravel, mud and sand fractions suggest that the sediments are primarily muddy sand in texture (Fig. 2). In this plot the average percentages of gravel, sand and mud was found to be 0.0%, 76.7%, 32.3% respectively. Proportion of sand was higher than mud and gravels indicating that the nature of river was turbulent.

Many studies have attempted to distinguish between the sediments of modern depositional environments using the grain size distribution. Friedman (1961) proposed that river, beach and dune sands could be differentiated by movement parameters which reflect differences in the mode and energy of sediment transport. Glaister and Nelson (1974) and Sagoe and Visher (1977) suggested that environment of deposition can be interpreted on the basis of the shapes of grain size cumulative curves. The energy conditions and sediment supply within river systems can be considerably differ from one river to another river and even within different parts of the same river system. Thus, in some cases, the grain size characteristics of sediments may show higher variability within different parts of the same environmental conditions (Boggs, 2014). The particle size in a particular deposit reflects weathering and erosion, which generate particles of various sizes, and the nature of subsequent transport processes. Finally, since the size and sorting of sediment grains may reflect sedimentation mechanisms and depositional conditions, grain size data are assumed to be useful for interpreting the depositional environments of ancient sediments or sedimentary rocks (Boggs, 2014). The grain size data show high contribution of medium sand followed by fine sand and very fine sand. The silt fraction is composed of very course silt with a low percentage of coarse, medium and fine silts. The grain size data shows both sand and silt content in variable proportions, which suggesting varying energy conditions.

XRD Analysis

The XRD patterns and results reflected the presence of quartz, kaolinite, illite, chlorite, K-feldspar, plagioclase and the main reflections of the

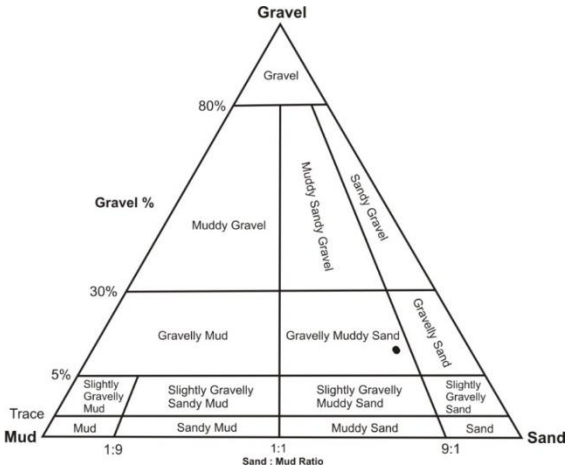

Fig. 2: Ternary plot for sediment classification based on Folk's scheme

major minerals such as quartz (78.38; 2θ), (120.87; 2θ), kaolinite (10.78; 2θ), (13.67; 2θ), illite (10.78;

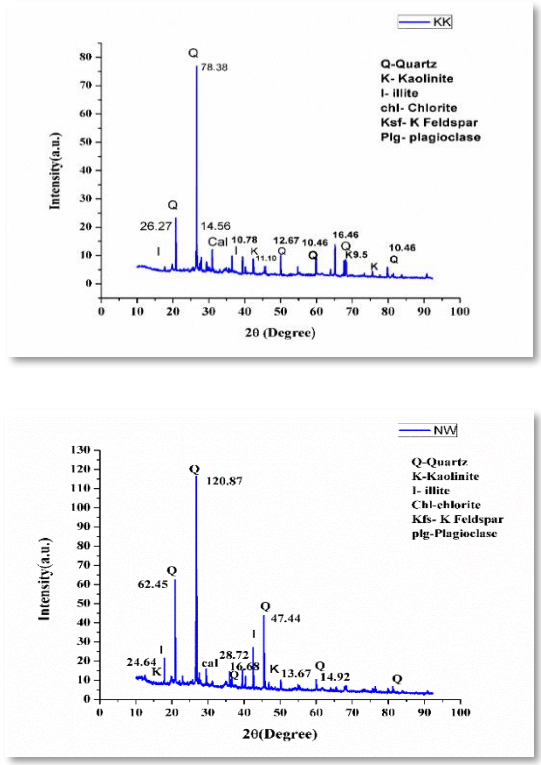

Fig. 3: X-ray Diffraction (XRD) spectra for the Assi river sediments

2θ), (28.72; 2θ) were found, probably derived from igneous and sedimentary rocks (Fig. 3) (Maity and Maiti, 2016; Khan et al., 2020). Presence of different clay mineral indicates a significant change in the physico-chemical conditions operating within the system. Weathering of k-feldspar under acidic condition produces mainly the kaolinite group without any exchangeable cations, whereas illite and chlorite are derived by alteration of mica, K-feldspars, biotite, etc. under alkaline conditions (Kotoky et al., 2006).

Kaolinite formation is favoured under tropical to subtropical humid climate (Chamley, 1989; Hallam et al., 1991). In addition, detrital origin of kaolinite may also develop by diagenetic processes due to the circulation of acidic solutions (Ghandour et al., 2003). Presence of illite and kaolinite suggests prominent chemical weathering of feldspar and muscovite. Under acidic conditions, weathering or hydrothermal alteration of alumino-silicate minerals facilitate leaching of Ca, Mg, Na and Fe ions (Sheldon and Tabor, 2009).

FTIR analysis

The band position or location of the peaks from the conspicuous FTIR absorption peaks are used in qualitative analysis to detect the primary and minor constituent minerals present in the samples. The FTIR spectra of the samples were recorded. The observed wave numbers are analyzed, and the

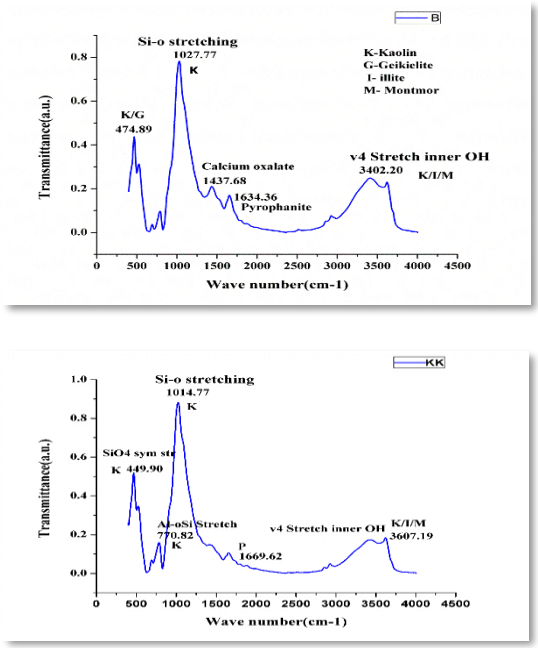

Fig. 4: FTIR spectra for the sediment samples showing the presence of various minerals

minerals are assigned using available literatures (Ramasamy et al., 2006). FTIR spectra revealed the presence of kaolinite, illite, montmorillonite, and Geikielite in different sediment samples (Fig. 4).

Quartz is a non-clay mineral that is found in abundance in all the samples. The strongest bonds in the silicate structure are the Si-O bonds, which may be seen in the infrared spectra of such minerals. The presence of quartz in the sediment samples can be explained by Si-O asymmetrical bending vibrations around 464 cm^{-1}, Si-O symmetrical bending vibrations around 694 cm^{-1}, Si-O symmetrical stretching vibrations at around 778 and 796 cm^{-1}, while the 1082 and 1162 cm^{-1} absorption

region arises from Si-O asymmetrical stretching vibrations due to low Al for Si substitution. The infrared determination of quartz in sediments has been characterized by Chester and Green (1968). Kaolinite, illite and montmorillonite are most important clay minerals. The presence of absorption band at or around 3690, 3620, 1030 and 1015 cm^{-1} indicates kaolinite (Ramasamy et al., 2006). The intensity of the bands varies from sample to sample, which shows the quantity. If four peaks are observed in the minerals between 3697 and 3620 cm^{-1} they are said to be ordered state (Russell, 1987; Ramasamy et al., 2005). Kotoy et al. (2006), have highlighted the use of Fourier Transform Infrared Spectra to establish mineral association of kaolinite with traces of illite and chlorite. Calcite is one of the most common carbonate mineral in sediments. From the existence of a peak in the range 1420-1438 cm^{-1} it is easily recognized that the calcite is present in the studied samples.

SEM-EDS analysis

The size, shape, composition, crystallography, and other physico-chemical aspects of a specimen are studied in the SEM (Ural, 2021). SEM allows for a high-resolution image to be created by analyzing the material to be inspected with an electron beam generated in a vacuum environment and thinned with electromagnetic lenses in the same environment (Armstrong-Altrin, 2020). Sediment samples were subjected to SEM-EDS analysis in order to determine the presence of characteristic micro-morphology of the clay minerals and their relationship to non-clay minerals (Bassin, 1975). During the EDX measurement different areas were focus and the corresponding peaks are shown. The studied samples are composed mainly of Si, Al, Fe, Mg, K, Ca, and P etc. (Fig. 5). Percentage of elements present in the sediment samples is given in Table 1.

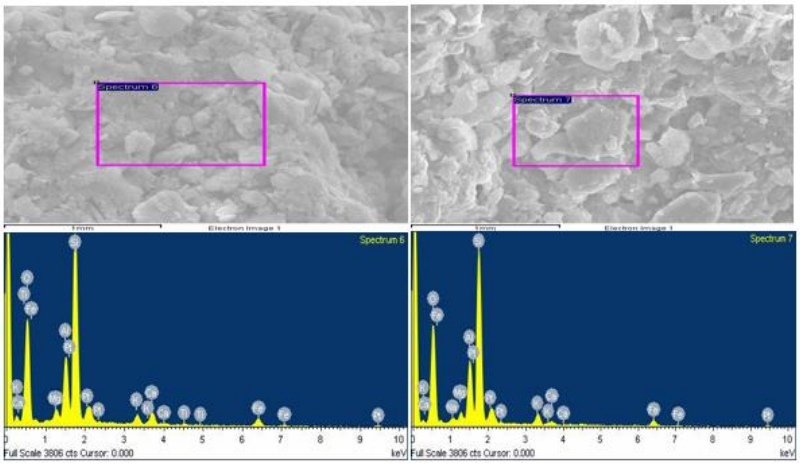

Fig. 5: Scanning Electron Microscopy (SEM-EDS) spectra and results of studied sediment samples at selected points

Table 1: Average percentage of elements present in the studied sediment samples

Element	Weight%	Atomic%
O K	53.75	70.61
Na K	0.97	0.89
Mg K	1.32	1.14
Al K	7.90	6.15
Si K	24.19	18.10
K	2.11	1.14
Ca K	0.48	0.25
Fe K	2.70	1.01
Pt M	6.57	0.71
Total	100.00	100.00

Results indicate that mineralogical characterization of sediments is an important tool to understand source of sediments, hydrodynamic conditions, mode of transportation and deposition. The drainage pattern of Varanasi environs is primarily controlled by Assi and Varuna rivers (Shukla and Raju, 2008). At Varanasi, the River Ganga carries mixed load sediments derived both from Himalaya and peninsular craton including Vindhyan rocks (Shukla and Raju, 2008). The sand is fine-to-medium grained and grey coloured with significant mica content. Sand is mainly point bars deposits flanked by narrow flood plains confined to river valley. Presence of kaolinite indicates acidic environment and sediments derived from weathering of granite and Ca-poor igneous and metamorphic rocks (Kotoky et al., 2006). Kaolinite forms in both reducing and oxidizing environmental conditions (Kotoky et al., 2006). Montmorillonite is the alteration product of basic rocks, where alteration of stable minerals formed in alkaline conditions due to availability of Ca and Mg, whereas illite is a stable alteration product of acidic rocks due to high weathering conditions in humid climate and confined to shale (Ramasamy et. al., 2004). Chlorite is possibly derived from aggradations of less oxidized sheet minerals and degradation of pre-existing ferromagnesian bearing minerals (Rajkumar et al., 2012).

CONCLUSIONS

Grain size analysis, chemical and mineralogical compositions are the three basic parameters to infer sediment provenance. A precise approximation of the parametric distributions of particle size is needed for the modelling of sediment transport, particularly to predict erosion and depositional conditions. The mineralogical characterization of sediments reflects the geological history of transport and sorting processes. Moreover, the scientific studies of the

identification of minerals in sediments lead to useful information about possible origin of minerals. In the present work, grain size, XRD, SEM and FTIR techniques were applied for the mineralogical components of the Assi river sediments. The Himalayan rivers carries the micaceous greywacke sand towards peninsular craton probably under increased water budget conditions. They were interacting with NE flowing southern rivers carrying pink arkosic sand from craton side near Varanasi. This led to mixing and superposition of sediments derived from two different sources across the zone of present-day water of Ganga. The interpreted source rocks for the Assi river sediments are Himalayan derived grey micaceous sands, were being carried by the southward flowing rivers beyond the present-day water divide of Ganga and mixed with pink arkosic sand brought by the northward flowing peninsular rivers.

ACKNOWLEDGEMENT

The authors are grateful to the Head, Department of Environmental Science, BBAU, Lucknow for providing the necessary facilities. The authors also express sincere gratitude to the Director, University Science Instrumentation Centre (USIC), BBAU for providing instrumentation facilities. We are grateful to the two reviewers for their comments, which significantly improved our presentation.

Declaration of Conflicting Interest: The Author(s) declare(s) that there is no conflict of interest.

REFERENCES

Armstrong-Altrin, J.S. (2020). Detrital zircon U-Pb geochronology and geochemistry of the Riachuelos and Palma Sola beach sediments, Veracruz State, Gulf of Mexico: a new insight on palaeoenvironment. Journal of Palaeogeography, v. 9 (4), article no. 28.

Armstrong-Altrin, J.S., Machain-Castillo, M.L., Rosales-Hoz, L., Carranza-Edwards, A., Sanchez-Cabeza, J.A. and Ruíz-Fernández, A.C. (2015). Provenance and depositional history of continental slope sediments in the Southwestern Gulf of Mexico unraveled by geochemical analysis. Continental Shelf Research, v. 95, pp. 15–26.

Armstrong-Altrin, J.S., Ramos-Vázquez, M.A., Madhavaraju, J., Marca-Castillo, M.E., Machain-Castillo, M.L. and Márquez-Garcia, A.Z. (2022a). Geochemistry of marine sediments adjacent to the Los Tuxtlas Volcanic Complex, Gulf of Mexico: Constraints on weathering and provenance. Applied Geochemistry, v. 141, no. 105321.

Armstrong-Altrin, J.S., Ramos-Vázquez, M.A., Madhavaraju, J., Verma, S.K., Macías-Martínez, K. and Martínez-Ruíz, D. (2022b). Quartz grain microtextures in the Boca del Cielo and Chocohuital beaches in the Mexican Pacific, Chiapas state: implication on palaeoenvironment. Arabian Journal of Geosciences, v. 15, number 1086.

Balagurunathan, R. and Shanmugasundaram, T. (2015). Microbial biodiversity of selected major river basins of India. In Ramkumar, M., Kumaraswamy, K, and Mohanraj, R. (Eds.), Environmental Management of River Basin Ecosystems. Springer, P. 575-591.

Bassin, N.J. (1975). Suspended marine clay mineral identification by scanning electron microscopy and energy-dispersive x-ray analysis. Limnology and Oceanography, v. 20(1), pp. 133-137.

Blum, M.D. and Törnqvist, T.E. (2000). Fluvial responses to climate and sea-level change: a review and look forward. Sedimentology, v. 47, pp. 2-48.

Boggs, S. (2014), Principles of sedimentology and stratigraphy. 5th ed. Pearson New International Publishers, USA, p. 560.

Chamley, H. (1989). Clay Mineralogy. Springer Publishers, Berlin, Germany, p. 623.

Chaurasia, A.K., Pandey, H.K., Tiwari, S.K., Prakash, R., Pandey, P. and Ram, A. (2018). Groundwater quality assessment using water quality index (WQI) in parts of Varanasi District, Uttar Pradesh, India. Journal of the Geological Society of India, v. 92, pp. 76-82.

Chester, R. and Green, R.N. (1968). The infrared determination of quartz in sediments and sedimentary rocks. Chemical Geology, v. 3(3), pp. 199-212.

Das, P. and Tamminga, K.R. (2012). The Ganges and the GAP: an assessment of efforts to clean a sacred river. Sustainability, v. 4(8), pp. 1647-1668.

Dickinson, W.R. (1985). Interpreting provenance relations from detrital modes of sandstones. In Zuffa G.G. (Eds.), Provenance of Arenites. Dordrecht, The Netherlands: Reidel Publishing Company Reidel, p. 231–247.

Flemming, B.W. (2000). A revised textural classification of gravel-free muddy sediments on the basis of ternary diagrams. Continental Shelf Research, v. 20(10-11), pp. 1125-1137.

Folk, R.L. (1980). Petrology of sedimentary rocks. Hemphill Publishing Company, Austin, Texas, p. 182.

Folk, R.L. and Ward, M.C. (1957). Brazos River bars: a study in the significance of grain size parameters. Journal of Sedimentary Research, v.27, pp. 3–27.

Friedman, G.M. (1961). Distinction between dune, beach and river sands from their textural characteristics. Journal of Sedimentary Petrology, v. 31, pp. 514-529.

Friedman, G.M. (1967). Dynamic processes and statistical parameters compared for size frequency distribution of beach river sands. Journal of Sedimentary Research, v. 37, pp. 327–354.

Garzanti, E., Andò, S., Vezzoli, G. (2009). Grain-size dependence of sediment composition and environmental bias in provenance studies. Earth and Planetary Science Letters, v. 277, pp. 422–432.

Ghandour, I.M., Harue, M. and Wataru, M. (2003). Mineralogical and chemical characteristics of Bajocian-Bathonian shales, G. Al-Maghara, North Sinai, Egypt: climatic and environmental significance. Geochemical Journal, v. 37, pp. 87–108.

Ghaznavi, A.A., Quasim, M.A., Ahmad, A.H.M. and Ghosh, S.K. (2019). Granulometric and facies analysis of Middle–Upper Jurassic rocks of Ler Dome, Kachchh, western India: an attempt to reconstruct the depositional environment. Geologos, v. *25*(1), pp. 51-73.

Ghosh, S.K. and Chatterjee, B.K. (1994). Depositional mechanisms as revealed from grain-size measures of the palaeoproterozoic Kolhan siliciclastics, Keonjhar District, Orissa, India. Sedimentary Geology, v. 89, pp. 181–196.

Glaister, R.P., and H.W. Nelson. (1974). Grain-size distributions, an aid to facies identifications. Canadian Petroleum Geology Bulletin, v. 22, pp. 203–240.

Gupta, A. and Mishra, A. (2022). Trend Analysis and Change Point Detection of Annual and Seasonal Precipitation Timeseries Over Varanasi District, Uttar Pradesh. In Phartiyal B, Mohan R, Chakraborty S, Dutta V, Gupta AK (Eds.), Climate Change and Environmental Impacts: Past, Present and Future Perspective, Cham: Springer International Publishing, P. 267-286.

Hallam, A., Grose, J.A. and Ruffell, A.H. (1991). Paleoclimatic significance of changes in clay mineralogy across the Jurassic-Cretaceous boundary in England and France. Palaeogeography, Palaeoclimatology, Palaeoecology, v. 81, pp.173–187.

Hartmann, D. (2007). From reality to model: operation-alism and the value chain of particle size analysis of natural sediments. Sedimentary Geology, v. 202, pp. 383–401.

Hlavay, J., Jonas, K., Elek, S. and Inczedy, J. (1978). Characterisation of the particle size and the crystallinity of certain minerals by IR spectrometry and other instrumental methods – II. Investigations on quartz and feldspar. Clays and Clay Minerals, v. 26(2), pp. 139.

Johnsson, M.J. (1993). The system controlling the composition of clastic sediments. In Johnsson MJ, Basu A (Eds.), Processes controlling the composition of clastic sediments. Geological Society of America, v. 284, p. 1–19.

Kanhaiya, S. and Singh, B.P. (2014). Spatial variation of textural parameters in a small river: An example from Khurar River, Khajuraho, Chhaterpur District, Madhya Pradesh, India. Global Journal of Earth Science and Engineering, v. 1, pp. 34–42.

Kanhaiya, S., Singh, B.P. and Srivastava, V.K. (2017). Surface textures of detrital quartz grains derived from Bundelkhand granite in the Khurar River, central India. Vietnam: Geo-spatial technology and Earth resources. Publishing House for Science and Technology, pp. 575–581.

Khan, Z., Quasim, M.A., Amir, M. and Ahmad, A.H.M. (2020). Provenance, tectonic setting, and source area weathering of Middle Jurassic siliciclastic rocks of Chari Formation, Jumara Dome, Kachchh Basin, Western India: Sedimentological, mineralogical, and geochemical constraints. Geological Journal, v. 55(5), pp. 3537-3558.

Kotoky, P., Bezbaruah, D., Baruah, J., Borah, G.C. and Sarma, J.N. (2006). Characterization of clay minerals in the Brahmaputra river sediments, Assam, India. Current Science, pp. 1247-1250.

Kumar Maity, S., Maiti, R., Kumar Maity, S. and Maiti, R. (2018). Identification of the Sediment Sources Using X-Ray Diffraction (XRD) Technique. Sedimentation in the Rupnarayan River. Estuarine Environment of Deposition, v. 2, pp. 57-78.

Madejova, J. (2003). FTIR techniques in clay mineral studies. Vibrational Spectroscopy, v. 31, pp.1-10.

Maity, S.K. and Maiti, R. (2016). Understanding the sediment sources from mineral composition at the lower reach of Rupnarayan River West Bengal India–XRD-based analysis. GeoResJ, v. 9(12), pp. 91–103.

Mishra, M. and Raju, K.P. (2022). Groundwater evidences in confirmation of palaeo-course of Assi River in Uttar Pradesh, India. Current Science, v. 122(3), pp. 333-336.

Mishra, M., Raju, K.N.P. and Raju, P.V. (2020). Palaeo and present channel of Assi river, Uttar Pradesh, India. Current Science, v. 118, pp. 630–639.

Moila, R. J and Weiser, D. (1968). Textural parameters: An evaluation. Journal of Sedimentary Petrology, v. 38, pp. 45-53.

Rajkumar, K., Ramanathan, A.L. and Behera, P.N. (2012). Characterization of clay minerals in the Sundarban mangroves river sediments by SEM/EDS. Journal of the Geological Society of India, v. 80, pp. 429-434.

Raju, J.N. (2012). Arsenic exposure through groundwater in the middle Ganga plain in the Varanasi environs, India: A future threat. Journal of the Geological Society of India, v. 79, pp. 302-314.

Raju, J.N., Shukla, U.K. and Ram, P. (2011). Hydrogeochemistry for the assessment of groundwater quality in Varanasi: a fast-urbanizing centre in Uttar Pradesh, India. Environmental Monitoring and Assessment, v. 173, pp. 279-300.

Ramasamy, N., Roy, P.D., Kessler, F.L., Jong, J., Dayong, V. and Jonathan, M.P. (2017). An integrated study of geochemistry and mineralogy of the Upper Tukau formation, Borneo Island (East Malaysia): sediment provenance, depositional setting and

tectonic implications. Journal of Asian Earth Sciences, v. 143, pp. 77–97.

Ramasamy, V., Murugesan, S. and Mullainathan, S. (2004). Characterization of minerals and relative distribution of quartz in Cauvery river sediments from Tamilnadu, India-A FTIR study. Bulletin Pure Applied Science, v. 23, pp. 1-2.

Ramasamy, V., Murugesan, S. and Mullainathan, S. (2005). Distribution and characterization of minerals in Cauvery river sediments by grain size analysis- A new approach by FT-IR study. The Indian Mineralogist, v. 39(2), pp. 91-93.

Ramasamy, V., Rajkumar, P. and Ponnusamy, V. (2006). FTIR spectroscopic analysis and mineralogical characterization of Vellar river sediments. Bulletin of Pure and Applied Science, v. 25(1), pp. 49-55.

Russel, J.D. (1987). Infrared methods- A hand book of determinative methods in clay mineralogy. In: Wilson, M.J. (Eds.), Blackie and Son Ltd., New York, P. 133.

Sagoe, K.M.O. and Visher, G.S. (1977). Population breaks in grain size distributions of sand—A theoretical model. Journal of Sedimentary Petrology, v. 47, pp. 285–310.

Sahu, B.K. (1983). Multi group discrimination of depositional environments using size distribution statistics. Indian Journal of Earth Science, v. 10, pp. 20–29.

Sastri V.V., Bhandari L.L., Raju A.T.R. and Dutta A.K. (1971). Tectonic framework and subsurface stratigraphy of the Ganga Basin. Journal Geological Society of India**,** v. 12, pp. 222–233.

Sheldon, N.D. and Tabor, N.J. (2009). Quantitative paleoenvironmental and paleo-climatic reconstruction using paleosols. Earth Science Review, v. 95, pp.1–52.

Shukla, U.K. and Raju, N.J. (2008). Migration of Ganga River and its implication on hydro-geological potential of Varanasi area, U. P. Journal of Earth System Sciences, v. 117(4), pp. 489–498.

Singh, M., Singh, I.B. and Müller, G. (2007). Sediment characteristics and transportation dynamics of the Ganga River. Geomorphology, v. 86(1-2), pp. 144-175.

Singh, R.P., Shukla, V., Kumar, S., Soni, D.K. and Kumar, N. (2022). Assessing surface and ground water quality, for Irrigation and drinking purpose, along the course of Assi River, Varanasi, India. National Journal of Life Sciences, v. 19, p.1-7.

Sopie, F.T., Ngueutchoua, G., Armstrong-Altrin, J.S., Njanko, T., Sonfack, A.N., Sonfack, A.N., Ngagoum, Y.S.K., Fossa, D. and Tembu, L.T. (2023). Provenance, weathering, and tectonic setting of the Yoyo, Kribi, and Campo beach sediments in the southern Gulf of Guinea, SW Cameroon. Journal of Earth System Science, v. 132, article no. 92.

Srivastava, A.K. and Mankar, R.S. (2008). Grain size analysis and depositional pattern of upper Gondwana sediments (Early Cretaceous) of Salbardi area, districts Amravati, Maharashtra and Betul, Madhya Pradesh. Journal of the Geological Society of India, v. 73, pp. 393–406.

Srivastava, M., Goel, A. and Ohri, A. (2017). Land Use Classification and Watershed Analysis of Assi River, Varanasi, Uttar Pradesh, India. Journal of Advanced Research in Construction & Urban Architecture, v. 2, pp. 32-37.

Tawfik, H.A., Salah, M.K., Maejima, W., Armstrong-Altrin, J.S., Abdel-Hameed, A-M.T. and Ghandour M.M.E. (2018). Petrography and geochemistry of the Lower Miocene Moghra sandstones, Qattara Depression, north Western Desert, Egypt. Geological Journal, v. 53, pp. 1938-1953.

Tripathi, A. and Hota, R.N. (2013). Granulometric Analysis of Ib River Sediments near Sundargarh, Odisha. Vistas in Geological Research. Utkal University Special Publication in Geology, pp. 74–79.

Ural, N. (2021). The significance of scanning electron microscopy (SEM) analysis on the microstructure of improved clay: An overview. Open Geosciences, v. 13(1), pp. 197-218.

Verma, S.P. and Armstrong-Altrin, J.S. (2013). New multidimensional diagrams for tectonic discrimination of siliciclastic sediments and their application to Precambrian basins. Chemical Geology, v. 355, pp. 117–133.

Zou, S.H., Wu, C.J., Xu, D.R., Shan, Q., Zhang, X.W., Hollings, P. and Hou, M.Z. (2016). Provenance and depositional setting of Lower Silurian siliciclastic rocks on Hainan Island, South China: implications for a passive margin environment of South China in Gondwana, Journal of Asian Earth Sciences, v. 123, pp. 243–262.

Received on: Feb 13, 2024
Revised accepted on: Aug 10, 2024

JOURNAL INDIAN ASSOCIATION OF SEDIMENTOLOGISTS ISSN NO 2582 – 2020
Vol. 41, Issue II, 2024, pp. 13 – 22
DOI: https://doi.org/10.51710/jias.v41iII.350

Lithofacies and Granulometric Analysis of Middle Siwalik Sandstones of Jammu, NW Himalaya, India

S. K. Pandita, Sumit Johar*, Shifali Chib, Yudhbir Singh, G. M. Bhat and S.S. Kotwal
Department of Geology, University of Jammu, Jammu-180006 (India)
*Email: sumit.johar@jammuuniversity.ac.in

ABSTRACT

In the Northwest Himalaya, the Siwalik Group of rocks are exposed in the Suruin-Mastgarh anticlinal folded succession and has been classified into Lower, Middle and Upper subgroups. The Middle Siwalik Subgroup is exposed at various locations in the Jammu region and is primarily made up of multistoried sandstones embedded with thin beds of mudstone. In the present study, these rocks have been studied to understand the depositional history using the sediment size of sandstones and the lithofacies in addition to the paleocurrent analysis. The multistoried nature of the sandstone and the scour fills observed in these rocks imply that there were frequent and periodic strong stream encounters at the depositional site where saltation was the dominant process of transportation of sediments. The data obtained on grain size, lithofacies, cross beddings, and the type of contacts between different lithofacies suggest that the southerly flowing braided river system underwent multiple episodes of avulsion and abandonment of the channel system during the deposition of the Middle Siwalik subgroup in Jammu region.

KEYWORDS: Middle Siwalik, Lithofacies, Grainsize, Paleocurrent, Paleoenvironment.

INTRODUCTION

The Himalayan Foreland Basin is a component of the marginal fold and thrust belt that resulted from the collision of the Indian and Eurasian plates. This foreland basin encompasses Tertiary rocks including the Subathu, Murree and Siwalik groups. The Siwalik extends from the Potwar plateau in the northwest all along the Himalaya arc to the Brahmaputra valley in the east, forming a series of parallel-dissected ridges. The Siwalik Group of rocks (consolidated to semi-consolidated) comprise a 5-6 km thick pile of late Cenozoic freshwater molasse sedimentary succession that forms the youngest mountain belt in the form of Himalayan foothills. The Siwalik Group of sediments were deposited in two coarsening up megacycles consisting of sandstone-clay alternations in the lower portion passing gradually into coarse sandstones and/or conglomerates towards the top (Parkash et al., 1980; Pandita and Bhat, 1999). Prominent structural units i.e. Udhampur Syncline, Udhampur Thrust, the Suruin-Mastgrah anticline and Kishanpur Thrust (Dasarathi, 1968) distinguish the Jammu foothills. The Siwalik Group of rocks are exposed in the Suruin-Mastgarh anticlinal folded succession. Sandstone, mudstone, and conglomerate make up the majority of the Siwalik succession in Jammu region (Pandita et al., 2014).

The Siwalik Group has been classified into three subgroups: Lower, Middle, and Upper Siwalik**.** The Lower Siwalik subgroup consists of indurated sandstone, mudstone and siltstone and has been interpreted as deposited within the meandering river system (Pandita et al., 2014). The Middle Siwalik subgroup is composed of dominantly thick semiconsolidated and consolidated multistoried-sandstone (90%) embedded with thin mudstone (10%) beds. The Upper Siwalik subgroup comprises of semiconsolidated conglomerates, sandstones and mudstones. The Siwalik sediments have been studied for palaeontology (Gupta and Verma, 1988; Ranga Rao et al., 1988; Nanda and Sehgal, 1993; Kundal and Prasad, 2011), sedimentology (Pandita and Bhat, 1999; Sharma et al., 2001; Bhat et al., 2008; Pandita et al., 2011, Irfan et al., 2022), structural geology (Dasarathi, 1968; Karunakaran and Ranga Rao, 1979) and petrography (Krynine, 1937; Bhatia, 1970; Pandita and Bhat, 1995, Pandita et al., 2014). Besides, magnetostratigraphy (Ranga Rao, 1993) and fission track dating of the bentonite beds in the upper Siwalik (Ranga Rao et al., 1988 and Mehta et al., 1993) have been carried out. The current study aims to discuss the depositional environment of the Middle Siwalik subgroup in the Jammu region by examining the lithofacies and granulometric analysis of these sediments.

STUDY AREA

The area under investigation displays some of the spectacular exposures of Siwalik Group extending for tens of kilometres along the strike and for 5 to 6 km in thickness (in different hillocks) and offers opportunity to study these sediments in Jammu Region. To understand the depositional history of the Middle Siwalik subgroup in Jammu region, three stratigraphic sections exposed near Bantalao (Nandni-Nagrota section), Aitham (Bajalta-Aitham section) and Parmandal (Parmandal-Utterbehni section) (Fig. 1) were

studied laying emphasis on recording lateral and vertical facies variations within the sediment bodies; the nature of stacking, grain size and sedimentary structures.

MATERIALS AND METHODS

Three well-exposed sections of Middle Siwalik at Bantalao in Nandni-Nagrota, at Aitham in Bajalta area and near Parmandal in Parmandal-Uttarbehni lithosections were studied in detail to understand the sedimentation pattern for interpreting the depositional environment. The lithosections were measured and different lithofacies were recorded in the field. The attitude of beddings and cross beddings was recorded for understanding the paleoflow direction in the area. A total of 30 (10 from each locality) semi-consolidated sandstone samples were collected for granulometric analysis. The sandstone samples were disintegrated and dry sieved in the sedimentology laboratory of the Department of Geology, University of Jammu. From each sample, 100 grams of the representative sediment sample was taken to perform sieve analysis by employing a series of standard sieves with 1Φ class interval using a mechanical sieve shaker. The weight of the sample size left in each sieve was recorded and the cumulative grain size distribution curves were prepared to calculate size statistical parameters as outlined by Lindholm (1987).

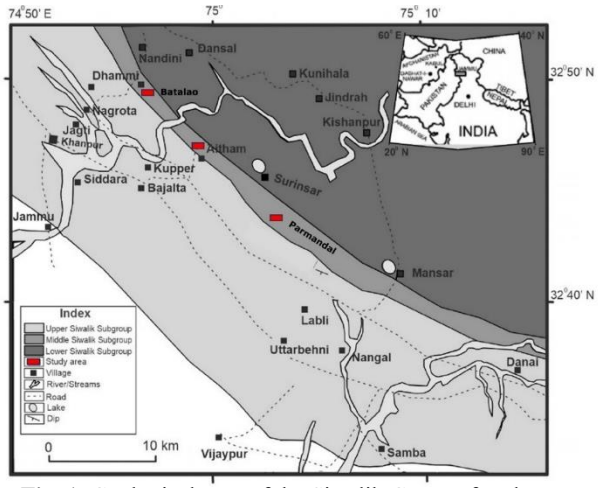

Fig. 1. Geological map of the Siwalik Group of rocks in the southern limb of the Suruin- Mastgarh anticline in Jammu region (after Pandita et al., 2014)

FIELD OBSERVATIONS

Nandni-Nagrota Lithosection

In this lithosection, Middle Siwalik is exposed along the Nandni-Nagrota Road near Bantalao area and a 97m thick stratigraphic succession comprising of sandstone-mudstone couplets (Fig. 2A) was measured. The sandstone beds are grey-coloured, medium to coarse-grained, friable, 1.0 to 11.2 m thick with an average thickness of 8 m. These sandstone beds mostly grouped as multi-storeyed sandstone bodies display large scale trough and planar cross bedding throughout the succession. Hard calcareous sand balls and sand lenses are distributed irregularly throughout the lithosection. Extra formational clasts are either unevenly distributed or oriented along bedding, cross-bedding and erosional bases of the sandstone bodies. The erosional surfaces are marked by the presence of intra formational mud balls, mud pellets and sand balls, and extra formational clasts. Deformation in the bedding and cross bedding due to liquefaction is observed at places. Channel cut and fill structures containing thin laminated sand beds are also observed. Sand nodules associated with coarse to medium sandstone are also observed.

The mudstones are yellow, brown, grey, variegated in colour, and range in thickness from 0.40 to 2.80 m with an average thickness of 1 m. These mudstones are thinly laminated, nodular, flaky and at places calcretised. The mudstones have mostly erosional contacts with overlying sandstone bodies but at places show sharp contacts also.

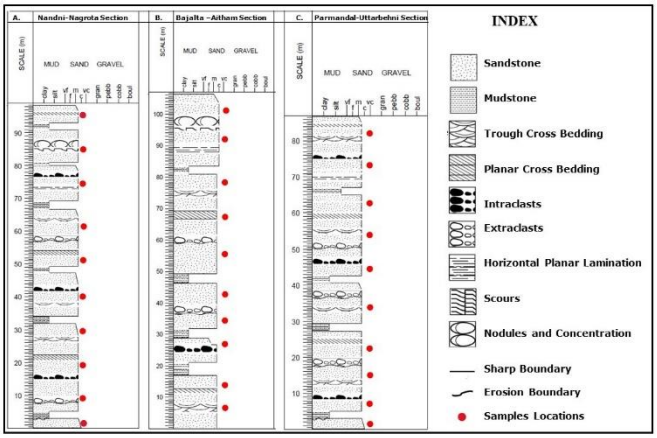

Fig. 2. Lithologs of the measured stratigraphic sections of Middle Siwalik in Jammu region: (A) Nandni-Nagrota section; (B) Bajalta-Aitham section; and (C) Parmandal-Uttarbehni section

Bajalta-Aitham Lithosection

A 106 m thick stratigraphic section of the Middle Siwalik subgroup was measured near Aitham, which embeds an alternation of sandstone and mudstone couplets (Fig. 2B). The sandstone beds are grey in colour, medium to coarse-grained. The basal contacts of the sandstone beds with mudstone/sandstone beds are erosional and sharp at places, whereas, the overlying contacts are mostly sharp but occasionally erosional. Various sandstone storeys are stacked one above the other and separated by erosional contacts. The erosional contacts are represented by the scour filling with intra formational mud balls, mud pellets and extra formational clasts of sandstone and quartzite composition. Various mud lenses are observed within the sandstone beds. At some places, sand balls are also observed within sandstone beds. The sandstone beds display planar and trough cross-stratification.

Parmandal-Uttarbehni Lithosection

In this lithosection, the Middle Siwalik subgroup is composed of an alternation of thick sandstone and thin mudstone beds. The total measured thickness of the Middle Siwalik rocks in this area is 86 m (Fig. 2C). The sandstone beds are grey and buff, medium to coarse-grained, friable and range in thickness from 2.8 to 20 m with an average thickness of 11.06 m. Some sandstone beds contain extra formational clasts disseminated either unevenly or form layers along the erosional base of the overlying cross-laminated beds. Few carbonaceous lenses are embedded in coarse-grained grey sandstone beds, which have a maximum thickness of 10 cm. Different sandstone beds are separated from the overlying and underlying sandstone beds, by erosional surfaces. These erosional surfaces are characterised by intraformational mud balls, mud pellets, mud layers, and extra formational clasts. Sand balls are also observed at places. The sandstone units display planar and trough cross-stratification. At places small mud pellets, mud balls and pebbles are oriented along the cross bedding. Occasionally, these cross-bed sets are deformed. Calcareous hard sandstone lenses are observed within sandstone beds. Thin mud lenses are present within the thick sandstone beds at different levels. In some places, the coarse-grained sandstone beds display channel cut filling. The mudstones are brown, grey, and blackish with various tints and variegated, and range in thickness from 0.40 to 1.18 m. These mudstones in some places are thinly laminated, nodular, hard and friable.

LITHOFACIES ANALYSIS

During the fieldwork, various lithofacies were identified and recorded and have been named as per the scheme adopted by Miall (1977, 1978). These lithofacies were encountered at different stratigraphic levels in the three lithosections (Fig. 3).

Pebbly Sandstone (Sp_1-facies)

In this facies, pebble size clasts constitute 5-70% of the rock. The maximum clast size ranges up to 10 cm. The thickness of individual bed sets varies from 0.10 to 1.70 m. This facies is characterised by pebble imbrication, horizontal- and cross-stratification, and intraformational mud balls and pellets. The underlying contact of the facies is generally erosional.

Trough Cross Bedded Sandstone (St-facies)

This facies is composed of fine to coarse-grained, poorly to well sorted, bright grey, grey and buff coloured, and trough cross bedded sandstones generally showing normal grading. At some places, mud clasts and pebbles are oriented along cross-bedding. Trough cross-bedding is occasionally distorted. In some cases, small mud lenses are aligned along the basal contacts of this facies. In normal grading, the lower pebbly cross-bedded set is followed by the trough cross-bedded set. Occasionally, the lower contact of this facies is characterised by a thin layer of small clasts. At some places, this facies shows sharp contacts with underlying Fm-, Sp- or Sh-facies, but mostly the underlying contacts are erosional. The St-facies is poorly cemented. However, hard calcareous coarse sandstone lenses occur along the bedding planes of this facies. These hard sandstone lenses sometimes display convolute structures. The thickness of individual bed sets varies from 0.15 to 2.0 m and that of the cosets varies from 0.60 to 3.0 m.

Planar Cross Bedded Sandstone (Sp-facies)

This facies is composed of fine to coarse-grained light grey, grey and buff, planar cross-bedded sandstones. Individual sets range in thickness from 0.10 to 1.50 m and different sets are superimposed over one another along either a sharp contact or scoured base. At places, the Sp-facies are underlain by either St- or Sh-facies. Sometimes this facies display reactivation surfaces, extra formational and intraformational clasts. Hard coarse calcareous sandstone lenses are occasionally seen in this facies.

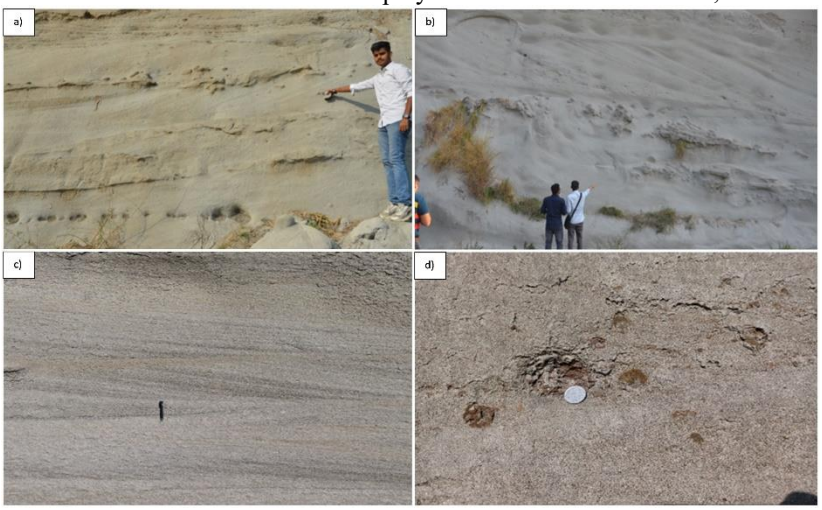

Fig. 3. Field photographs displaying a) planar crossbedding, sand lenses and concretions; b) Planar and trough cross bedding, Erosional scour surfaces with mud balls and pebbles; c) Planar cross bedding; d) Mud balls in a scour surface.

Horizontally Bedded Sandstone (Sh-facies)

This facies is composed of fine to coarse grained, laminated, grey and buff coloured sandstones ranging in thickness from 0.05 to 5 m. This facies is generally followed either by Sp or St-

facies. The upper and lower contacts of this facies are mostly sharp but occasionally erosional. In some cases, calcareous coarse sandstone lenses and distorted planar bedding in this facies are observed.

Erosional Scour Fill (Ss-facies)

Scour surfaces with a maximum relief of 0.5 to 1.0 m are observed at the upper contact of mudstone facies with sandstone facies and within the multistoried sandstone complexes. These scour fills consist of extraformational clasts of sandstone and quartzite and intraformational mudballs and mud pellets and at places thin mud lenses.

Massive Mottled and Nodular Mudstone (Fm-facies)

This facies is composed of massive, variegated, brown, yellow, grey and blackish coloured mudstones. This facies show generally sharp contact with underlying sandstone facies but at places gradational contacts are observed. The upper contact with sandstone is mostly sharp but gradational/erosional contacts are also seen. This facies is characterised by nodular and mottled mudstone showing root casts and mud cracks.

PALAEOCURRENT ANALYSIS

The data on directional features were collected from the sandstone units possessing extensive and clear cross-beddings. The azimuths of planar and trough cross-beddings at different stratigraphic levels in the three studied lithosections were recorded. These data were corrected for tectonic tilt following the method outlined by Potter and Pettijohn (1963). The tilt corrected azimuthal data were grouped at the class interval of 20^0 and plotted as rose diagrams (Fig. 4). Vector means and vector magnitudes were determined both graphically and trigonometrically following the procedure outlined by Lindholm (1987).

For the Nandni-Nagrota section, the rose diagram shows a polymodal distribution with five prominent modes in the 80°-100°, 120°-160°, 200°-220°, 240°-260°, and 280°-300° class intervals (Fig. 4A). The trigonometric vector mean and vector magnitudes are 138° and 51% respectively whereas, the graphic vector mean and vector magnitude are 138° and 51% respectively. For the Bajalta-Aitham lithosection, the rose diagram shows a polymodal distribution with four prominent modes in the 100°-120°, 120°-160°, 200°-240° and 240°-260° class intervals (Fig. 4B). The trigonometric vector mean and vector magnitudes are 186° and 39% respectively whereas, the graphic vector mean and vector magnitude are 185° and 40% respectively. For the Parmandal-Uttarbehni lithosection, the rose diagram shows a polymodal distribution with three prominent modes in the 140°-160°, 160°-180° and 240°-280° class intervals (Fig. 4C). The trigonometric vector mean and vector magnitudes are 181° and 59% respectively whereas, the graphic vector mean and vector magnitudes are 181° and 59% respectively. For all three lithosections, the trigonometric and graphic vector means and vector magnitudes are in well agreement with one another indicating south-easterly palaeoflow for Nandni-Nagrota, south-south-westerly palaeoflow direction for Bajalta-Aitham lithosection and southerly palaeoflow for Parmandal-Uttarbehni area (Fig. 4).

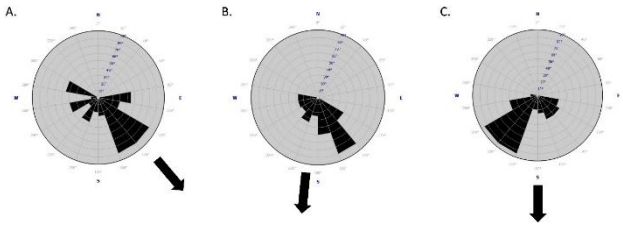

Fig. 4. Rose diagrams displaying the azimuthal data of the cross beddings recorded in Middle Siwalik of the three studied lithosections A) Nandni-Nagrota, B) Bajalta-Aitham, C) Parmandal-Uttarbehni.

GRANULOMETRIC ANALYSIS

The granulometric analysis is a well-known technique that provides additional information about the sedimentary depositional environment, energy conditions and sediment transport. Size statistical textural parameters with environmental significance including graphic mean, standard deviation (sorting), kurtosis and skewness are useful in comprehending synsedimentary hydrodynamic factors of transportation and deposition in a basin (Folk and Ward, 1957; Srivastava and Mankar, 2009; Vijaya Lakshmi et al., 2010; Weltje and Prins, 2007; Kanhaiya et al., 2017). The grain size data obtained from sieve analysis were used to calculate various statistical parameters (Table 1) and are discussed as under:

Textural Parameters

Textural parameters are quantitative measures used to describe the characteristics of sediment based on their grain size distribution. Different textural parameters are graphically derived using size analysis data plotted on cumulative frequency curves. Cumulative frequency curves are plotted on the arithmetic scale with the class interval (phi) at the X-axis and cumulative weight percentage at the Y-axis. These curves offer grain size information values of phi (Φ) which are employed in mathematical calculations of statistical parameters devised by Folk and Ward (1957). Cumulative curves approximately reflect an S-shape trend when plotted on an arithmetic scale. The slope of the central portion of the curve reflects the sorting of the sample; if there is a steep slope, it indicates good sorting and a very gentle slope means poor sorting. The cumulative frequency curves of the analysed sandstone samples in the present study are approximately S-type (Fig. 5) showing that the

majority of the sediment was deposited by the saltation process with traction and suspension load contribution as well.

In this study, the size statistical parameters (textural parameters) namely graphic mean (Mz), graphic standard deviation (σ_I), graphic skewness (S_K), and graphic kurtosis (K_G) have been used. These parameters are useful for interpreting sedimentary processes that occur in depositional environments (Sengupta, 1977; Sun et al., 2002; Bartholdy et al., 2007; Le Roux and Rojas, 2007; Lakshmi et al., 2010).

Graphic Mean (M_z)

The graphic mean (M_z) represents the average particle size of the sediment and is calculated by the formula Φ16+ Φ50+Φ84)/3 (Folk, 1957). This parameter measures the average kinetic energy of the depositing energy as well as the average grain size of the particle population in terms of energy.

Graphic Standard Deviation (σ_I)

Graphic standard deviation(σ_I) is a mathematical expression which measures the degree of the sorting and is calculated by the formula (Φ84 - Φ16)/4 + (Φ95- Φ5)/6.6 (Folk and Ward, 1957). The sorting is a measure of the magnitude of grain size distribution around the mean size. The standard deviation indicates the fluctuations in the kinetic energy conditions prevailing during transport.

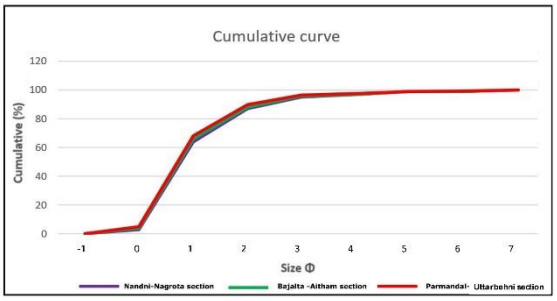

Fig. 5. Average cumulative curve of size analysis studied of lithosections.

Graphic Skewness (S_k)

The graphic skewness (S_k) measures the asymmetry in the frequency curves in terms of the domination of coarse or fine grained fractions (usually represented as negative or positive skewness). It is calculated by formula [(Φ84+ Φ16 - 2Φ50) / 2(Φ84- Φ16)] + [(Φ5+ Φ95-2 Φ50) / 2(Φ95- Φ5)] (Folk and Ward, 1957). This is the most accurate way to measure skewness because it accounts for both the tails and the central portion of the frequency curve in size analysis. The curve's tails essentially display the significant variations between samples.

Graphic Kurtosis (K_G)

Kurtosis (K_G) represents the distribution of grain size population between tails and central portion of the frequency curve. It is calculated by the formula K_G = (Φ95 - Φ5) / [2.44 (Φ75 - Φ25)]. Leptokurtic nature is due to better sorting in the central portion as compared to the tails in a frequency curve. Strongly platykurtic curves often represent a bimodal nature with subequal amounts of the two modes (Folk, 1980).

Interpretation of textural parameters:

Nandni-Nagrota section

For the Nandni-Nagrota section, the size statistical parameters of the Middle Siwalik subgroup show mean grain size varying from 0.31 to 1.30Φ (average = 0.85Φ) reflecting a coarse to medium grained nature for these sediments. The standard deviation ranges between 1.00 to 1.82 Φ (average=1.33 Φ) reflecting moderately to poorly sorted sands. The skewness ranges between -0.09 and 0.48 (average = 0.17Φ and reflects the coarse to finely skewed nature of these sands. The Kurtosis values range from 0.73 to 1.25Φ (average = 0.95Φ) and reflect platykurtic to leptokurtic nature for these sands (Table 1).

Bajalta-Aitham section

The sandstones of the Bajalta-Aitham section have mean grain size ranging from 0.67 to 1.87Φ (average=1.03Φ) and reflect coarse to medium grained nature. The standard deviation varies from 0.89 to 1.46Φ and reflects a moderately to poorly sorted nature with an average of 1.11Φ (poorly to moderately sorted). These sediments appear to be nearly symmetrical to very finely skewed (skewness -0.04 to 0.46Φ) averaging at 0.25Φ (finely skewed) and platykurtic to leptokurtic in nature (K=0.84 to1.29Φ) with an average kurtosis equal to 1.02 Φ (Table 1).

Parmandal-Uttarbehni section

In the Parmandal-Uttarbehni section**,** the mean size ranges from 0.43 to 1.30Φ (average = 0.78Φ) indicating medium to coarse-grained nature. The sediments are moderately to poorly sorted with a standard deviation of 0.96 to 1.16Φ averaging at 1.08Φ (poorly sorted). The skewness varies from 0.05 to 0.39Φ (average 0.27Φ and reflects a finely to near symmetrical skewed nature. The kurtosis ranges from 0.79 to 1.25Φ indicating platykurtic to leptokurtic (average 0.90Φ=platykurtic) nature (Table 1).

Interrelationship among Textural Parameters

The relationship between the textural parameters is important for understanding the transport and depositional environment of sediments and is an excellent tool for identifying different

Table 1. Grain size textural parameters for the studied Middle Siwalik sandstones (NN: Nandni-Nagrota Section; BA: Bajalta-Aitham Section; PU: Parmandal-Uttarbehni Section)

Sample ID	Mean (M_Z)	Interpretation	Standard deviation (σ_I)	Interpretation	Skewness (S_K)	Interpretation	Kurtosis (K_G)	Interpretation
NN-1	0.31	Coarse sand	1.51	Poorly sorted	0.10	Fine-skewed	0.73	Platykurtic
NN-2	0.42	Coarse sand	1.69	Poorly sorted	0.18	Fine-skewed	1.25	Leptokurtic
NN-3	0.88	Coarse sand	1.73	Poorly sorted	0.36	Very fine-skewed	0.78	Platykurtic
NN-4	0.90	Coarse sand	1.82	Poorly sorted	0.48	Very fine-skewed	1.23	Leptokurtic
NN-5	0.97	Coarse sand	1.13	Poorly sorted	0.13	Fine-skewed	0.81	Platykurtic
NN-6	0.77	Coarse sand	1.00	Moderately sorted	0.20	Fine-skewed	0.87	Platykurtic
NN-7	0.87	Coarse sand	1.14	Poorly sorted	0.11	Very fine-skewed	0.99	Mesokurtic
NN-8	1.08	Medium sand	1.14	Poorly sorted	0.19	Fine-skewed	0.75	Platykurtic
NN-9	0.98	Coarse sand	1.09	Poorly sorted	-0.09	Near-symmetrical	1.23	Leptokurtic
NN-10	1.30	Medium sand	1.16	Poorly sorted	0.05	Near-symmetrical	0.85	Platykurtic
BA-1	1.13	Medium sand	1.07	Poorly sorted	0.27	Fine-skewed	1.29	Leptokurtic
BA-2	0.67	Coarse sand	1.08	Poorly sorted	0.29	Fine-skewed	0.84	Platykurtic
BA-3	1.87	Medium sand	1.16	Poorly sorted	0.41	Very fine-skewed	0.92	Mesokurtic
BA-4	0.75	Coarse sand	1.15	Poorly sorted	0.28	Fine-skewed	0.96	Mesokurtic
BA-5	0.85	Coarse sand	0.98	Moderately sorted	0.46	Very fine-skewed	0.98	Mesokurtic
BA-6	1.02	Medium sand	0.89	Moderately sorted	-0.04	Near-symmetrical	0.88	Platykurtic
BA-7	0.83	Coarse sand	1.25	Poorly sorted	0.39	Very fine-skewed	0.95	Mesokurtic
BA-8	1.40	Medium sand	1.07	Poorly sorted	-0.07	Near-symmetrical	0.94	Mesokurtic
BA-9	0.98	Coarse sand	1.07	Poorly sorted	0.22	Fine-skewed	1.18	Mesokurtic
BA-10	0.88	Coarse sand	1.46	Poorly sorted	0.25	Fine-skewed	1.08	Mesokurtic
BA-1	1.13	Medium sand	1.07	Poorly sorted	0.27	Fine-skewed	1.29	Leptokurtic
BA-2	0.67	Coarse sand	1.08	Poorly sorted	0.29	Fine-skewed	0.84	Platykurtic
BA-3	1.87	Medium sand	1.16	Poorly sorted	0.41	Very fine-skewed	0.92	Mesokurtic
BA-4	0.75	Coarse sand	1.15	Poorly sorted	0.28	Fine-skewed	0.96	Mesokurtic
PU-1	0.57	Coarse sand	1.12	Poorly sorted	0.39	Very fine-skewed	0.81	Platykurtic
PU-2	0.53	Coarse sand	0.96	Moderately sorted	0.11	Fine-skewed	1.25	Leptokurtic
PU-3	0.65	Coarse sand	1.08	Poorly sorted	0.24	Fine-skewed	0.83	Platykurtic
PU-4	1.00	Coarse sand	1.04	Poorly sorted	0.09	Near-symmetrical	0.96	Mesokurtic
PU-5	1.30	Medium sand	1.16	Poorly sorted	0.05	Near-symmetrical	0.81	Platykurtic
PU-6	0.77	Coarse sand	1.15	Poorly sorted	0.24	Fine-skewed	0.79	Platykurtic
PU-7	0.43	Coarse sand	0.95	Moderately sorted	0.16	Fine-skewed	0.91	Mesokurtic
PU-8	0.72	Coarse sand	1.13	Poorly sorted	0.24	Fine-skewed	0.96	Mesokurtic
PU-9	0.83	Coarse sand	1.16	Poorly sorted	0.11	Fine-skewed	0.91	Mesokurtic
PU-10	1.05	Medium sand	1.14	Poorly sorted	0.07	Near-symmetrical	0.87	Platykurtic

sedimentation processes. Bivariate plots are prepared using different pairs of size statistical parameters. For the current study the plots based on mean versus skewness and standard deviation show that most of the sediments are plotted in the river channel zone (Fig. 6). The bivariate plot between mean grain size and standard deviation (sorting) (Fig. 7) shows that the sediments are poorly to moderately sorted and composed primarily of coarse to medium-grained sand particles. The mean size versus skewness plot (Fig. 8) shows mostly finely skewed nature of the sediments. The scatter plot between mean grain size and kurtosis shows platykurtic to mesokurtic in nature (Fig. 9).

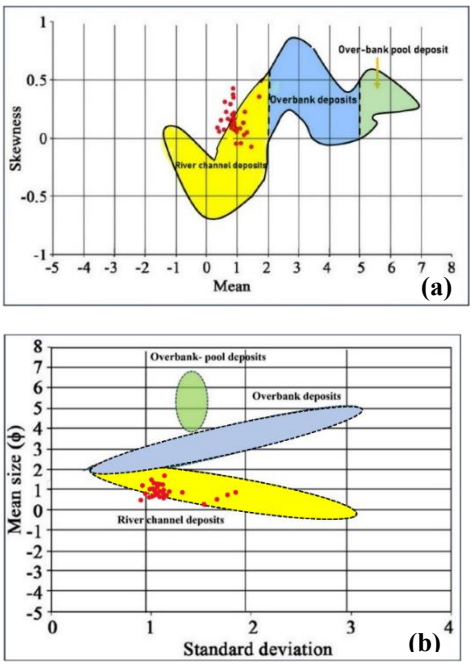

Fig. 6. Bivariate plots a) Mean and skewness b) Standard deviation and mean (after Mycielska-Dowgiallo, 2007; Ludwikowska-kedzia, 2000).

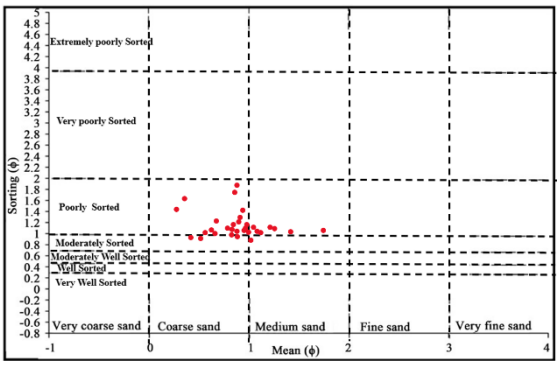

Fig. 7. Bivariate plot of mean grain size and sorting (after Blott and Kenneth, 2001).

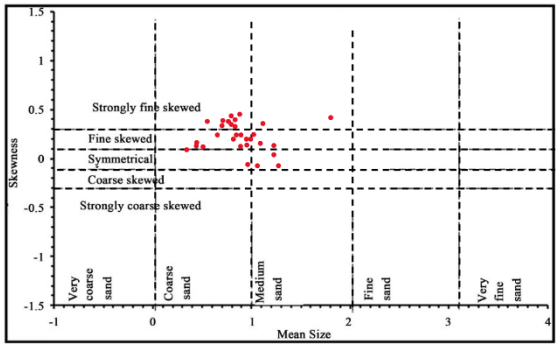

Fig. 8. Bivariate plot of mean grain size and skewness (after Blott and Kenneth, 2001).

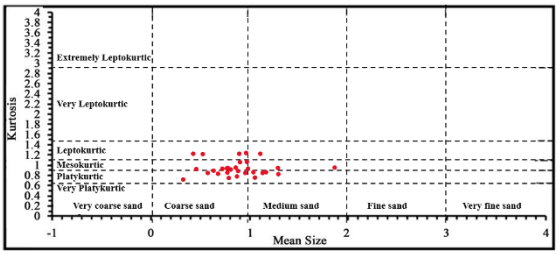

Fig. 9. Bivariate plot of mean grain size and kurtosis (after Blott and Kenneth, 2001).

RESULTS AND DISCUSSION

Grain size analysis of the sediments reveals that the sediments are medium to coarse grained in nature. The predominance of medium to coarse-grained sediment indicates moderate to high energy depositional conditions, where the current velocity was strong enough to transport sand in saltation and suspension mode. The occurrence of pebble clasts lower within the channel deposits and an overall increase in up section mean grain size observed in the Middle Siwalik subgroup in this study supports the existence of a large channel system of modestly increased depositional slope with coarse sediment load. The large lateral extent of the sand bodies suggests relatively low sinuosity streams (Keller, 1977) flowing on a broad alluvial plain like the modern Indo-Gangetic plain. The sediments of Middle Siwalik are moderately to poorly sorted, symmetrical to finely skewed and platykurtic to mesokurtic indicating deposition under fluctuating energy conditions in different geomorphic domains within fluvial settings. Strongly platykurtic curves often represent bimodal nature with subequal amounts of the two modes (Folk, 1980). The symmetrical nature of the sediments suggest that the hydrodynamic conditions may have caused the removal of fine particles due to the periodic encounters of strong stream currents at depositional sites (Pandita and Bhat, 1995).

The dominance of channel sandstone bodies and vertical and lateral stacking patterns of storeys within these sandstone bodies reflect the increased number and size of the active channels. The alternation of buff and grey sandstone strata demonstrates paleocurrent fluctuations over time and most likely reflects different river systems draining areas with diverse source material. The planar cross-bedding in sandstone facies indicates the linguoid depositional bars. Large scale trough cross-stratification lower in storeys suggests that the deeper channel bars were sinuously crested in nature. Vertical variation in grain size (fining-upward) and sedimentary structures (large scale trough cross stratification to planar strata or cross lamination) reflect variation in fluid flow during the single depositional event. Minor erosion surfaces may be related to local scouring and modification of bed form geometry during flash floods. Bioturbation and mottling of fine tops of bed sets suggest either the emergence of bed forms during low flow regime or abandonment of channels (Bridge et al., 1986) within a large braided river system (Pandita and Bhat, 1995). According to Singh (1977), channel bars migrate laterally during floods by depositing material in the form of extensive foreset laminae on the lee face. Additionally, during a flood, fluctuations in velocity causes scouring of the sedimentary surface and concurrent rapid deposition of sediments. Under turbulent flow conditions, the migration and development of the lee face of the bar are punctuated by strong scouring and filling action of the flow. Such large-scale bedforms that can produce planar sets comparable to those present here have been recorded in the large present-day river Brahmaputra (Coleman, 1969). The migration of three-dimensional dunes or scour origins lead to the development of trough cross-bedding (Miall, 1977; Reineck and Singh, 1980). The scale of the bedform that can produce the observed cross-beds is quite large and is only stable in deeper waters (Tyler and Ethridge, 1983; Singh and Kumar, 1974). The major channels of rivers like the Yamuna (Singh and Kumar, 1974) and Brahmaputra (Coleman, 1969) have reported similar-sized undulatory megaripple bedforms. Erosional surfaces separate various sandstone storeys (channel deposits), indicating the removal of fine-grained facies (over bank deposits). In confined rivers, episodic floods increase the probability of substrate erosion/scouring (Singh et al., 2006). The presence of scour-fill facies indicates

that floods occurred during the Middle Siwalik sedimentation and there were periodic and frequent encounters at the depositional site. This indicates that the upper part of the sequence was eroded before the deposition of a complete cycle due to channel abandonment caused by avulsion (Miall, 1977).

Mudstone units associated with braided rivers are typically found on bar tops and in abandoned channels (Williams and Rust, 1969). Mudstone intraclasts related to braided river sandstone units have been described as fragmented, desiccated and eroded from bar tops and flood plains (Karcz, 1969). However, in most instances, broad lags of massive mudstone intraclasts are formed as a result of the collapse of muddy river banks, which is aided by desiccation fissures.

The palaeoflow trends in different sections of the area at the same stratigraphic levels are consistent with a small river system on a vast transverse sediment fan. The majority of the present fans in the Himalayan basins have low-relief braided channel patterns and sediment sources in the northwest (Willis, 1993). The variation reported in this study reflects only mountain proximal drainage system-induced local variation, as suggested for Pakistan's Siwalik belt (Willis, 1993). The distinct palaeocurrent direction shifts reflect local variations in basin physiography and depositional slope. The general palaeoflow pattern is due SE in the Nandni-Nagrota section, SSW in the Bajalta-Aitham lithosection and due south in the Parmandal-Uttarbehni lithosection suggesting an overall southerly drainage pattern during deposition of these sediments.

Sediment texture analysis reveals frequent strong stream encounters and saltation-dominated sediment transport, reflected in the multistoried sandstone bodies with trough and planar cross-bedding. The presence of erosional surfaces and channel cut-fill structures suggests multiple avulsion events and channel abandonments in a generally southerly drainage pattern in a braided river system.

The geometry of the Siwalik basin is thought to be substantially identical to those of the modern-day Himalayan frontal basin as rates of continental convergence have remained relatively consistent since the Miocene Period. Therefore, the contemporary Himalayan drainage system may have an identical resemblance to the Miocene and later river systems that left their imprints in the Siwalik strata. The presence of pebble clasts lower in the channel deposits, as well as an overall rise in up-section mean grain size seen in the Middle Siwalik subgroup, support the existence of a wide channel system with a significantly enhanced depositional slope and coarse sediment load. The wide lateral extent of the sand deposits suggests relatively low sinuosity streams moving across a broad alluvial plain similar to the contemporary Indo-Gangetic plane (Keller, 1977). The laterally interfingering sand and mudstone facies indicate simultaneous active and interchannel areas of the braided river system. The comparatively significant variations in facies and palaeocurrent direction are evident in meter-scale facies sequences indicating periodic channel belt avulsion. The braided pattern of these channels is replicated by cross-cutting erosional surfaces that surround lensoid facies sequences.

CONCLUSION

The Middle Siwalik sandstones were investigated in three stratigraphic sections in Jammu region to understand the depositional history of these rocks. These multistoried sandstone bodies with erosional basal contacts embedded with minor mudstone beds were deposited in a southerly flowing braided river system.

ACKNOWLEDGEMENTS

We express our sincere gratitude to the Department of Geology, University of Jammu for providing facilities to complete this work.

CONFLICT OF INTEREST:

The authors declare no conflict of interest.

REFERENCES

Bartholdy, J., Christiansen, C., & Pedersen, J. B. (2007). Comparing spatial grain-size trends inferred from textural parameters using percentile statistical parameters and those based on the log-hyperbolic method. *Sedimentary Geology*, *202*(3), 436-452.

Bhat, G. M., Kundal, S. N., Pandita, S. K., and Prasad, G. V. R. (2008). Depositional origin of tuffaceous units in the Pliocene upper Siwalik Subgroup, Jammu (India), NW Himalaya. *Geological Magazine*, *145*(2), 279-294.

Bhatia, T. R. (1970). Petrology of the Siwalik Formations of Jammu Hills. *Unpublished Ph. D. Thesis*, University of Jammu, Jammu, 1-272.

Blott, S. J., and Pye, K. (2001). GRADISTAT: a grain size distribution and statistics package for the analysis of unconsolidated sediments. *Earth surface processes and Landforms*, 26(11), 1237-1248.

Bridge, J. S., Smith, N. D., Trent, F., Gabel, S. L., and Bernstein, P. (1986). Sedimentology and morphology of a low-sinuosity river: Calamus River, Nebraska Sand Hills. *Sedimentology*, *33*(6), 851-870.

Cautley, P. T. (1835). Letter noticing the discovery of further fossils in vast quantity in the Siwalik Range. *J. Asia. Soc. Bengal*, 4, 585-587.

Coleman, J. M. (1969). Brahmaputra River: channel processes and sedimentation. *Sedimentary Geology,* 3(2-3), 129-239.

Dasarathi, N. (1968). A note on certain geological aspects of Tawi Valley Tertiaries. *Kashmir Science,* 5(1-2), 222-232.

Folk, R. L., & Ward, W. C. (1957). Brazos River bar [Texas]; a study in the significance of grain size parameters. *Journal of sedimentary research*, *27*(1), 3-26.

Folk, R. L. (1980). *Petrology of sedimentary rocks*. Hemphill publishing company.

Friedman, G. M. (1962). On sorting, sorting coefficients, and the lognormality of the grain-size distribution of sandstones. *The Journal of Geology,* 70(6), 737-753.

Friedman, G. M. (1967). Dynamic processes and statistical parameters compared for size frequency distribution of beach and river sands. *Journal of Sedimentary Research*, 37(2), 327-354.

Gupta, S. S., and Verma, B. C. (1988). Stratigraphy and vertebrate fauna of the Siwalik Jammu district Group, Mansar-Uttarbani section, J & K. *J Palaeont Soc India,* 33, 117-124.

Irfan, M., Singh, B. P., & Kanhaiya, S. (2022). Textural behaviour, facies, and depositional environments of the Middle Siwalik Subgroup of the Jammu area, Jammu & Kashmir State, NW Himalaya. *Journal of the Palaeontological Society of India*, *67*(1), 85-92.

Kanhaiya, S., Singh, B. P., Tripathi, M., Sahu, S., & Tiwari, V. (2017). Lithofacies and particle-size characteristics of late Quaternary floodplain deposits along the middle reaches of the Ganga river, central Ganga plain, India. *Geomorphology*, *284*, 220-228.

Karcz, I. (1969). Mud pebbles in a flash floods environment. *Journal of Sedimentary Research*, *39*(1), 333-337.

Karunakaran, C., and Ranga Rao, A. (1979). Status of exploration for hydrocarbon in the Himalayan Region. Himalayan Geol. Seminar. New Delhi 1976. *Jour. Geol. Surv. India,* Misc. Publ, 41, 1-66.

Keller, E. A. (1977). The fluvial system: selected observations. In Riparian forests in California: Their ecology and conservation: A Symposium (pp. 39-46).

Krumbein, W. C., and Pettijohn, F. J. (1938). Manual of sedimentary petrology. *Appleton-Century-Crofts. Inc., New York*, 549.

Krynine, P. D. (1937). Petrography and genesis of the Siwalik Series. *American Journal of Science,* 5(204), 422-446.

Kundal, S. N., and Prasad, G. V. R. (2011). Late Pliocene-Early Pleistocene microvertebrates from the Upper Siwalik Subgroup of Jammu, Jammu and Kashmir, India. *Earth Science India,* 4.

Le Roux, J. P., & Rojas, E. M. (2007). Sediment transport patterns determined from grain size parameters: Overview and state of the art. *Sedimentary Geology*, *202*(3), 473-488.

Lindholm, R. C. (1987). *A Practical Approach to Sedimentology*, Allen & Unwin,276pp.

Ludwikowska-Kędzia, M. (2000). Evolution of the middle segment of the Belnianka River valley in the Late Glacial and Holocene. Dialog Press, Warsaw, 180.

Mehta, Y. P., Thakur, A. K., Lal, N., Shukla, B., and Tandon, S. K. (1993). Fission track age of zircon separates of tuffaceous mudstones of the Upper Siwalik subgroup of Jammu–Chandigarh sector of the Panjab Sub-Himalaya. *Current Science*, 519-521.

Miall, A. D. (1977). A review of the braided-river depositional environment. *Earth-Science Reviews*, 13(1), 1-62.

Miall, A. D. (1978). Lithofacies types and vertical profiles in braided river systems: A summary. *Fluvial sedimentology: Calgary, Canadian Society Petroleum Geologists, Memoir*, *5*, 597-604.

Mycielska-Dowgiałło, E. (2007). Research methods for textural features of clastic deposits and the significance of interpretational results. Research into the Textural Features of Quaternary Sediments and Some Dating Methods, *The Family Alliance School of Higher Education Press, Warsaw*, 95-180.

Nanda, A. C. and Sehgal, R. K. (1993). Siwalik mammalian faunas from Ramnagar (J. & K.) and Nurpur (HP) and lower limit of Hipparion. *Geological Society of India*, 42(2), 115-134.

Pandita, S. K. and Bhat, G. M. (1999). Vertical and lateral facies variations, and their cyclicity in Middle and Upper Siwalik Subgroups, Jammu. *Journal of Indian Association of Sedimentologists*, 18: 159-185

Pandita, S. K., and Bhat, G. M. (1995). Petrographic and Facies Evaluation of Middle Siwalik Subgroup of Jammu, Himalaya. *Journal Geological Society of India*, 46, 369-374.

Pandita, S. K., Bhat, S. K., and Kotwal, S. S. (2011). Facies evaluation of boulder conglomerate formation, Upper Siwalik, Jammu Himalaya. *Him. Geol*, *32*(1), 63-69.

Pandita, S. K., Kotwal, S. S., Thakur, K. K., Bhat, G. M., and Singh, Y. (2014). Lithofacies association and depositional history of Boulder Conglomerate Formation, Upper Siwalik Subgroup, Jammu Himalaya. *Himalayan Geology*, 35(2), 135-145.

Parkash, B., Sharma, R. P., and Roy, A. K. (1980). The Siwalik Group (molasse)—sediments shed by collision of continental plates. *Sedimentary Geology*, *25*(1-2), 127-159.

Potter, P. E. and Pettijohn, F. J. (1963). Basin analysis and the sedimentary model. *Paleocurrents and Basin Analysis*, 224-251.

Rao, A. R. (1989). Neogene-quaternary boundary in the Siwalik of Northwest Himalayan foothills, India. *Geological Society of India*, *33*(2), 95-103.

Rao, A. R. (1993). Magnetic-polarity stratigraphy of Upper Siwalik of north-western Himalayan foothills. *Current Science*, 863-873.

Rao, A. R., Agarwal, R. P., Sharma, U. N., Bhalla, M. S., and Nanda, A. C. (1988). Magnetic polarity stratigraphy and vertebrate palaeontology of the Upper Siwalik Subgroup of Jammu Hills, India. *Geological Society of India,* 31(4), 361-385.

Reineck, H. E., and Singh, I. B. (1980). Depositional Sedimentary Environments *Springer-Verlag. New York.*

Sahu, B. K. (1964). Significance of the size distribution statistics in the interpretation of depositional environments. *Res. Bull. Panjab Univ.(ns),* 15, 213-219.

Sengupta, S. (1977). Experimental approach to grain-size data interpretation. *Indian Journal of Earth Science*, 92–102.

Sharma, S., Sharma, M., and Singh, I. B. (2001). Facies characteristics and cyclicity of Lower Siwalik sediments, Jammu area: a new perspective. *Geological Magazine*, 138(4), 455-470.

Singh, I. B. (1977). Bedding Structures in a channel sand bar of the Ganga River near Allahabad, Uttar Pradesh, India. Journal of Sedimentary Research, 47 (2), 747 – 752.

Singh, B. P., Mithila and Pawar, J. S. (2006). Lithofacies of a small Himalayan braided river, Tawi River, India. *Himalayan Geology*, 27: 1-13.

Singh, I. B., and Kumar, S. (1974). Mega-and giant ripples in the Ganga, Yamuna, and Son rivers, Uttar Pradesh, India. *Sedimentary Geology*, 12(1), 53-66.

Srivastava, A. K., & Mankar, R. S. (2009). Grain size analysis and depositional pattern of upper Gondwana sediments (Early Cretaceous) of Salbardi area, districts Amravati, Maharashtra and Betul, Madhya Pradesh. *Journal of the Geological Society of India*, *73*, 393-406.

Sun, D., Bloemendal, J., Rea, D. K., Vandenberghe, J., Jiang, F., An, Z., & Su, R. (2002). Grain-size distribution function of polymodal sediments in hydraulic and aeolian environments, and numerical partitioning of the sedimentary components. *Sedimentary geology*, *152*(3-4), 263-277.

Tanner, W. F. (1991). Suite statistics: the hydrodynamic evolution of the sediment pool. Principles, methods and application of particle size analysis, 225-236.

Tyler, N., and Ethridge, F. G. (1983). Fluvial architecture of Jurassic Uranium-bearing sandstones, Colorado Plateau, Western United States. Modern and ancient fluvial systems, 533-547.

Vijaya Lakshmi, C. S., Srinivasan, P., Murthy, S. G. N., Trivedi, D., and Nair, R. R. (2010). Granularity and textural analysis as a proxy for extreme wave events in southeast coast of India. *Journal of Earth System Science*, *119*, 297-305.

Weltje, G. J., & Prins, M. A. (2007). Genetically meaningful decomposition of grain-size distributions. *sedimentary geology*, *202*(3), 409-424.

Williams, P. F., and Rust, B. R. (1969). The sedimentology of a braided river. *Journal of Sedimentary Research*, *39*(2).

Willis, B. (1993). Evolution of Miocene fluvial systems in the Himalayan foredeep through a two-kilometre-thick succession in northern Pakistan. *Sedimentary Geology*, *88*(1-2), 77-121.

Received on: Feb 26, 2024
Revised accepted on: Dec 13, 2024

JOURNAL INDIAN ASSOCIATION OF SEDIMENTOLOGISTS ISSN NO 2582 – 2020
Vol. 41, Issue II, 2024, pp. 23 – 31
DOI: https://doi.org/10.51710/jias.v41iII.361

Geochemistry of sandstones from the Imphal Valley, Indo-Myanmar Ranges

Salam Ranjeeta Devi
Department of Earth Sciences, Manipur University, Imphal-795003, India
Email: ranjeeta_27@rediffmail.com

ABSTRACT

Spheroidal weathered siliciclastic rocks of the Imphal Valley, Indo-Myanmar Ranges were studied to determine paleoclimate, paleoweathering and mineral alteration based on the geochemical and mineralogical compositions. The Chemical Index of Alteration (CIA) suggests low-intermediate chemical weathering. Plagioclase Index of Alteration (PIA) value indicates incipient plagioclase alteration. Mineralogical Index of Alteration (MIA) reveals incipient to intermediate mineralogical alteration and the A-CN-K ternary plot of the studied samples suggests a low rate of alteration. The results suggest semi-arid climate, which ranges from warm-arid to warm cool conditions. Geochemistry and mineralogy indicate felsic, mafic and ultramafic compositions for the siliciclastic rocks.

Keywords: Spheroidal Weathering, Imphal Valley, Indo-Myanmar Ranges, paleoweathering and mineral alteration, paleoclimate

INTRODUCTION

An understanding of weathering processes is essential, since these fundamental processes are responsible for the geomorphological evolution of landscapes (Stallard, 1995; Turkington et al., 2005; Brantley et al., 2011; Hall et al., 2012) and environmental planning (Ehlen, 2005). The knowledge on weathering of the siliciclastic rock is useful in designing road, quarries, excavation and in planning for reclaimation at surface mines, an idea of the durability of different sedimentary rocks types in desirable. Unlike crystalline rocks, the study of siliciclastic rock weathering is complicated by lateral and vertical variations in lithology which make it difficult to compare weathered material with unweathered rock. Homogeneous rocks like basalts and coarse-grained granite show spheroidal weathering processes during regolith generation. Spheroidal weathering, also termed concentric or onion-skin weathering, is defined as the process where rocks scale off in concentric shells, producing rounded boulder-like forms (Chapman and Greenfield, 1949; Ollier, 1971). When those rocks are well jointed, the corners of a boulder suffer attacks in all directions and, often, there is an abrupt physical change between the unweathered rock and the weathered rock. The combination of chemical and physical processes in spheroidal weathering enhances the weathering rate. Many studies are carried out on spheroidal weathering to discuss mineralogical changes, geochemical processes (Babechuk et al., 2014), landscape evolution (Fletcher et al., 2006; Brantley et al., 2011) or weathering rates calculation (Chabauxe et al., 2013).

Geochemistry of major, trace and REEs of the clastic sedimentary rocks are widely used to infer provenance, paleoweathering, mineral composition, depositional environment and paleoclimate conditions and the elemental ratios of these elements signify the source rocks, paleoclimate and paleoweathering condition (Bhatia, 1983; McLennan et al. 1993; Hernández-Hinojosa et al., 2018; Anaya-Gregorio et al., 2018; Armstrong-Altrin, 2020). The chemical weathering has effect on the geochemistry and mineralogy of sediments (Nesbitt and young, 1982; McLennan, 1993; Bhatia and Crook, 1986; Roser and Korsch, 1986; Sopie et al., 2023). The present study determines paleoclimate, paleoweathering and mineral alteration, as well as geochemical and mineralogical composition of spheroidal weathered sandstones from the Imphal valley, Indo-Myanmar Ranges (IMR). The objective of this study is to infer the weathering and provenance of sandstones from the Imphal valley.

GEOLOGICAL SETTING

The Imphal valley and its surrounding areas consist of the Disang Group (Late Cretaceous to Eocene), Disang-Barail transition (Late Eocene- Early Oligocene) and Barail Group (Oligocene) with an alluvium deposit (Fig. 1). The Disang Group consists of dark grey splintery shales with silty shale and fine sandstone, sometimes giving rise to rhythmic character. The gradational contact between the Disang and Barail Group runs nearly parallel to the western margin of the Imphal valley and continue northerly towards the Naga Hills and southerly along Mizo-Hills of the Indo-Myanmar Ranges. The Imphal valley is bounded by two prominent thrust faults, the one in the eastern side is the Thoubal Thrust (TT) while the other in the western side is the Churachandpur Mao-Thrust (CMT), which also partly serves as the tectonic contact between the Disang and Barail Groups.

The Disang-Barail transition sequence of the Imphal Valley are characterized by intercalation of thin, flaggy, well cemented siltstone, fine-grained sandstone and sandy or silty shales (Devi, 2021) with

plant impression such as leave, twigs, bark etc. The Barail Group occupies the western side of the Imphal valley and as outliers in the eastern sides of the valley forming cappings of the Disang Group. Alluvium, which consists of black carbonaceous clay, silt and sand of fluvio-lacustrine origin, covers a wide area of the valley, above the Barail. Stratigraphic Succession of the Imphal Valley of the Indo-Myanmar ranges is given in Table 1.

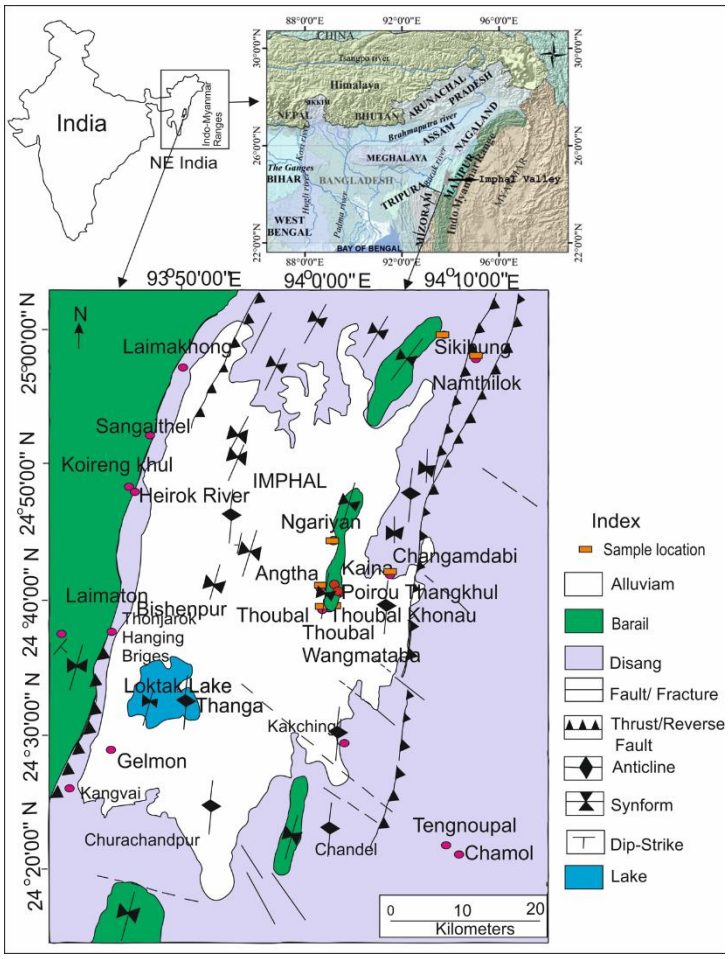

Figure 1. Geological map of the Imphal Valley, Indo-Myanmar Ranges showing the sample locations (modified after Devi, 2022).

Table 1. Stratigraphic succession of the Imphal Valley (Soibam, 1997)

Group	Lithology	Age
Alluviums	Dark grey to black clay, silt and sand deposits of fluvial-lacustrine origin. Flood plain deposits of the rivers and streams. Clay, sand, gravel and boulder deposits of the foothills and old river terraces. Possibly including lower deposits of the Imphal Valley.	(Quaternary: Holocene to Pleistocene (?) Older)
----------Stratigraphic Break----------		
Barails	Shale, sandy shale, massive siltstone, intercalation of bedded sandstone with shales showing turbidite character.	Oligocene
Disang-Barail Transition sequence (Gradational or local tectonic contact) consist of thick siltstone, fine-grained sandstone and sandy or silty shale (Late Eocene –Early Oligocene)		
Disangs	Dark grey splintery shale interbedded with thin siltstone and sandstones showing rhythmites nature.	Late Cretaceous to Late Eocene
~~ Unconformity ~~~~~~~~~~~~~~~~~~~~~~~~~~~~~~~~		
Basement Complex	Unseen (?) Early Mesozoic/Paleozoic or Precambrian rocks	(?) Early Mesozoic/ Paleozoic

METHODOLOGY

Sandstone, siltstone and shale samples of spheroidal weathering rocks were collected from the Imphal valley along the road cut and small quarries (Fig. 1). For geochemical analysis, sandstones are thoroughly washed, dried and homogenized in an agate mortar. All concentrations in this work were expressed with reference to dry weight. Samples were powdered by 200 ASTM. Major element concentrations for sample were determined using a RIGAKU ZSX Primus II X-ray Fluorescence Spectrometer system and analyzed in pressed powder briquettes. The accuracy of major elements of each sample was taken in 3 ml savillexR vials, supra pure acid mixture of HF+HNO_3+HCl in 7:3:1 proportion was added, and heated for about 48 h on a hot plate at a temperature of 110°C with lids closed. The samples were repeatedly treated with HNO_3 + HCl until clear solutions were obtained. The solutions were dried, re-dissolved with 2% HNO_3 and diluted to 50 ml in polypropylene (PP) storage bottles. The stock solution was further diluted to ~7500 times with 2% HNO_3, and trace and REE concentrations were measured using Inductively Coupled Plasma-Quadrapole Mass Spectrometer (ICPMS, Thermo X-Series) at the Department of Earth Sciences, Pondicherry University. USGS standards AGV-2, BCR-2, SCO-1 and multi-element standards were used for calibration, and 10 ppb Rhodium solution was used as an internal standard. To check the accuracy of data, USGS standard BHVO-2, AGV-2 were repeatedly analysed as unknown and the replicate analysis show precision of 2% for the REE, and better than 5% for other elements. Geochemistry data is listed in Tables 2 and 3.

Table 2. Major element contentrs (wt. %) of sandstones of the Imphal Valley

	CH-2	TB-2K-1	TB-W-1	NL-1	NL-3	Ng-3	RTH1
SiO_2	66.53	72.24	70.90	68.18	72.94	69.05	56.61
TiO_2	0.58	0.71	0.69	0.40	0.35	0.71	0.81
Al_2O_3	10.65	11.44	10.49	12.14	11.05	11.56	19.49
Fe_2O_3t	5.74	4.97	4.93	5.15	3.97	5.25	7.61
MnO	0.10	0.06	0.11	0.05	0.05	0.08	0.05
MgO	4.08	2.63	2.87	5.08	4.08	3.24	2.77
CaO	3.19	0.78	1.64	1.01	0.24	1.51	0.48
Na_2O	2.05	2.53	2.25	3.12	3.50	2.92	0.66
K_2O	0.67	0.79	0.8	0.53	0.53	0.90	3.15
P_2O_5	0.10	0.13	0.12	0.09	0.09	0.14	0.12
L.O.I.	5.93	3.51	4.84	4.18	2.82	4.50	9.42
CIA	51.82	63.97	58.11	61.66	62.07	57.61	78.41
ICV	2.00	1.24	1.53	1.74	1.60	1.54	0.70
PIA	18.74	15.86	16	18.18	16.34	17.77	17.69
MIA	3.65	27.94	16.22	23.32	24.15	15.22	56.81

Table 3. Trace element including REE (ppm) of the sandstones of the Imphal Valley

	CH-2	TB-2K-1	TB-W-1	NL-1	NL-3	Ng-3	RTH1
Sc	11.10	7.76	12.52	10.41	8.99	11.9	16.40
V	71.89	46.98	92	71.08	58.06	91.4	155
Cr	235.8	200.6	548	224.5	254	526	194
Co	14.99	9.77	16.78	19.22	13.3	18.36	22
Ni	32.50	12.05	24.26	42.92	26.90	27.93	205
Cu	24.73	8.02	17.62	16.39	11.48	24.14	49.00
Zn	73.24	30.89	67.99	68.52	48.87	68.37	110
Rb	29.28	23.17	34.91	23.13	15.96	37.96	145
Sr	97.60	52.85	95.92	86.84	142	109	110
Zr	69.90	37.57	114.69	57.79	45.62	96.30	151
Ba	73.4	51.6	89.47	73.66	130	93.36	258
La	30.83	13.59	24.43	13.16	16.66	23.12	29.53
Ce	47.46	24.71	50.18	27.71	35.68	47.71	62.33
Pr	4.59	3.04	6.00	3.23	4.25	5.63	6.83
Nd	17.50	11.48	22.06	13.01	17.02	21.35	29.28
Sm	3.31	2.15	3.88	2.61	3.52	3.87	6.02
Eu	0.74	0.48	0.84	0.65	0.99	0.85	1.36
Gd	3.06	1.92	3.65	2.47	3.67	3.61	4.39
Tb	0.48	0.30	0.52	0.37	0.55	0.60	0.70
Dy	2.73	1.71	3.13	2.36	3.16	3.38	3.88
Ho	0.56	0.35	0.65	0.46	0.63	0.67	0.81
Er	1.64	0.89	1.77	1.26	1.70	1.90	2.49
Tm	0.23	0.15	0.29	0.20	0.26	0.28	0.38
Yb	1.57	0.91	1.77	1.22	1.44	1.77	2.26
Lu	0.22	0.12	0.25	0.17	0.21	0.25	0.36
Ga	4.86	2.70	5.28	5.50	5.35	5.41	24

RESULTS

Major and Trace element concentrations

The sandstones are with the high concentrations of Cr (CH-2, Fig. 2 and 3), with CIA value of 51.82 (Table 2). Also, sandstones are high in Al_2O_3, K_2O, V, Ni, Rb and Ba contents (Figs. 2 and 3).

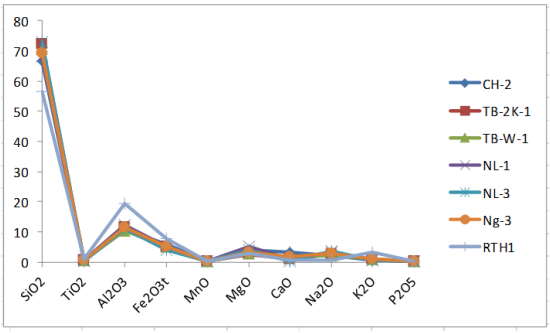

Figure 2. Major element contents in sandstones.

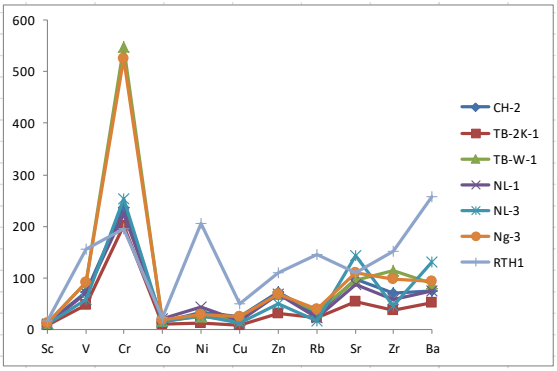

Figure 3. Trace element contents in sandstones.

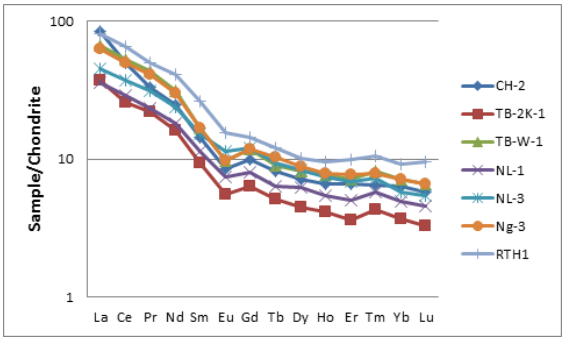

Figure 4. Chondrite normalized diagram for the sandstones from the Imphal Valley.

MINERALOGY

For mineralogical study, finely powdered samples were mounted in a glass slide and were scanned from 5° to 80° with step size of 0.02° 2Θ and with a scan spaced of 10s/step, using nickel filter copper radiation in a Panalytical XpertPro X-Ray diffractometer at the Department of Earth Sciences, Pondicherry University. The mineral phases were identified by using proprietary software Xpert High score.

XRD data (Table 4) show that quartz, albite and clinochlore are the dominant minerals in the studied samples. Clay minerals are kaolinite, vermiculite and montmorillonite (Fig. 5). Albite is mostly related to albitization of feldspars or from low grade metamorphism. Clinochlore occurs as a hydrothermal alteration product of amphiboles,

Table 4. Mineralogical data of sandstones from the Imphal Valley	
Sample No.	Minerals
CH-2	Quartz, Clinochlore, albite, Kaolinite
Ng-3	Quartz, Clinochore, Albite,
TB-W-1	Quartz, Clinochlore, Albite, Montmorillonite
NL-1	Quartz, Clinochore, Albite, Muscovite
TB-2K-1	Quartz, Albite, Kaolinite, Vermiculite
NL-3	Quartz, Clinochore, Albite
R-1	Quartz, Clinochlore, Rutile

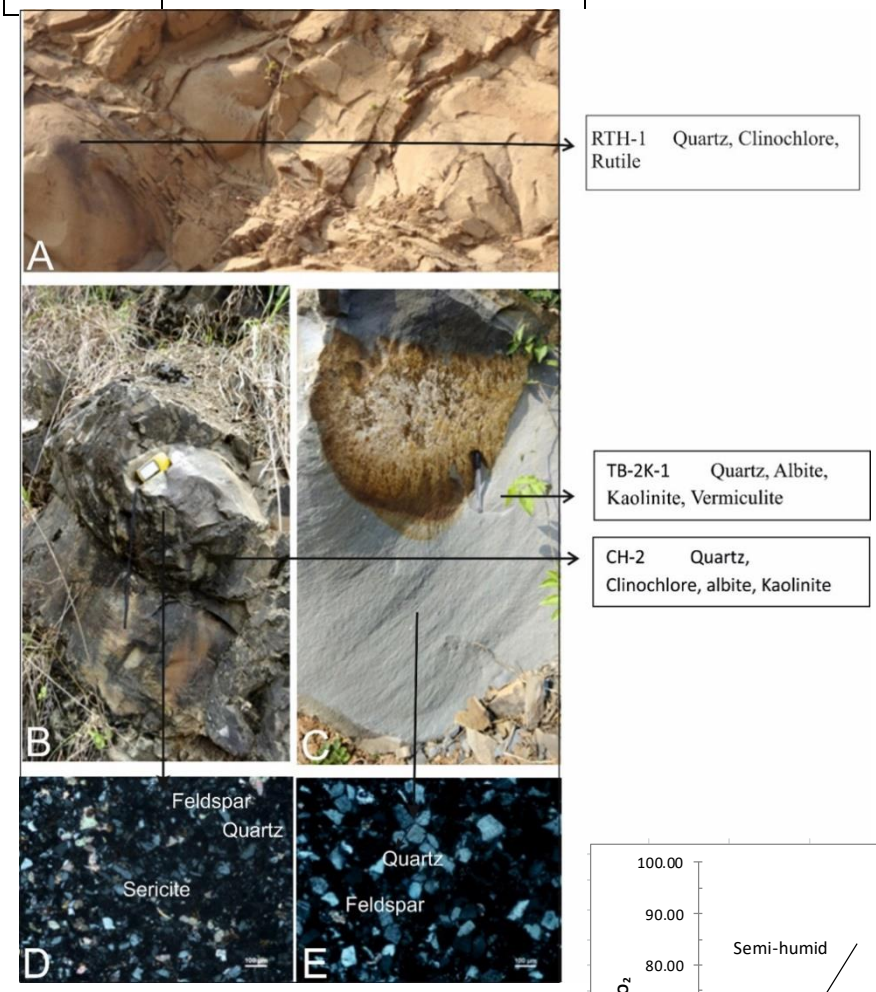

Figure 5. Spheroidal weathering produces rounded boulders within the outcrops (A, B, and C) and photomicrograph of spheroidal weathering (D and E).

pyroxene and biotite. This sediment underwent moderate alteration suitable to clay mineral product as montmorillonite and vermiculite. Alteration of plagioclase allows to form kaolinite. This study suggests the mineralogical composition of the siliciclastic rock of spheroidally weathered from the Imphal Valley. Several primary/secondary mineral pairs can he considered as reflecting the degree of spheroidally weathering. It is agreed that mineralogy of the incipient stage of rock alteration contained a significant proportion of primary mineral. Albite/montmorillonite are primary/secondary mineral in this study.

PALEOCLIMATE

Climate and tectonic activity control the alteration of mineral process (Wronkiewicz and Condie, 1987). The high mineral alteration matches the low grade of tectonic and climate fluctuation to hot and moist conditions conducive to mineral degradation in the deposition area (Jacobson and Blum, 2003). The $SiO_2/(K_2O + Na_2O + Al_2O_3)$ ratio is widely used to discriminate paleoclimate conditions (Suttner and Dutta 1986) because during the alteration phase, K_2O, Na_2O and Al_2O_3 are easily leached compared to SiO_2. SiO_2 and $(K_2O + Na_2O + Al_2O_3)$ diagram suggested that the siliciclastic rock from the study area was deposited in the semi-arid climatic conditions (Fig. 6).

Furthermore, the Ga/Rb vs Sr/Cu ratios for the sediments are widely referred to constrain the paleoclimate condition (Xie et al., 2018). Galium is mostly associated with fine-grained aluminosilicate portion and is high in kaolinite, reflecting hot and moist climate conditions whereas, Rubidium is related with illite and indicates poor intensity of alteration, indicating warm and cool weather conditions (Roy and Roser, 2013a). Therefore, the Ga/Rb value decreases in sediments (Roy and Roser,

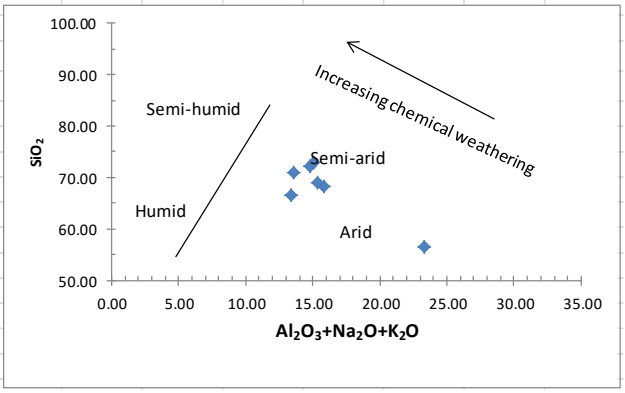

Figure 6 Bivariate plot of SiO_2 vs $K_2O + Na_2O + Al_2O_3$ to discriminate paleoclimatic conditions (Suttner and Dutta 1986).

2013b) in cold and dry climate conditions, whereas the Ga/Rb value increase in warm and humid climate conditions.

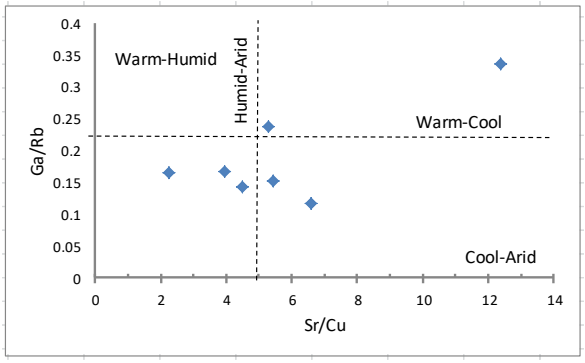

Figure 7. Sr/Cu and Ga/Rb ratios for sandstones from the Imphal Valley (Beckmann et al., 2005; Roy and Roser, 2013 a).

High Ga/Rb and low Sr/Cu proportion value in sediments usually suggest dry and moist weather conditions (Xu et al., 2017) . The Sr/Cu proportion value varies between 1.3 and 5.0 in deposits is thought to reveal humid conditions, while values above 5.0 indicate dry conditions (Sarki Yandoka et al., 2015; Xu et al., 2017). The diagram of Ga/Rb and Sr/Cu ratio (Fig. 7) shows low Ga/Rb and Sr/Cu ratio values, which ranges from 2 to 12 for Ga/Rb and 0.1 to .35 for Sr/Cu in most samples. This result reveals the humid-arid and warm cool climate conditions in the source region.

PALEOWEATHERING and MINERAL

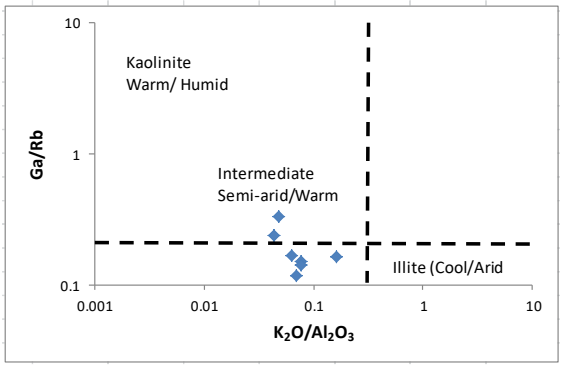

Figure 8. Ga/Rb vs. K_2O/Al_2O_3 diagram (Roy and Roser, 2013a).

ALTERATION

Chemical weathering influence the chemical composition of the siliciclastic sediments (Nesbitt and Young, 1982, 1984; Johnson et al., 1988; McLennan et al., 1993; Fedo et al., 1995). During this process, Ba and Al are stable in the sediments compared to Ca, Na and Sr that are carried away (Fedo et al., 1996; Nath and Kunzendorf, 2000). According to Nesbitt and Young (1982), the CIA is a good proxy for evaluating sediments alteration and expressed by CIA = 100 X (Al_2O_3/ (Al_2O_3+CaO∗+Na_2O + K_2O). The CIA values are widely used in various studies (Armstrong-Altrin et al., 2019, 2021a, b; 2022; Ekoa Bessa et al., 2021a, b). The various components are in molar proportions where CaO∗ is the quantity of CaO added into silicate fraction of sample. The equation yields values between 50 and 60 for incipient weathering, between 60 and 80 for intermediate weathering, and more than 80 for intense to extreme weathering. In hot and humid tropical condition, sediment have a high CIA value (85-100) and the sediment deposited in the warm humid paleoclimatic have a medium CIA value (70-85) while the lower CIA value (50-70) represents the cold and dry paleo climate, hence, the CIA have been widely used to determine the paleoclimate (Fedo et al., 1995).

The CIA values of this study is varying from 51.82 to 78.41 (Table 2) indicating incipient to intermediate chemical weathering and paleoclimate is varying from cold and dry climate to warm humid climate. The CIA values are integrated into a triangular diagram of Al_2O_3–CaO+Na_2O–K_2O or A–CN–K (Fig. 9). The siliciclastic rock is close to A-CN axis and suggests a low rate of alteration.

The index of compositional variability ICV >1 is immature and suggests to tectonically active settings (Cox et al., 1995). While those with ICV <1 is mature and deposited in a tectonically stable or cratonic setting, where sediment recycling is active. Accordingly, in this study, the ICV values are >2 with 0.70 of RTH-1 implying that samples are immature and deposited in a tectonically active setting and ICV <1 indicates mature and highly weathered.

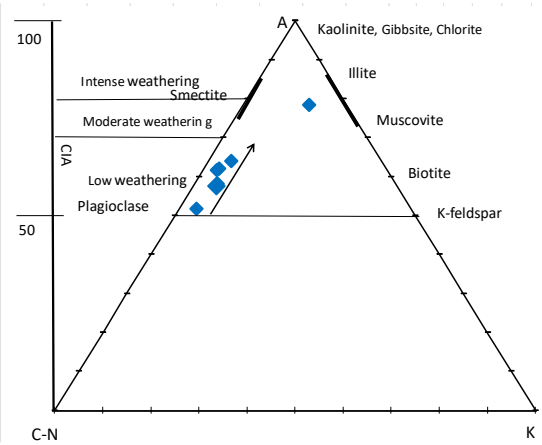

Figure 9 A– CN–K diagram with the CIA values (Nesbitt and Young, 1984)

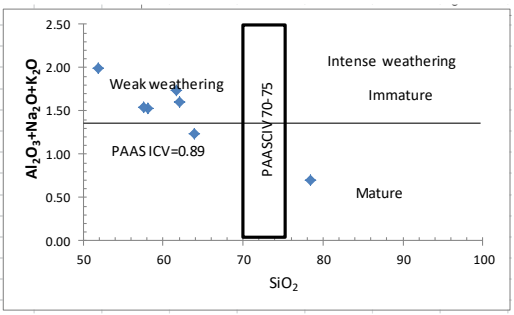

Figure 10. CIA vs ICV binary diagram (Cox et al., 1995; Long et al., 2012).

The binary plot CIA vs ICV (Fig. 10) shows that most of the siliciclastic rocks are geochemically immature and were derived from weakly weathered source rock.

The Plagioclase Index of Alteration (PIA) by Fedo et al. (1995) is used to determine the plagioclase weathering and expressed by PIA=(Al_2O_3-K_2O/(AL_2O_3+CaO^*+Na_2O-K_2O)) X 100 where Al_2O_3, CaO, NaO and K_2O are molecular proportions and CaO^* in the amount of CaO content in the silicate fraction of the rocks. PIA values from 15.7 to 18.7 suggest the incipient weathering of plagioclase. CIA and PIA values for siliciclastic rock show low to moderate silicate weathering (Fig. 11, Roy et al., 2008). The CIA values are in good agreement with those of PIA (Fig. 11).

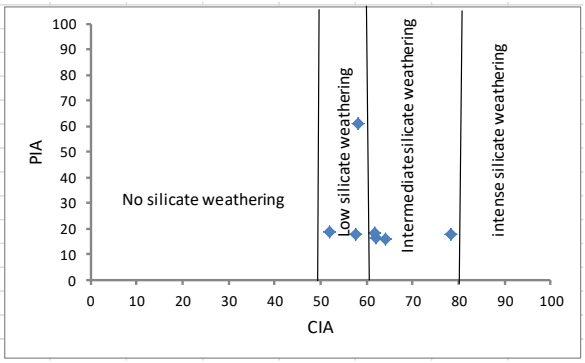

Figure 11. Scatter plots of chemical index of alteration CIA vs. PIA showing the degrees of silicate weathering.

In addition to this, the mineralogical index of alteration (MIA) is used to know the magnitude of the mineralogical weathering of rock formation and is given by

MIA= 2X (CIA-50)

The mineralogical index of alteration suggests the degree of mineralogical weathering, i.e. the transformation ratio of a primary mineral into its equivalent alteration mineral. MIA values ranges between 0 and 100, and reflects incipient (MIA<20), intermediate (MIA = 20-60), and intense to extreme (MIA>60) mineralogical transformation. The value of 100 means complete transformation of a primary mineral into its equivalent alteration product. The MIA values from 3.65 to 56.81 suggest incipient to intermediate mineral alteration for the sandstones.

GEOCHEMICAL and MINERALOGICAL VARIATIONS

According to Cullers (2000), Th/Sc ratios near a value of 1.0 are typical of the upper continental crust which tends to be more enriched in the incompatible element Th; whereas, a more mafic component has a ratio near 0.6 and tends to be more enriched in the compatible element Sc (Fig. 12). Intermediately weathered rocks consist more felsic composition.

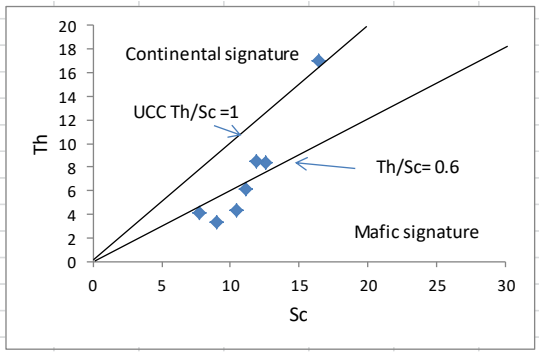

Figure 12. Th vs. Sc plot for the sandstones.

Cr/V-Y/Ni ratios also provide estimates of preferential concentration of chromium over other ferromagnesian elements (Hiscott, 1984; McLennan et al., 1993; Armstrong-Altrin et al., 2014). The Cr/V ratio measures enrichment of Cr with respect to other ferromagnesian elements, whereas the Y/Ni ratio evaluates the relationship between the ferromagnesian trace elements (represented by Ni) and the HREE, using Y as a proxy (McLennan et al., 1993). Y/Ni ratios generally range across values typical of intermediate to felsic calc-alkaline rocks. Sediments derived from ultrabasic sources usually have high Cr/V ratios much greater than 1 coupled with low Y/Ni less than 1 (Hiscott, 1984). The Cr/V ratio for siliciclastic rock is greater than 1.06 and the Y/Ni ratio is less than 1, indicating a contribution of ultramafic rock.

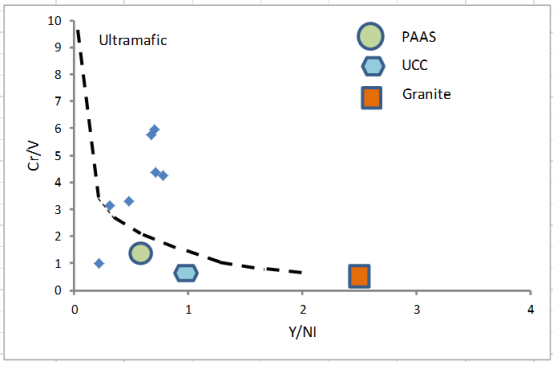

Figure. 13 Cr/V vs Y/Ni diagram for the sandstones.

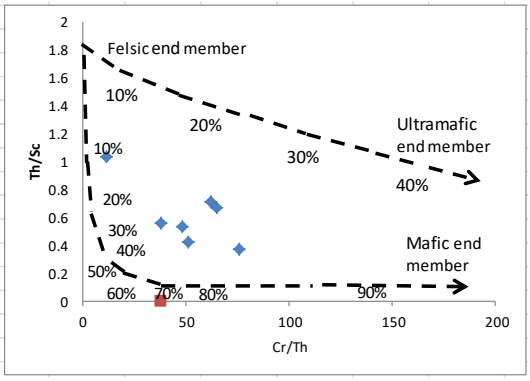

Figure 14. Th/Sc vs Cr/Th ratio in the sandstones (Condie and Wronkiewicz, 1990).

To better constrain the mafic or ultramafic versus felsic character, elemental ratios such as Cr/Th and Th/Sc were considered (Fig. 14). According to Hofmann et al (2003), high values of these ratios reflect enrichment in mafic-ultramafic and felsic components, respectively. The siliciclastic rock indicates a mixing between felsic and mafic end members with a major contribution from the felsic end member for intermediately weathered. This study suggests the geochemical and mineralogical compositions of the weathered rock. Spheroidally weathered originates as a result of expansion during chemical decomposition of the rock.

CONCLUSIONS

The sandstones from the Imphal valley, Indo-Myanmar Ranges constitute felsic, mafic and ultramafic compositions. Clinochlore suggests hydrothermal alteration of amphibole, pyroxene and biotite. Vermiculite is formed by weathering or hydrothermal alteration of biotite. The rocks were subjected to low – intermediate silicate weathering and low- intermediate mineral alteration. Semi-arid climate condition ranges from humid arid to warm cool prevailed during spheroidal weathering. The moderately weathered rock has dominantly felsic composition than the mafic and ultramafic compositions of less weathered rock. Spheroidal weathered structure originates because of expansion during variations in temperature.

ACKNOWLEDGEMENTS

The author sincerely thanks the Head, Department of Earth Sciences, Manipur University and Prof. Soibam Ibotombi of the department for providing necessary facilities and support. The author also acknowledged Nurul Absar, Department of Earth Sciences, Pondicherry University and John S. Armstrong-Altrin for geochemical analyses. I thank two reviewers for their useful comments on the manuscript. Author received financial assistance from Department of Science and Technology, New Delhi under the DST project No: SR/WOS-A/EA31/2016 dated 06-01-2017.

REFERENCES

Anaya-Gregorio, A., Armstrong-Altrin, J.S., Machain-Castillo, M.L., Montiel-García, P.C., Ramos-Vázquez, M.A. (2018). Textural and geochemical characteristics of late Pleistocene to Holocene fine-grained deep-sea sediment cores (GM6 and GM7), recovered from southwestern Gulf of Mexico. Journal of Palaeogeography, v. 7(3), pp. 253-271.

Armstrong-Altrin, J.S. (2020). Detrital zircon U-Pb geochronology and geochemistry of the Riachuelos and Palma Sola beach sediments, Veracruz State, Gulf of Mexico: a new insight on palaeoenvironment. Journal of Palaeogeography, v. 9 (4), article no. 28.

Armstrong-Altrin, J.S., Nagarajan, R., Lee, Y.I., Kasper-Zubillaga, J.J. and Córdoba-Saldaña, L.P. (2014). Geochemistry of sands along the San Nicolás and San Carlos beaches, Gulf of California, Mexico: implications for provenance and tectonic setting. Turkish Journal of Earth Sciences, v. 23 (5), pp. 533-558.

Armstrong-Altrin, J.S., Botello, A.V., Villanueva, S.F.and Soto, L.A. (2019). Geochemistry of surface sediments from the northwestern Gulf of Mexico: implications for provenance and heavy metal contamination. Geological Quarterly, v. 63 (3), pp. 522-538.

Armstrong-Altrin, J.S., Ramos-Vázquez, M.A., Hermenegildo-Ruiz, N.Y. and Madhavaraju, J. (2021a). Microtexture and U-Pb geochronology of detrital zircon grains in the Chachalacas beach, Veracruz State, Gulf of Mexico. Geological Journal, v. 56 (5), pp. 2418-2438.

Armstrong-Altrin, J.S., Madhavaraju, J., Vega-Bautista, F., Ramos-Vázquez, M.A., Pérez-Alvarado, B.Y., Kasper-Zubillaga, J.J. and Ekoa Bessa, A.Z. (2021b). Mineralogy and geochemistry of Tecolutla and Coatzacoalcos beach sediments, SW Gulf of Mexico. Applied Geochemistry, v. 134, pp. 105103.

Armstrong-Altrin, J.S., Ramos-Vázquez, M.A., Madhavaraju, J., Marca-Castillo, M.E., Machain-Castillo, M.L. and Márquez-Garcia, A.Z. (2022). Geochemistry of marine sediments adjacent to the Los Tuxtlas Volcanic Complex, Gulf of Mexico: Constraints on weathering and provenance. Applied Geochemistry, v. 141, pp. 105321.

Babechuk, Mg., Widdowson, M. and Kamber, Bs. (2014). Quantifying chemical weathering intensity and trace element release from two contrasting basalt profiles, Deccan Traps, India. Chemical Geology, v. 363, pp. 56-75.

Beckmann, B., Flogel, S., Hofmann Schulz, M., and Wagner T. (2005). Orbital forcing of Cretaceous River discharge in tropical Africa and ocean response. Nature, v. 437, pp. 241–244.

Bhatia, M.R. (1983). Rare earth element geochemistry of Australian Paleozoic graywackes and mudrocks: Provenance and tectonic control. Sedimentary Geology, v. 45, pp. 97–113.

Bhatia, M.R. and Crook, K.A.W. (1986). Trace element characteristics of greywackes and tectonic setting discrimination of sedimentary basins. Contribution to Mineralogical Petrology, v. 92, pp. 181-193.

Brantley, S.l., Buss, H., Lebedeva, M., Fletcher, Rc and Ma, L. (2011). Investigating the complex interface where bedrock transforms to regolith. Applied Geochemistry, v. 26, pp. S12-S15.

Chabaux, F., Blaes, E., Stille, P., Di Chiara Roupert, R., Pelt, E., Dosseto, A., Ma, L., Buss, H.l. and Brantley, S.l. (2013). Regolith formation rate from U-series nuclides: Implications from the study of a spheroidal weathering profile in the Rio Icacos watershed (Puerto Rico). Geochimica et Cosmochimica Acta, v. 100, pp. 73-95.

Chapman, R.W. and Greenfield, M.A. (1949). Spheroidal weathering of igneous rocks, American Journal of Science, v. 247, pp. 407-429.

Condie, K.C., and Wronkiewicz, D.J. (1990). Cr/Th ratio in Precambrian pelites from the Kaapval craton as an index of craton evolution. Earth and Planetary Science Letters, v. 97, pp. 256-267.

Cox R., Lowe, D.R. and Cullers, R.L. (1995). The influence of sediment recycling and basement composition on evolution of mudrock chemistry in the southwestern United States. Geochimica et Cosmochimica Acta, v. 59, pp. 2919-2940.

Cullers, R.L. (2000) The Geochemistry of Shales, Siltstones and Sandstones of Pennsylvanian-Permian Age, Colorado, USA: Implications for Provenance and Metamorphic Studies. Lithos, v. 51, pp. 181-203.

Devi, S.R. (2021). Geochemistry, depositional and tectonic Setting of the Barail Group of the Indo-Myanmar Ranges. Journal Indian Association of Sedimentologists, v. 38, pp. 13-22.

Devi, S. R. (2022). Geochemistry of the Transitional beds between Disang and Barail Successions of the Imphal Valley, Indo-Myanmar Ranges. Journal Indian Association of Sedimentologists, v. 39, pp. 10-16.

Ehlen, J. (2005). Above the weathering front: contrasting approaches to the study and classification of weathered mantle. Geomorphology, v. 67, pp. 7-21.

Ekoa Bessa, A.Z., Armstrong-Altrin, J.S., Fuh, G.C., Betsi, T.B., Kelepile, T. and Ndjigui, P-D., (2021 a). Mineralogy and geochemistry of the Ngaoundaba Crater Lake sediments, northern Cameroon: implications for provenance and trace metals status. Acta Geochimica, v. 40, pp. 718-738.

Ekoa Bessa, A.Z., Paul-Désiré, N., Fuh, G.C., Armstrong-Altrin, J.S. and Betsi, T.B. (2021b). Mineralogy and geochemistry of the Ossa lake Complex sediments, Southern Cameroon: Implications for paleoweathering and provenance. Arabian Journal of Geosciences, v. 14, pp. 322.

Fedo C.M., Eriksson K.A. and Krogstad E.J. (1996). Geochemistry of shales from the Archean (~ 3.0 Ga) Buhwa Greenstone Belt, Zimbabwe: implications for provenance and source-area weathering. Geochemica Cosmochimica. Acta. v. 60, pp. 1751-1763.

Fedo, C.M., Nesbitt, H.W. and Young, G.M. (1995). Unraveling the effects of potassium metasomatism in sedimentary rocks and paleosols, with implications for paleoweathering conditions and provenance. Geology, v. 23, pp. 921-924.

Fletcher, Rc, Buss, H.l. and Brantley, S.l. (2006). A spheroidal weathering model coupling porewater chemistry to soil thicknesses during steady-state denudation. Earth and Planetary Science Letters, v. 244, pp. 444-457.

Hall, K., Thorn, C., and Sumner, P. (2012). On the persistence of weathering. Geomorphology, v. 149/150, pp. 1-10.

Hernández-Hinojosa, V., Montiel-García, P.C., Armstrong-Altrin, J.S., Nagarajan, R., Kasper-Zubillaga, J.J. (2018). Textural and geochemical characteristics of beach sands along the western Gulf of Mexico, Mexico. Carpathian Journal of Earth and Environmental Sciences, vol. 13(1), pp. 161-174.

Hiscott, R.N. (1984). Ophiolitic source rocks for Tectonic-age flysch: trace element evidence. Geological Society American Bulletin, v. 95, pp. 1261-1267.

Hofmann, A., Bolhar, R., Dirks, P.H.G.M. and Jelsma, H.A. (2003). The geochemistry of Archaean shales derived from a mafic volcanic sequence, Belingwe greenstone belt, Zimbabwe: provenance, source area unroofing and submarine vs subaerial weathering. Geochimica et Cosmochimica Acta, v. 67, pp. 421-440.

Jacobson, A.D. and Blum, J.D. (2003). Relationship between mechanical erosion and atmospheric CO_2 consumption in the New Zealand Southern Alps. Geology, v. 31, pp. 865–868.

Johnson, R.W., Perfit M.R., Chappell, B.W. and Jacques A.L. (1988). Volcanism in the New Ireland basin and Manus Island region: notes on the geochemistry and petrology of some dredged volcanic rocks from a rifted-arc region. Archives, v. 9, pp. 113.

Long, X., Sun, M., Yuan, C., Kröner, A. and Hu, A. (2012). Zircon REE patterns and geochemical characteristics of Paleoproterozoic anatectic granite in the northern Tarim Craton, NW China: implications for the reconstruction of the Columbia supercontinent. Precambrian Research, v. 222, pp. 474-487.

McLennan S.M. 1993. Weathering and glacial denudation. Journal of Geology, v. 101, pp 295-303.

McLennan, S.M., Hemming, S., McDaniel, D.K. and Hanson, G.N. (1993). Geochemical approaches to sedimentation, provenance, and tectonics. Johnsson M.J., Basu A., editors. Processes controlling the composition of clastic sediments. Geological Society of America Special Paper, v. 284, pp. 21-40.

Nath B.N. and Kunzendorf H. (2000). Influence of provenance, weathering, and sedimentary processes on the elemental ratios of the fine-grained fraction of the bedload sediments from the Vembanad, Lake and the Adjoining Continental Shelf, Southwest Coast of India. Journal of Sedimentary Research, v. 70(5), pp. 1081-1094.

Nesbitt H.W. and Young G.M. (1982). Early Proterozoic climates and plate motions inferred from major elements chemistry of lutites. Nature, v. 199, pp. 715-717.

Nesbitt H.W., Young G.M. 1984. Prediction of some weathering trends of plutonic and volcanic rocks based on thermodynamic and kinetic considerations. Geochemica et Cosmochimica Acta. v. 48, pp. 1523–1534.

Ollier, C.D. (1971). Causes of spheroidal weathering, Earth-Sciences Reviews, v. 7, pp. 127-141.

Roser, B.P. and Korsch, R.J. (1986). Determination of tectonic setting of sandstone-mudstone suites using SiO_2 content and K_2O/Na_2O ratio. The Journal of Geology, v. 94, pp. 635-650.

Roy D.K. and Roser B.P. (2013a). Climatic control on the composition of carboniferous-Permian Gondwana

sediments, Khalaspir, Bangladesh. Gondwana Research, v. 23, pp. 1163-1171.

Roy D.K. and Roser B.P. (2013b). Geochemical evolution of the Tertiary succession of the NW shelf, Bengal basin, Bangladesh: Implications for provenance, paleoweathering and Himalayan erosion. Journal of Asian Earth Sciences, v. 78:248–262.

Roy, P.D., M. Caballeroa, R. Lozanoc and W. Smykatz-Klossd (2008). Geochemistry of late quaternary sediments from Tecocomulco Lake, central Mexico: Implication to chemical weathering and provenance. Chemie der Erde, v. 68, pp. 383-393.

Sarki Yandoka B.M., Abdullah W.H., Abubakar M.B., Hakimi M.H. and Adegoke A.K. (2015). Geochemical characterization of Early Cretaceous lacustrine sediments of Bima Formation, Yola Sub-basin, Northern Benue Trough, NE Nigeria: Organic matter input, preservation, paleoenvironment and palaeoclimatic conditions. Marine and Petroleum Geology, v. 61, pp. 82-94.

Soibam, I. (1997). Structural control on ground water occurrence in shales: a case study of the Imphal valley. Indian Journal of Landscape Systems and Ecological Studies, v. 20, pp. 111-116.

Sopie, F.T., Ngueutchoua, G., Armstrong-Altrin, J.S., Njanko, T., Sonfack, A.N., Sonfack, A.N., Ngagoum, Y.S.K., Fossa, D. and Tembu, L.T. (2023). Provenance, weathering, and tectonic setting of the Yoyo, Kribi, and Campo beach sediments in the southern Gulf of Guinea, SW Cameroon. Journal of Earth System Science, 132, article no. 92.

Stallard Rf. (1995). Tectonic, environmental, and human aspects of weathering and erosion: A global review using steady-state perspective. Annual Review Earth and Planetary Sciences, v. 23, pp. 11-39.

Suttner L. and Dutta P. (1986). Alluvial sandstone composition and paleoclimate. I. Framework mineralogy. Journal of Sediments, v. 56, pp. 329-345.

Turkington Av, Phillips Jd and Campbell, Sw. (2005). Weathering and landscape evolution. Geomorphology, v. 67, pp. 1-6.

Wronkiewicz D.J. and Condie K.C. (1987). Geochemistry of Archean shales from the Witwatersrand Supergroup, South Africa: source-area weathering and provenance. Geochemica Cosmochimica Acta, v. 51, pp. 2401-2416.

Xie G., Shenc Y., Liuab S. and Haod W. (2018). Trace and rare earth element (REE) characteristics of mudstones from Eocene Pinghu Formation and Oligocene Huagang Formation in Xihu Sag, East China Sea Basin: Implications for provenance, depositional conditions and paleoclimate. Marine and Petroleum Geology, v. 92, pp. 20-36.

Xu, Q.L., Liu, B., Ma, Y.S., Song, X.M., Wang, Y.J. and Chen Z.X. (2017). Geological and geochemical characterization of lacustrine shale: A case study of the Jurassic Da'anzhai member shale in the central Sichuan Basin, southwest china. Journal of Natural Gas Science, v. 47, pp 124-139.

Received on: April 6, 2024
Revised accepted on: Oct 7, 2024

JOURNAL INDIAN ASSOCIATION OF SEDIMENTOLOGISTS ISSN NO 2582 – 2020
Vol. 41, Issue II, 2024, pp. 32 – 39
DOI: https://doi.org/10.51710/jias.v41iII.377

Micromorphology of basalt alterite and its implications on the geological processes during quiescence period of the Deccan volcanism, Kharghar hill, Maharashtra, India

Anshul Dhiman[1,*], Seema Singh[1], and Soumyajit Mukherjee[2]
[1]Department of Geology, Panjab University, Chandigarh 160 014, India
[2]Department of Earth Sciences, Indian Institute of Technology Bombay, Powai, Mumbai 400076, Maharashtra, India *E-mail address: danshul039@gmail.com

ABSTRACT

Palaeoweathering unearths hidden mysteries of the previously weathered (paleo) surfaces. Researchers have shown that each mineral weathers/alters in a particular manner and is process-specific. Micromorphology is the most reliable and well-established technique to identify process-specific features imparted in an alterite under a given set of conditions. The Indian Deccan traps form one of the world's largest flood basalt volcanic provinces and has numerous exposures. Notwithstanding, systematic micromorphological studies of Deccan flood basalts are lacking compared to such flood basalts of global occurrences. The episodic nature of Deccan volcanism provided subsequent phases of interaction with the Earth's surface processes, thereby making the basalt alterites an ideal repository of surficial conditions and subsequent duration. Deccan basalt alterite exposed in the Kharghar hill of Mumbai (Maharashtra) has been selected for detailed micromorphology. Micromorphological results from the top to bottom of >70 cm thick, buried basalt alterite show changes in specific pattern of primary mineral alteration, formation of secondary minerals, development and patterns of secondary porosity. For example, the top of studied alterite (i.e. top 30 cm) has irregular, speckled and patchy patterns of mineral alteration, intramineral secondary pores, dominance of secondary products and only isolated alteromorphs that too with large elongate patches. Whereas towards the bottom (i.e. below 30 cm), the alterite shows planar patterns of mineral alteration, which is preceded at places by a linear/speckled pattern and most distinct is the dominance of intermineral pore system connected with transmineral fractures. Therefore, the basalt alterite can be subdivided from top to bottom into two distinct layers namely, alloterite and isalterite. This distinction significantly indicates a change in process with time as well as duration of basalt interaction with then prevailing surficial conditions. Thus, it can be concluded that alteroplasmation was progressively and gradually replaced with pedoplasmation resulting in dominance of supergene processes over hypogene processes.

Keywords: Deccan Basalt; alterite; micromorphology; pedoplasmation

INTRODUCTION

Palaeoweathering studies are significant to understand past sub-aerial geologic processes comprising dominance of surficial processes, past climates, continental environments and evolution (e.g., Reimink and Smye, 2024). Perhaps the simplest way for palaeoweathering studies in varied weathered mantle is the geochemical approach. However, different geochemical proxies have limitations in specific rock types. Nonetheless these are commonly used as powerful approach. Continental flood basalt eruptions have captivated the scientific community for long period of geologic time, driven by their paramount significance as elucidated by Ross et al. (2005). In particular Ross et al. (2005) showed that continental flood basalt eruptions had potential atmospheric impacts and catastrophic influence on biodiversity, including mass extinction events. Self et al. (2014) rightly stated continental flood basalt provinces as the subaerial expression of large igneous province volcanism. Earth's geologic history is rich in large igneous provinces comprising numerous flood basalt eruptions, which formed through multiple volcanic eruptions within a short geologic time (Self et al., 2008).

The Deccan flood basalt is an excellent example of continental flood basalt in Indian context forming longest lava flow known (Mukherjee et al., 2017), which mainly comprises pahoehoe lava flows erupted within a period of < 1 Ma (Courtillot et al., 1988). Krishnan (1953) estimated its original extent ~ 1.5 million km^2 when extended beneath the Arabian Sea. It covers an area of > ~ 500,000 km^2 (Watts et al., 1989 and others) across western and central India. Self et al. (2022) documented typical Deccan eruption rates as ~ 50–250 km^3 y^{-1} of lava with individual eruptions lasting for a few hundred to thousand years, separated by hiatuses of 3,000–6,000 yrs that makes them significant repositories for understanding of supergene processes. Deccan volcanic province is also rich in vertebrate biodiversity remains and vertebrate fauna (e.g., Khosla et al., 2003; Prasad et al., 2014). The Deccan

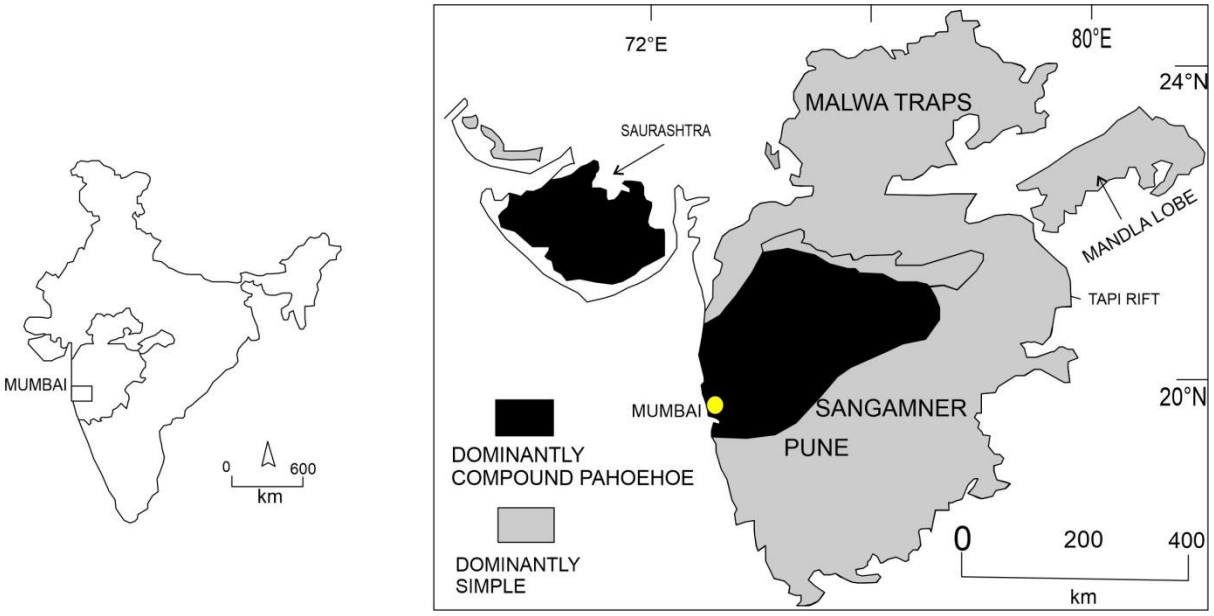

Fig. 1. Map showing the extent of Deccan Volcanic Province, India (After Bondre et al., 2004). Broad location of the study area is shown by yellow colour filled circle.

flood basalt has been extensively investigated geochemically (e.g., Alexander et al., 1977; Peng et al., 1998; Sano et al., 2001; Basu et al., 2020), petrographically (e.g., Shrivastava et al., 2002, 2008; Paul et al., 2008) and by isotopic means (Alexander et al., 1977; Lightfoot et al., 1988; Peng et al., 1998; Ravizza et al., 2003).

What remained a due was the systematic micromorphologic studies of the Deccan flood basalts. Such studies have alredy been performed in continental flood basalts across the globe (Paisani et al., 2013; Spinola et al., 2017; Zhang et al., 2022). Various Deccan basalt alterite outcrops are available in India and the episodic nature of Deccan volcanism serve excellent archives of prevalent surficial/palaeoweathering conditions before the next volcanic phase.

The term *'alterite'* refers to weathered mantle that is the result of weathering/supergene processes (Delvigne, 1998). Researchers have shown that each mineral alters in a particular manner and is process-specific. Systematic micromorphology is the essential technique to identify process-specific features imparted in an alterite under a given set of conditions. Therefore, buried Deccan basalt alterites have been explored in and around Mumbai (Maharashtra) with the major objective of systematic micromorphological studies. The aim of this study is to understand the geologic processes during the quiescence period of the Deccan volcanism.

STUDY AREA

DECCAN TRAPS: GEOLOGY AND STRATIGRAPHY

Several researchers have documented the geology and stratigraphy of Deccan Volcanic Igneous Province, DVIP (Beane et al., 1986; Jay et al., 2008 and others). Detailed account of lithostratigraphy of Deccan traps has been done by Godbole et al. (1996); Solanki et al. (1996) and others (also see Misra and Mukherjee 2017). Whereas the chemostratigraphic advances were presented by Beane et al. (1986) and Peng et al. (1994). Mahoney et al. (1982) deduced chemostratigraphy of lava piles by studying changes in major and trace elements and Sr-Nd ratios. Detailed trace element studies were done by Cox and Hawkesworth (1984). DVIP constitutes of simple and compound flows with western part dominated by compound lava flows (Mahoney, 1988; Bondre et al., 2004; Duraiswami et al., 2012; Fig.1).

Various other researchers documented the magnetostratigraphy of the DVIP (Deutsch et al., 1958; Sahsrabudhe, 1963; Wensink and Klootwijk, 1971) . Absolute ages or chronostratigraphy/ geochronology has been done in detail (Courtillot et al., 1986; Vandamme et al., 1991; Chenet et al., 2007; Schoene et al., 2015 and others). Beane et al. (1986) divided the DVIP of the Western Ghats (India) into three subgroups and 10 formations. Beginning with the lowermost (i.e. stratigraphically oldest) the Kalsubai Subgroup includes five formations- Jawhar, Igatpuri, Neral, Thakurvadi and Bhimashankar. The Lonavala Subgroup overlies The Kalasubai Subgroup and comprises an older Khandala Formation and a younger Bushe Formation. The Wai Subgroup is the youngest of the three subgroups and consists of Poladpur, Ambenali and Mahabaleshwar Formation from bottom to top.

LOCATION OF THE STUDY AREA

The Deccan basalt outcrops in and around Mumbai have been explored for weathered/

pedogenised profiles/units through fieldwork and the interest was to find a buried unit. A buried, Deccan basalt alterite exposed in Kharghar hills of Mumbai was selected for the present study (Fig. 2). This section forms part of the Bhimashankar Formation (= Upper Ratangarh Formation) of the Kalsubai Subgroup. It comprises of dense aphyric to phyric flows, with moderately porphyritic pahoehoe flows intermingling (Misra et al., 2014 and references therein). The selected buried profile in the

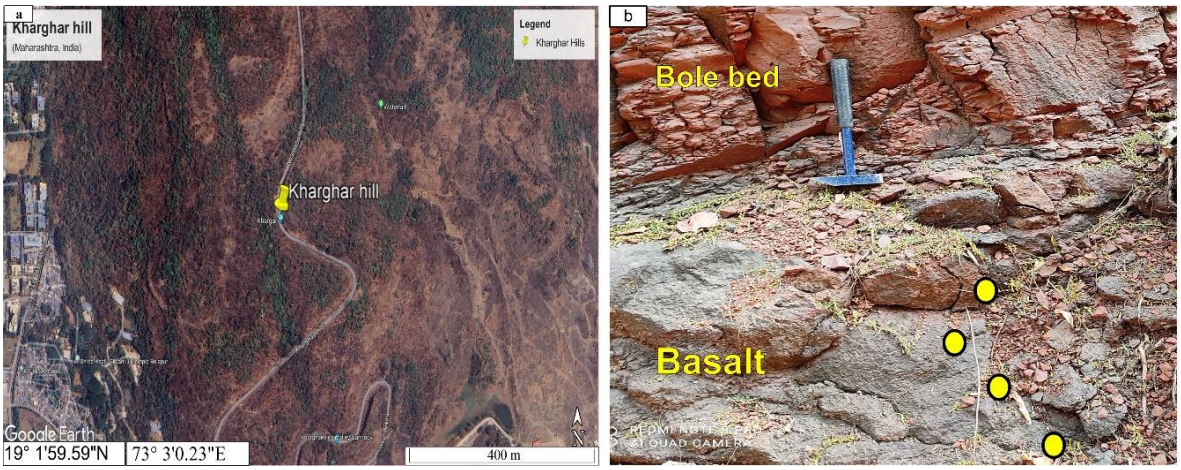

Fig. 2 a). Google Earth image showing the Kharghar hill location (Mumbai), wherefrom basalt alterite was sampled. b): Representative field photograph of the studied basalt alterite. The yellow-coloured circles show sampling locations. Geological hammer used as scale is ~ 30 cm long.

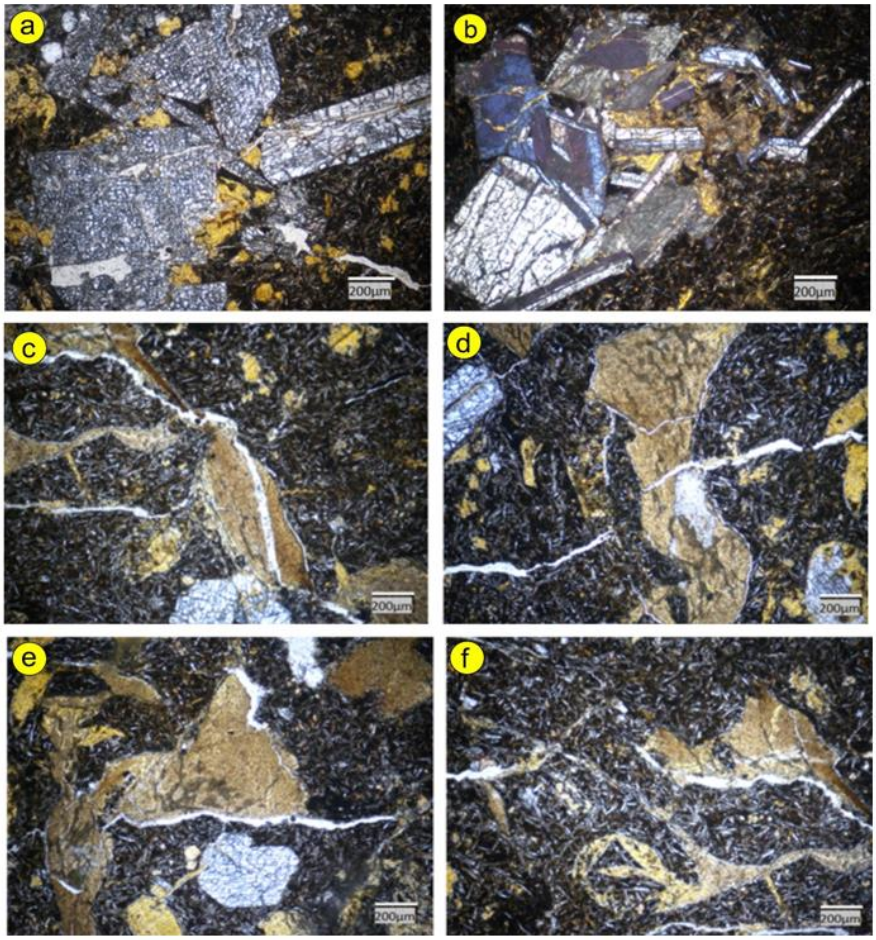

Fig. 3: From the bottommost basalt alterite, representative photomicrographs showing fractured plagioclase laths and secondary products/clay minerals deposited around the mineral grains in (a-b); trans-mineral pore system connected with inter-mineral pores in (c-d) and inter-mineral pore space surrounding the mineral grains in (e-f).

Kharghar hill was recognised in the field based on morphologic criteria as per Hencher and Martin (1982), Retallack (1988) and Ollier et al. (1996). The preliminary weathering stages in the field have been identified following Hencher and Martin (1982) and Ollier et al. (1996). In general, alterite and soil features have been recognized in the field on the basis of obliteration of basalt rock fabric and texture, which resulted in changes in colour, texture and/or structure.

METHODOLOGY

The studied basalt laterite is >70cm thick and has been carefully examined in the field based on changes in morphological features from top to bottom. A total of four representative samples of basalt alterite were collected for micromorphology. For thin-section studies, undisturbed *in-situ* samples have been collected in Kubiena tin boxes of

dimension 10 cm * 12 cm * 16 cm and 5 cm* 6 cm * 8 cm and were prepared as per Miedema et al. (1974) and Jongerius and Heintzberger (1975). These were described by following Delvigne (1998), and Stoops (2003). All the micromorphological/ thin-section observations have been done under Carlz Zeiss and Radical polarizing microscopes at the Department of Geology (Panjab University, Chandigarh, India).

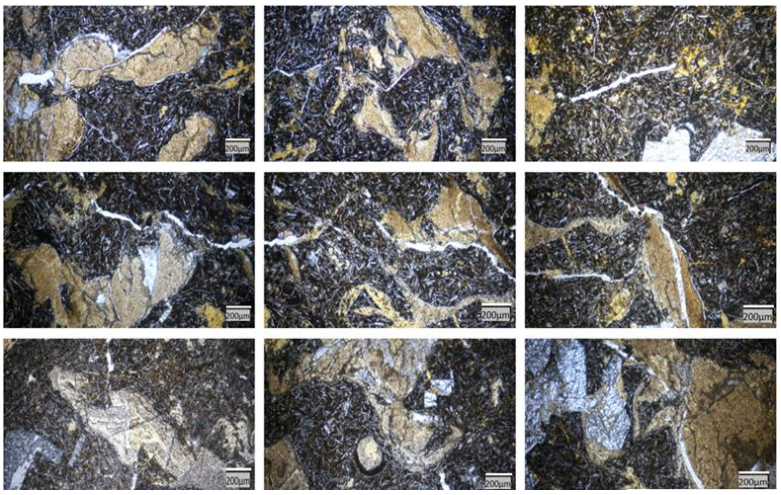

Fig. 4. From the bottommost basalt alterite, representative photomicrographs showing moderate connectivity between inter-mineral pore network.

RESULTS

The investigated, > 70 cm thick, buried basalt alterite, below the bole bed unit, shows distinct micromorphological characterstics from top (i.e. ~ 30 cm thick) part to bottom part of alterite. For example, micromorphological results from the top to bottom of basalt alterite show changes in specific pattern of primary mineral alteration, formation of secondary minerals and development of secondary porosity. Representative photomicrographs showing changes in micromorphologic features (Figs. 3-6). The bottom extent of basalt alterite is unexposed whereas the top part has clear and irregular boundary contact with the overlying bole bed. A number of process-specific micromorphologic features indicative of *in-situ* weathering/pedogenesis have been identified in the logged basalt alterite.

The bottom part of basalt alterite (below ~ 30 cm) shows predominant mineral grains e.g., plagioclase, secondary clay minerals and a fine grained groundmass composed primarily of plagioclase laths and opaques (Fig. 3). Large well developed crystals (phenocrysts) are embedded in fine- grained matrix/ groundmass, and serves distinct primary porphyritic texture. Majority of plagioclase grains are fractured and are bordered by secondary deposition of clay minerals (Fig. 3). Also, the alterite shows development of secondary porosity. Prominent presence of trans-mineral pore space is observed in the bottom alterite traversing the rock and cutting the mineral without following rock boundaries (Fig. 3). Further, the transmineral pores are seen connected with intermineral pores that surrounds the mineral grains without cutting through them (Fig. 3). Furthermore, this bottom part of basalt alterite shows not only intermineral porosity but moderate connectivity has been observed between the inter-mineral pores (Fig. 4).

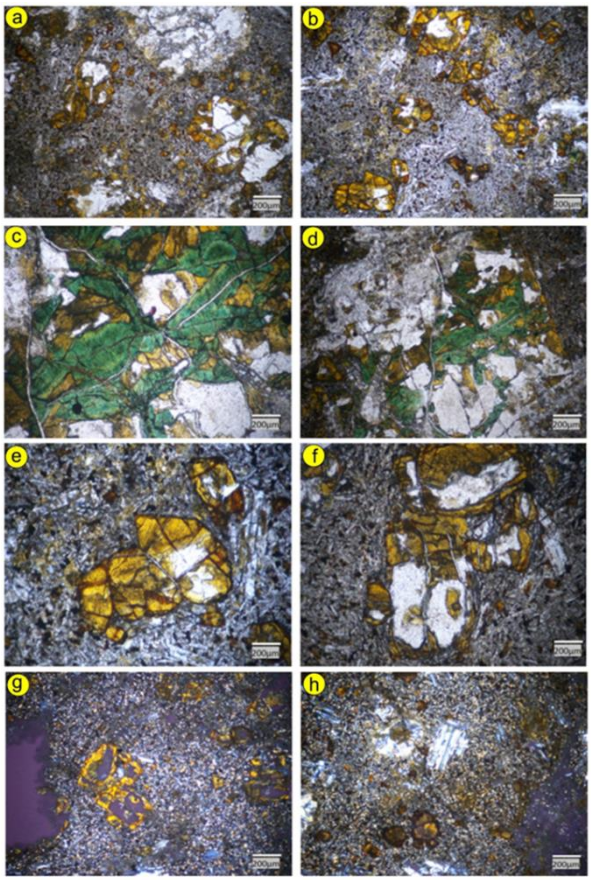

Fig. 5: From the topmost basalt alterite, representative photomicrographs showing patchy pattern of mineral alteration in (a-b); planar radial voids in (c-d); chemical weathering phenomenon by alteration of mineral from outward to inward in (e-f); and dominance of weathered micromass (g-h)

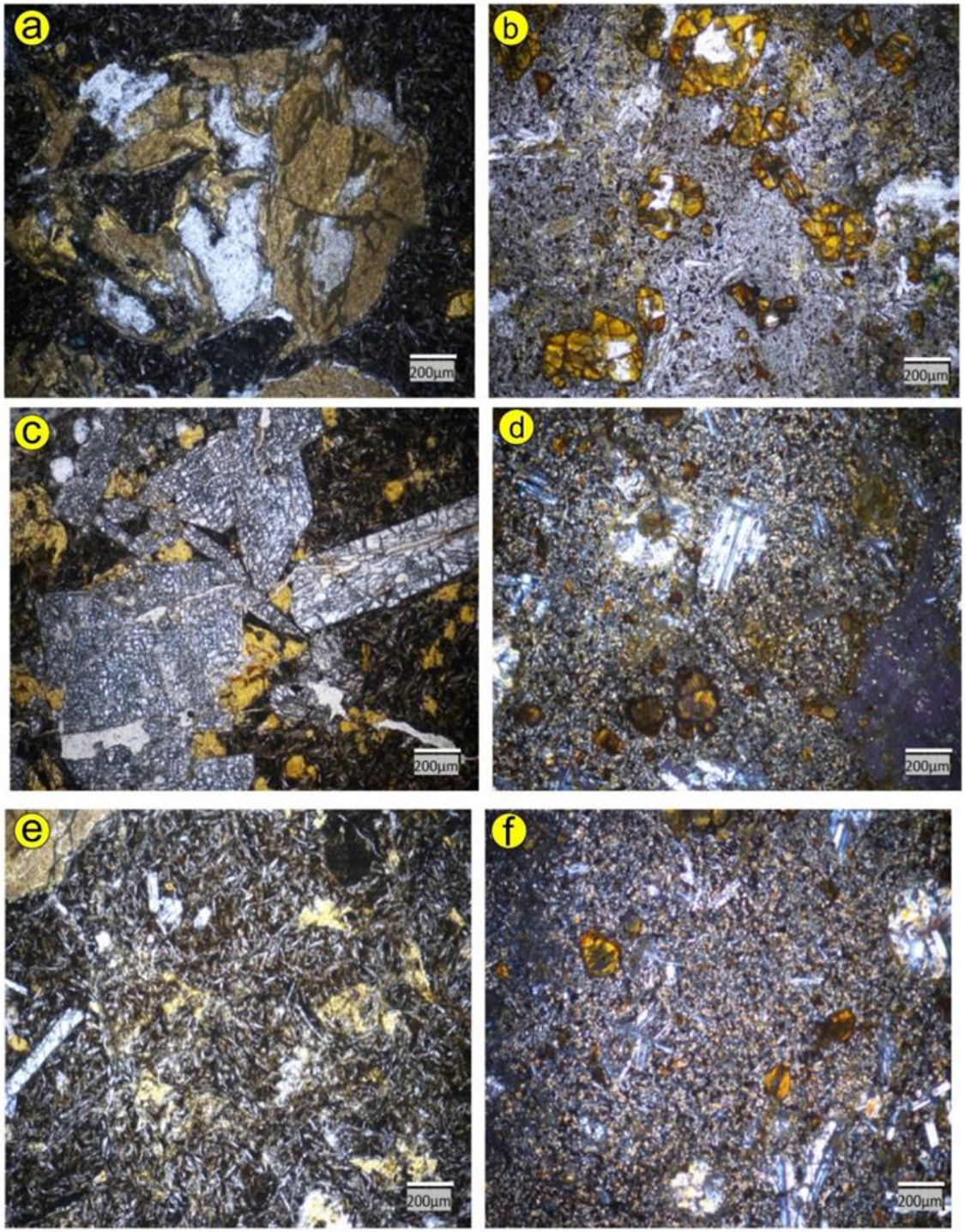

Fig. 6. Representative photomicrographs showing complete disappearance of original rock fabric from bottom (a) to top (b) alterite; Reduction in mineral grain size and increase in porosity from bottom (c) to top (d) alterite; (e-f) shows the relative increase in percentage of opaques from bottom (e) to top (f) alterite.

Towards the top, the basalt alterite shows extensive alteration of primary minerals, where olivine and plagioclase form the major primary minerals alongwith some secondary infillings and amydgules (Fig. 5). The groundmass is fine-grained and consists primarily of plagioclase laths and opaque minerals (Fig. 5). Large well-developed crystals (phenocrysts), primarily altered olivines are embedded in fine- grained matrix (groundmass) clearly indicate porphyritic texture. These mineral grains are partially to completely altered. The alteration is from outward to inward of the mineral grains (Fig. 5). Also, patchy alteration of minerals have been identified along with planar radial voids (Fig. 5). The micromass is more weathered than the bottom alterite and isolated alteromorphs are commonly present (Fig. 5).

Thus, a change in micromorpologic features have been observed from bottom towards the top of the investigated basalt alterite. There is almost complete disappearance of original fabric of the rock in the top when compared with the bottom part of the basalt alterite (Fig. 6). As compared to bottom, the top alterite shows more isolated alteromorphs (Fig. 6). There is significant reduction in grain size due to extensive fractures in mineral such as plagioclase from bottom towards the top of basalt alterite (Fig. 6). Altered micromass with porosity/voids is common in top alterite than the bottom one and there is greater percentage of opaques in top alterite than the bottom part of alterite (Fig. 6).

INTERPRETATIONS AND DISCUSSIONS

Micromorphology acts as an apropriate tool to study the peculiar patterns of mineral alteration. Each mineral species weathers uniquely under given set of conditions and the patterns of alteration are controlled largely by the nature and characteristics of primary mineral (Delvigne, 1998; Delvigne et al., 2000).

In the studied basalt alterite, the bottom alterite (i.e. below 30 cm) shows presence of transmineral pore system that primarily results from fracturing and fissuring of mineral grains. The pore network in a mineral grain facilitates the movement of fluids for better facilitation of weathering processes. The moderate interconnectivity between intermineral pores observed in the bottom alterite connotes that it is a less weathered portion. Whereas towards the top (i.e. 30 cm), alterite shows irregular, speckled and patchy patterns of mineral alteration. Isolated alteromorphs with large elongate patches are observed that shows the intensity of weathering processes that has operated over the top alterite. The weathering progression of minerals from outward to inward is a strong signature of chemical weathering process, which is documented prominently in the top alterite. The presence of planar radial voids indicates dominance of supergene processes.

The micromorphologic features observed at the top part of basalt alterite suggest pedoplasmation. For example, disappearance of original rock fabric, reduced grain size, dominance of alteration products comprising clays, opaques and extensively altered micromass resulting in isolated alteromorphs and voids. Therefore, micromorphology aids in understanding that the transition from alteroplasmation to pedoplasmation that occurred gradually, resulting in the prevalence of supergene processes over hypogene processes.

CONCLUSIONS

1. Based on systematic micromorphological studies, the investigated basalt alterite can be subdivided in to top alterite designated as *alloterite* and the bottom alterite as *isalterite*.
2. Alteroplasmation was progressively and gradually replaced with pedoplasmation resulting in dominance of supergene processes over hypogene processes.

ACKNOWLEDGEMENTS

Authors AD and SS are thankful to the Chairperson, Department of Geology, Panjab University, Chandigarh (India) for providing research facilities. AD acknowledges the financial support through the Department of Science & Technology's Inspire fellowship (grant number DST/ INSPIRE Fellowship/ 2022/IF220417). This paper comes partly from the M.Sc. and partly from the pre-Ph.D. course work carried out by AD**.** SM was funded by IIT Bombay for conducting fieldwork in the Kharghar area. We are thankful for the two reviewers for their comments, which significantly improved our presentation.

REFERENCES

Alexander, P.O. and Paul, D.K. (1977). Geochemistry and strontium isotopic composition of basalts from the eastern Deccan volcanic province, India. Mineralogical Magazine, v. 41(318), pp. 165-171.

Basu, A.R., Saha-Yannopoulos, A. and Chakrabarty, P. (2020). A precise geochemical volcano-stratigraphy of the Deccan traps. Lithos, v. 376, pp.105754.

Beane, J.E., Turner, C.A., Hooper, P.R., Subbarao, K.V. and Walsh, J.N. (1986). Stratigraphy, composition and form of the Deccan basalts, Western Ghats, India. Bulletin of Volcanology, v. 48, pp. 61 83.

Bondre, N.R., Duraiswami, R.A. and Dole, G. (2004). A brief comparison of lava flows from the Deccan Volcanic Province and the Columbia-Oregon Plateau Flood Basalts: Implications for models of flood basalt emplacement. Journal of Earth System Science, v. 113, pp. 809-817.

Chenet, A.L., Quidelleur, X., Fluteau, F., Courtillot, V. and Bajpai, S. (2007). 40K–40Ar dating of the Main Deccan large igneous province: Further evidence of KTB age and short duration. Earth and Planetary Science Letters, v. 263(1-2), pp. 1-15.

Courtillot, V., Besse, J., Vandamme, D., Montigny, R., Jaeger, J.J. and Cappetta, H. (1986). Deccan flood basalts at the Cretaceous/Tertiary boundary? Earth and Planetary Science Letters, v. 80(3-4), pp. 361-374.

Courtillot, V., Feraud, G., Maluski, H., Vandamme, D., Moreau, M.G. and Besse, J. (1988). Deccan flood basalts and the Cretaceous/Tertiary boundary. Nature, v. 333(6176), pp. 843-846.

Cox, K.G. and Hawkesworth, C.J. (1984). Relative contribution of crust and mantle to flood basalt magmatism, Mahabaleshwar area, Deccan Traps. Philosophical Transactions of the Royal Society of London. Series A, Mathematical and Physical Sciences, v. 310(1514), pp. 627-641.

Deutsch, E.R., Radakbishnamurty, C. and Sahasrabudhe, P.W. (1958). The remanent magnetism of some lavas in the Deccan traps. Philosophical Magazine, v. 3(26), pp. 170-184.

Duraiswami, R.A., Subhajyoti, D. and Shaikh, T.N. (2012). Hydrogeological framework of aquifers from the Deccan Traps, India: some insights. Memoir Geological Society of India, v. 80, pp. 1-15.

Godbole, S.M. and Chatterjee, A.K. (1999). A note on the Geochemistry of Lava pile Nazardeo, Jalgaon Dist, Maharashtra. Gondwana Geological Magazine, v. 2, pp. 81-88.

Hencher, S.R. and Martin, R.P. (1982). November. The description and classification of weathered rocks in Hong Kong for engineering purposes. In Proceedings of 7th South-east Asian geotechnical conference, Hong Kong. v. 1, pp. 125-142.

Jay, A.E. and Widdowson, M. (2008). Stratigraphy, structure and volcanology of the SE Deccan continental flood basalt province: implications for eruptive extent and volumes. Journal of the Geological Society, v. 165(1), pp. 177-188.

Jongerius, A. and Heintzberger, G. (1975). Methods in soil micromorphology: a technique for the preparation of large thin sections (No. 10). Stichting voor Bodemkartering Wageningen.

Khosla, A. and Sahni, A. (2003). Biodiversity during the Deccan volcanic eruptive episode. Journal of Asian Earth Sciences, v. 21(8), pp. 895-908.

Krishnan, M.S., 1960. Geology of India and Burma.

Lightfoot, P. and Hawkesworth, C. (1988). Origin of Deccan Trap lavas: evidence from combined trace element and Sr-, Nd-and Pb-isotope studies. Earth and Planetary Science Letters, v. 91(1-2), pp. 89-104.

Mahoney, J., Macdougall, J.D., Lugmair, G.W., Murali, A.V., Das, M.S. and Gopalan, K. (1982). Origin of the Deccan Trap flows at Mahabaleshwar inferred from Nd and Sr isotopic and chemical evidence. Earth and Planetary Science Letters, v. 60(1), pp. 47-60.

Miedema, R., Pape, T. and Van de Waal, G.J. (1974). A method to impregnate wet soil samples, producing high-quality thin sections. Netherlands Journal of Agricultural Science, v. 22(1), pp. 37-39.

Misra, A.A. and Mukherjee S. (2017) Dyke-brittle shear relationships in the Western Deccan Strike Slip Zone around Mumbai (Maharashtra, India). In: Mukherjee S, Misra AA, Calvès G, Nemčok M. (Eds) Tectonics of the Deccan Large Igneous Province. Geological Society of London, Special Publications, v. 445, pp. 269-295.

Mukherjee, S., Misra, A.A., Calvès, G. and Nemčok, M. (2017). Tectonics of the Deccan Large Igneous Province: an introduction. In: Mukherjee S, Misra AA, Calvès G, Nemčok M. (Eds) Tectonics of the Deccan Large Igneous Province. Geological Society of London, Special Publications, v. 445, pp. 1-9.

Ollier, C. and Pain, C. (1996). Regolith. Soils and Landforms, pp. 316.

Paisani, J.C., Pontelli, M.E., de Barros Corrêa, A.C. and Rodrigues, R.A.R. (2013). Pedogeochemistry and micromorphology of oxisols–a basis for understanding etchplanation in the Araucárias Plateau (Southern Brazil) in the Late Quaternary. Journal of South American Earth Sciences, v. 48, pp. 1-12.

Peng, Z.X., Mahoney, J.J., Hooper, P.R., Macdougall, J.D. and Krishnamurthy, P. (1998). Basalts of the northeastern Deccan Traps, India: isotopic and elemental geochemistry and relation to southwestern Deccan stratigraphy. Journal of Geophysical Research, Solid Earth, v. 103(B12), pp. 29843-29865.

Prasad, G.V. and Sahni, A. (2014). Vertebrate fauna from the Deccan volcanic province: Response to volcanic activity. Geological Society of America Special Papers, v. 505, pp. 193-211.

Ravizza, G. and Peucker-Ehrenbrink, B. (2003). Chemostratigraphic evidence of Deccan volcanism from the marine osmium isotope record. Science, v. 302(5649), pp. 1392-1395.

Reimink, J.R. and Smye, A.J. (2024). Subaerial weathering drove stabilization of continents. Nature, pp. 1-7.

Retallack, G.J. and Reinhardt, J. (1988). Field recognition of paleosols. Geological Society of America Special Paper, v. 216, pp. 1-20.

Retallack, G.J. (2000). ATLAS OF MICROMORPHOLOGY OF MINERAL ALTERATION AND WEATHERING. By Jean E. Delvigne. Canadian Mineralogist, Special Publication No. 3, Ottawa, Ontario, 1998, 494 p. Hardbound 125(100 for members of the Mineralogical Association of Canada).

Ross, P.S., Peate, I.U., McClintock, M.K., Xu, Y.G., Skilling, I.P., White, J.D. and Houghton, B.F. (2005). Mafic volcaniclastic deposits in flood basalt provinces: a review. Journal of Volcanology and Geothermal Research, v. 145(3-4), pp. 281-314.

Sahasrabudhe, P.W. (1999). Palaeomagnetism and the geology of the Deccan traps. Memoirs, Geological Society of India, v. 2, pp. 171-172.

Sano, T., Fujii, T., Deshmukh, S.S., Fukuoka, T. and Aramaki, S. (2001). Differentiation processes of Deccan Trap basalts: contribution from geochemistry and experimental petrology. Journal of Petrology, v. 42(12), pp. 2175-2195.

Schoene, B., Samperton, K.M., Eddy, M.P., Keller, G., Adatte, T., Bowring, S.A., Khadri, S.F. and Gertsch, B. (2015). U-Pb geochronology of the Deccan Traps and relation to the end-Cretaceous mass extinction. Science, v. 347(6218), pp. 182-184.

Self, S., Blake, S., Sharma, K., Widdowson, M. and Sephton, S. (2008). Sulfur and chlorine in Late Cretaceous Deccan magmas and eruptive gas release. Science, v. 319(5870), pp. 1654-1657.

Self, S., Mittal, T., Dole, G. and Vanderkluysen, L. (2022). Toward understanding Deccan volcanism. Annual Review of Earth and Planetary Sciences, v. 50, pp. 477-506.

Self, S., Schmidt, A. and Mather, T.A. (2014). Emplacement characteristics, time scales, and volcanic gas release rates of continental flood basalt eruptions on Earth. Geological Society of America Special Papers, v. 505, pp. 319-337.

Shrivastava, J.P. and Pattanayak, S.K. (2002). Basalts of the Eastern Deccan volcanic province, India. Gondwana Research, v. 5(3), pp. 649-665.

Shrivastava, J.P., Giridhar, M. and Kumar, R. (2008). Petrography, composition and petrogenesis of basalts from Chakhla-Delakhari intrusive complex, Eastern Deccan Volcanic province, India. Geophysics and Geochronology, pp. 83-108.

Solanki, J.N., Bhattacharya, D.D., Jain, A.K., Mukherjee, A., (1996) Stratigraphy and tectonics of the Deccan Traps of Mandla. Gondwana Geological Magazine, v. 2, pp. 101-114.

Spinola, D.N., de Castro Portes, R., Schaefer, C.E.G.R., Solleiro-Rebolledo, E., Pi-Puig, T. and Kühn, P. (2017). Eocene paleosols on King George Island, Maritime Antarctica: macromorphology, micromorphology and mineralogy. Catena, v. 152, pp. 69-81.

Stoops, G. (2003). Guidelines for the Analysis and Description of Soil and Regolith Thin Sections. SSSA. Madison, pp. 184.

Vandamme, D., Courtillot, V., Besse, J. and Montigny, R. (1991). Paleomagnetism and age determinations of the Deccan Traps (India): Results of a Nagpur-Bombay Traverse and review of earlier work. Reviews of Geophysics, v. 29(2), pp. 159-190.

Watts, A.B. and Cox, K.G. (1989). The Deccan Traps: an interpretation in terms of progressive lithospheric flexure in response to a migrating load. Earth and Planetary Science Letters, v. 93(1), pp. 85-97.

Wensink, H. and Klootwijk, C.T. (1971). Paleomagnetism of the Deccan traps in the Western Ghats near Poona (India). Tectonophysics, v. 11(3), pp. 175-190.

Zhang, M., Gong, Z., Zhou, Y., Liu, Y., Li, J. and Huang, C. (2022). Cooler Equatorial climate in the late Lopingian estimated from Paleosols developed on Emeishan Basalts. The Journal of Geology, v. 130(1), pp. 23-44.

Received on: June 6, 2024
Revised accepted on: Oct 8, 2024

JOURNAL INDIAN ASSOCIATION OF SEDIMENTOLOGISTS ISSN NO 2582 – 2020
Vol. 41, Issue II, 2024, pp. 40 – 51
DOI: https://doi.org/10.51710/jias.v41iII.382

Morphometric evaluation of diverse ripple structures in the Alwar Group at Jamwa Ramgarh in NE Rajasthan, North Delhi Fold Belt, NW India

Asha Saxena*, M. K. Pandit, Nirmal Kant Verma
Department of Geology, University of Rajasthan, Jaipur-302004 (India)
* E-mail Address: ashageo19@gmail.com
***** ORCID: 0000-0002-7983-3034

ABSTRACT

In this study we describe a complex set of well-preserved ripple structures from the Alwar Group quartzites (quartz arenite) of Mesoproterozoic Delhi Supergroup in NW India. Exposed in a road section near Jamwa Ramarh (to the east of Jaipur city), a large abundance and diversity in ripple shape, size, wave amplitude and mode of occurrence is unique for a small geographic area. The studied ripples are predominantly symmetric in shape, showing bifurcations, sinuous types, pointed crest with rounded trough, etc. Occasional current and criss-cross, and mega ripples are also present. Their symmetric shape suggests a wave dominant environment. The Vertical Form Index (VFI) values or Ripple Index values below 15 further rule out any possibility of a wind origin for them. The criss-cross and interference ripples point toward the presence of a high energy river system in the vicinity. The statistical analysis of ripple morphological parameters indicates deposition of quartz arenite under shallow water conditions (< 3 m depth). Based on various morphometric analyses, we infer continental shelf with variable depth for the development of these wave ripples. Based on the crest-line criterion, the inferred paleocurrent direction was from the NW.

Keywords: Ripples, classification, morphometric analysis, quartz arenite, Alwar Group, NW India

INTRODUCTION

One of the primary objectives of a sedimentological investigation is to reconstruct the depositional environment and infer the paleocurrent direction. While heavy minerals are reliable tools in source characterization, the primary sedimentary structures are the diagnostic indicators of paleo-sedimentary depositional processes. Ripple marks (also named, ripples, current marks, wave marks, and friction marks), are one of the most common primary structures preserved in the arenaceous (arenite) rocks (Tanner, 1982). Formed by non-cohesive materials under the action of water, waves or wind, the ripple marks are one of the most prevalent sedimentary structures and are regarded as significant indicators of the near-shore, fluvial and aeolian depositional environment. Different aspects of ripple morphology are commonly investigated, such as the shape, classification (Baird, 1962), formation and evolution (Bergman, 1979, Chang and Fleming, 2013) etc. that are useful in sedimentary environment modelling and paleoclimate reconstruction (De Vleeschouwer et al., 2015; Cheng et al., 2021). Physical parameters of ripples (morphology, length, and amplitude) also provide useful information for facies analysis, delineation of paleo-shore line, and evaluating hydrological characteristics of the basin and sediment transport (Harms, 1969; Tanner, 1970; Komar, 1976; Allen, 1984; Baas, 1999). The studies on ripple marks are based mainly on the recent siliciclastic deposits, using also experimental data and empirical morphological parameters. Ancient ripple marks are often poorly preserved due to post-sedimentation erosion (Romanovski, 1977; Allen, 1984). Although the application of ripples in deducing the sedimentary environment has been questioned because similar ripples could form at highly variable depths (Kindle and Bucher, 1926; Romanovski, 1977; Allen, 1984), and ripple size may not correctly elucidate the depth of water (Ewans, 1942), ripples are one of the most popular tools in working out sedimentation conditions. Despite their suitability for working out the sedimentary process, the poor preservation potential of ripples is a deterrent. They tend to get eroded and obliterated during the post-depositional processes and, therefore, are not abundant in nature. These structures are usually destroyed during the metamorphic reconstitution; therefore, quartzite is usually an unlikely candidate for such studies. However, wave-formed ripples in Proterozoic quartz arenites have been successfully used for Paleoenvironmental reconstruction in several studies (Clifton and Dingler, 1984; Aspleri, et al., 1994) including numerical estimates of water depth of ancient waves (Tanner, 1971). Cross bedding structures are used as a tool to decipher plaeo-tectonics and sedimentation history of Proterozoic Alwar Group. Such types of planer structures studies were also conducted for Gulcheru quartzite of Cuddapah basin (Sukanta et al., 2017).

The Mesoproterozoic quartzites exposed in a road section in the Jamwa Ramgarh area of Rajasthan in NW India display a variety of well-preserved ripple marks at several planes despite the rocks having undergone low to medium-grade metamorphism and recrystallization (Fig. 1). The

quartzite belongs to the Alwar Group of the Delhi Supergroup. The development of a large variety of ripple marks and diversity in their morphological parameters (shape, size, and amplitude). Therefore, it can be regarded as a unique site where maximum possible ripple types are exposed within sediment sequence of less than 2 m, implying rapidly changing depositional conditions due to unusual fluctuations in wave amplitude, energy and direction. This paper presents a detailed inventory of the Jamwa Ramgarh ripple marks and documents their megascopic characteristics. Morphological parameters of all ripple types were analysed for quantitative estimation of paleodepth and paleo-wave period along with orbital diameter and maximum wave period. The findings have been discussed to decipher the depositional environment at the southern margin of the Alwar – Jaipur sub-basin.

REGIONAL GEOLOGY AND STRATIGRAPHY

The NW Indian block, also known as the Aravalli Craton, is constituted by an Archean basement, the Banded Gneissic Complex (BGC - Heron, 1953) dated to 3.3 to 2.5 Ga (Roy and Kroner, 1996; Widenecke et al., 1996), over which supracrustal sequences of Aravalli (Paleoproterozoic) and Delhi (Meso-Neoproterozoic) Supergroup rocks were deposited (Roy and Jakhar, 2002; Deb and Thorpe, 2004; McKenzie et al., 2013). A Paleo- Mesoproterozoic Vindhyan Supergroup (Rasmussen et al., 2002; Ray et al., 2002; Gregory et al., 2006) occurs to the east of the Aravalli – BGC juxtaposed along a major fault, named the Great Boundary Fault (Fig. 1).

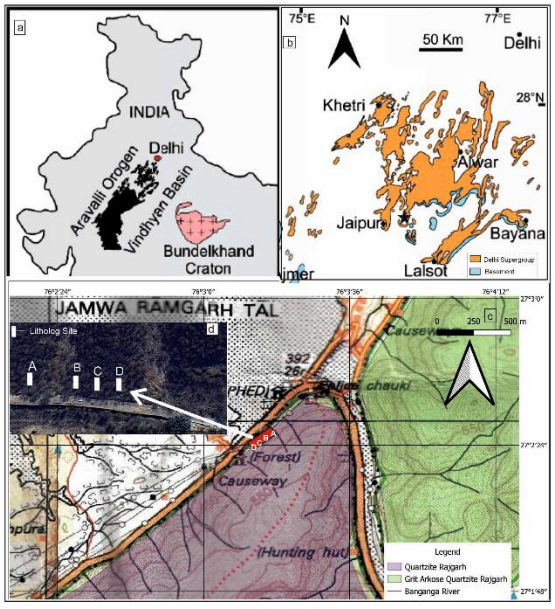

Figure 1 **a.** Location map of Aravalli Craton, NW India **b.** Geological map of North Delhi Fold Belt (Roy, 1988), **c.** Geological map of Jamwa Ramgarh section with study area, **d.** Google Earth image of study area

Delhi Supergroup, the dominant lithostratigraphic unit of the Aravalli Craton, was subdivided by Sinha Roy (1984) into two geographic domains, i.e. North Delhi Fold Belt (NDFB - older) and South Delhi Fold Belt (SDFB - younger). The diachronous sedimentation history, based entirely on the age of intrusive granites, was contested by some later workers (Bose et al., 1996; Roy and Kataria, 1999), however, more recent detrital zircon geochronologic studies support a diachronous sedimentation for the Delhi Supergroup (Wang et al., 2017). The NDFB is further subdivided into three, fault-bound, sub-parallel basins, namely, the Bayana-Lalsot, Alwar-Jaipur, and Khetri sub-basins (Sinha-Roy et al., 1998), from east to west. The Raialo Group (dolomitic limestone, quartzite and mafic volcanics) represents the oldest stratigraphic unit of the NDFB, followed by Alwar Group (arenaceous) and Ajabgarh Group (argillaceous – arenaceous facies), in stratigraphically ascending order (Gupta et al., 1997). Jamwa – Ramgarh, the area of present study, forms the southern part of the Alwar-Jaipur sub-basin (Fig. 1). Stratigraphy of the area is listed in Table 1.

Table-1a Stratigraphy of Delhi Supergroup

Supergroup	Group	Formation	Thickness (after Singh 1982)
Delhi Su-pergroup	Ajabh-garh	Bharkhol	100- 150m+
		Thanagazi	100 – 150m+
		Sariska	90- 150m+
		Kushalgarh	110- 200m+
	Alwar	Pratapgarh	900m+
		Kankanwari	100-250m
		Rajgarh	40- 1200m+
	Raialo	Tehla	1500 – 2020m+
		Serrate	200- 300m+

Table- 1b Lithology of Rajgarh Formation

Formation	Lithology
Rajgarh	Quartz-biotite schist with conglomerate **Quartzite** Dolomite Quartzite with basic flows at places Grit, Arkose, Quartzite Conglomerate with pebbly quartzite

STRATIGRAPHY OF JAMWA RAMGARH AREA

Stratigraphically, the Alwar- Jaipur sub-basin consists of Serrate and Tehla formations of the Raialo Group, Rajgrah, Kankwarhi and Pratapgarh formations of Alwar Group and Kushalgarh, Sariska, Thanagazi, and Bharkol formations of Ajabhgarh Group.

The studied quartzites (quartz arenite) belongs to the Rajgarh Formation of Alwar Group (Table 1). These quartz arenites are exposed along a

Table- 2 Morphological parameters of studied ripple marks in Jamwa Ramgarh quartz arenite									
Sr. No.	**Amplitude (H)**	**Wave Length (S)**	**RS = H/S**	**RI = S/H**	**Angle**	**d_0**	**Tm (Sec)**	**Wave height (cm)**	**Water Depth (cm)**
Small									
1	0.3	3	0.10	10	35	4.62	1.11	2.54	21.85
2	0.3	4	0.08	13.33	40	6.15	1.35	4.43	25.04
3	0.4	2.5	0.16	6.25	51	3.85	0.99	1.60	20.41
4	0.4	4	0.10	10	358	6.15	1.35	4.43	25.04
5	0.5	1.4	0.36	2.8	348	2.15	0.70	0.38	18.50
6	0.5	1.4	0.36	2.8	75	2.15	0.70	0.38	18.50
7	0.5	2.5	0.20	5	18	3.85	0.99	1.60	20.41
8	0.5	3.5	0.14	7	16	5.38	1.24	3.49	23.39
9	0.5	3.5	0.14	7	16	5.38	1.24	3.49	23.39
10	0.5	4	0.13	8	56	6.15	1.35	4.43	25.04
11	0.25	1.5	0.17	6	19	2.31	0.73	0.57	18.75
12	0.5	2.4	0.13	8	28	3.69	0.96	1.41	20.13
13	0.5	4	0.13	8	38	6.15	1.35	4.43	25.04
14	0.5	4	0.13	8	18	6.15	1.35	4.43	25.04
15	0.5	4	0.13	8	38	6.15	1.35	4.43	25.04
16	0.5	4.5	0.11	9	334	6.92	1.46	5.38	26.81
17	0.5	4.5	0.11	9	334	6.92	1.46	5.38	26.81
18	0.5	5	0.10	10	55	7.69	1.57	6.32	28.70
19	0.5	5	0.10	10	92	7.69	1.57	6.32	28.70
20	0.5	5	0.10	10	60	7.69	1.57	6.32	28.70
21	0.5	7	0.07	14	2	10.77	1.96	10.10	37.70
22	0.5	9	0.06	18	127	13.85	2.32	13.88	49.52
Medium									
1	0.6	4	0.15	6.67	74	6.15	1.35	4.43	25.04
2	0.6	4	0.15	6.67	55	6.15	1.35	4.43	25.04
3	0.6	4.5	0.13	7.50	340	6.92	1.46	5.38	26.81
4	0.7	3	0.23	4.29	20	4.62	1.11	2.54	21.85
5	0.8	3.5	0.23	4.38	32	5.38	1.24	3.49	23.39
6	0.8	4.5	0.18	5.63	6	6.92	1.46	5.38	26.81

7	0.9	3	0.30	3.33	40	4.62	1.11	2.54	21.85
8	1	4	0.25	4.00	12	6.15	1.35	4.43	25.04
9	1	4	0.25	4.00	17	6.15	1.35	4.43	25.04
10	1.1	6	0.18	5.45	30	9.23	1.77	8.21	32.89
11	1.1	4.7	0.23	4.27	20	7.23	1.50	5.75	27.55
Large									
1	0.6	2.5	0.24	4.17	38	3.85	0.99	1.60	20.41
2	0.6	5.5	0.11	9.17	50	8.46	1.67	7.27	30.72
3	0.7	7	0.10	10.00	11	10.77	1.96	10.10	37.70
4	0.8	6	0.13	7.50	350	9.23	1.77	8.21	32.89
5	0.8	6.8	0.12	8.50	81	10.46	1.92	9.72	36.69
6	1	5.5	0.18	5.50	26	8.46	1.67	7.27	30.72
7	1	5.5	0.18	5.50	31	8.46	1.67	7.27	30.72
8	1	6	0.17	6.00	26	9.23	1.77	8.21	32.89
9	1	6.5	0.15	6.50	45	10.00	1.87	9.16	35.21
10	1	7	0.14	7.00	345	10.77	1.96	10.10	37.70
11	1	7.5	0.13	7.50	25	11.54	2.05	11.05	40.36
12	1	8	0.13	8.00	28	12.31	2.14	11.99	43.21
13	1.1	6	0.18	5.45	30	9.23	1.77	8.21	32.89
14	1.1	7.5	0.15	6.82	16	11.54	2.05	11.05	40.36
15	1.2	6	0.20	5.00	14	9.23	1.77	8.21	32.89
16	1.2	7	0.17	5.83	69	10.77	1.96	10.10	37.70
17	1.2	12	0.10	10.00	105	18.46	2.81	19.55	74.56
18	1.4	6	0.23	4.29	9	9.23	1.77	8.21	32.89
19	1.4	8	0.18	5.71	65	12.31	2.14	11.99	43.21
20	1.4	11.5	0.12	8.21	27	17.69	2.73	18.61	69.65
21	1.4	21	0.07	15.00	31	32.31	4.08	36.56	254.49
22	1.5	6	0.25	4.00	28	9.23	1.77	8.21	32.89
23	1.5	8	0.19	5.33	25	12.31	2.14	11.99	43.21
24	1.5	9	0.17	6.00	355	13.85	2.32	13.88	49.52
25	1.5	10.5	0.14	7.00	21	16.15	2.57	16.72	60.77
26	1.7	17.5	0.13	8.00	51	26.92	3.61	29.95	157.88

27	1.5	19	0.08	12.67	109	29.23	3.82	32.78	193.73
28	1.6	7	0.23	4.38	18	10.77	1.96	10.10	37.70
29	1.6	7.5	0.21	4.69	18	11.54	2.05	11.05	40.36
30	1.7	7	0.24	4.12	23	10.77	1.96	10.10	37.70
31	1.8	9.5	0.19	5.28	23	14.62	2.40	14.83	53.02
32	1.8	10	0.18	5.56	23	15.38	2.49	15.77	56.76
33	1.9	13	0.15	6.84	42	20.00	2.96	21.44	85.46
34	2	8	0.25	4.00	10	12.31	2.14	11.99	43.21
35	2	8.5	0.24	4.25	6	13.08	2.23	12.94	46.26
36	2	10	0.20	5.00	44	15.38	2.49	15.77	56.76
37	2	11	0.18	5.50	27	16.92	2.65	17.66	65.06
38	2	13	0.15	6.50	44	20.00	2.96	21.44	85.46
39	2.2	14	0.16	6.36	40	21.54	3.11	23.33	97.95
40	2.3	15	0.15	6.52	330	23.08	3.26	25.22	112.26
41	2.5	8.5	0.29	3.40		13.08	2.23	12.94	46.26
42	2.5	11	0.23	4.40	16	16.92	2.65	17.66	65.06
43	2.5	12	0.21	4.80	27	18.46	2.81	19.55	74.56
44	2.6	12.5	0.21	4.81	18	19.23	2.89	20.50	79.83
45	2.8	16	0.18	5.71	8	24.62	3.40	27.11	128.67
46	2.8	18	0.16	6.43	20	27.69	3.68	30.89	169.03
47	3	11.5	0.26	3.83	30	17.69	2.73	18.61	69.65
48	3	13	0.23	4.33		20.00	2.96	21.44	85.46
49	3.1	19	0.16	6.13	58	29.23	3.82	32.78	193.73
50	3.2	10	0.32	3.13	16	15.38	2.49	15.77	56.76
51	3.3	20	0.17	6.06	37	30.77	3.95	34.67	222.04
52	3.6	20	0.18	5.56	15	30.77	3.95	34.67	222.04
53	3.7	25	0.15	6.76	92	38.46	4.58	44.12	439.16
54	3.8	18	0.21	4.74	21	27.69	3.68	30.89	169.03
55	4.5	24	0.19	5.33	44	36.92	**4.46**	42.23	383.16
Mega									
1	4.0	27	0.15	6.75	19	41.54	4.82	47.90	576.90
2	4.0	60	0.07	15.00	118	92.31	8.21	110.27	51992.85

3	4.2	27	0.16	6.43	22	41.54	4.82	47.90	576.90
4	4.5	35	0.13	7.78	16	53.85	5.73	63.02	1717.91
5	5.1	50	0.10	9.80	55	76.92	7.27	91.37	13291.25
6	5.3	35	0.15	6.60	35	53.85	**5.73**	63.02	1717.91

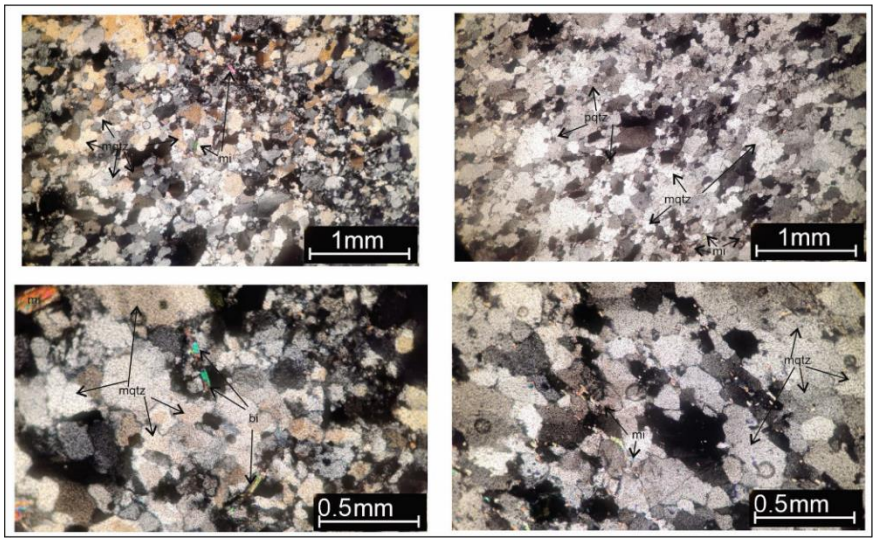

Figure 2 Photomicrograph of Rajgarh quartzite of Jamwa Ramgarh section, mqtz- monocrystalline quartz, pqtz- polycrystalline quartz, mi- muscovite

road section at the Jamwa Ramgarh reservoir, situated eastern side of Jaipur city (Fig. 1). The Rajgrah Formation, in Alwar- Jaipur basin, is marked by conglomerates and pebbly quartzites at the base, grading into coarse to medium grain (gritty to arkosic quartzite- DR map) and quartzite with basic flows at places, dolomite, massive quartzites and the uppermost litho-unit is a quartz-biotite schis with conglomerate (Gupta et al., 1997). The main direction of sediment transport was towards north-northwest for Rajgarh Formation. The massive quartzites at Jamwa Ramgarh host well-preserved ripple marks at several, still-preserved bedding planes.

FIELD AND LABORATORY METHODS

The study includes geological investigations along 250m travers near Jamwa Ramgarh reservoir which shows the best development of diverse types of ripple structures in quartz arenite. Detailed field studies comprising documentation of sedimentary features, orientation of planer structures and description of morphometric parameters of ripple mark at four spots A, B, C and D (Fig. 1). A total of ninety-four ripple marks (ripple surfaces) were documented from massive quartzite in Jamwa Ramgarh section. All ripples are preserved in a single direction along the road side. The strike is E 50- 55° N with moderate dips (20° to 40°) towards NW. They were studied in detail over a strike length of 250 m, where they show prolific development. The data of all ninety-four ripple marks is collected manually with the help of measuring tape and scale. Petrographic characters were observed and examined under a polarizing microscope. Based on field variation in term of variation in colour and texture, total fifteen samples were selected to examine grain size, texture and mineralogical features.

RESULTS

The thickness of individual quartzite bed varies from 2 to 50 cm. The petrographic studies of quartzite reveal uniformity in grain size, sorting,

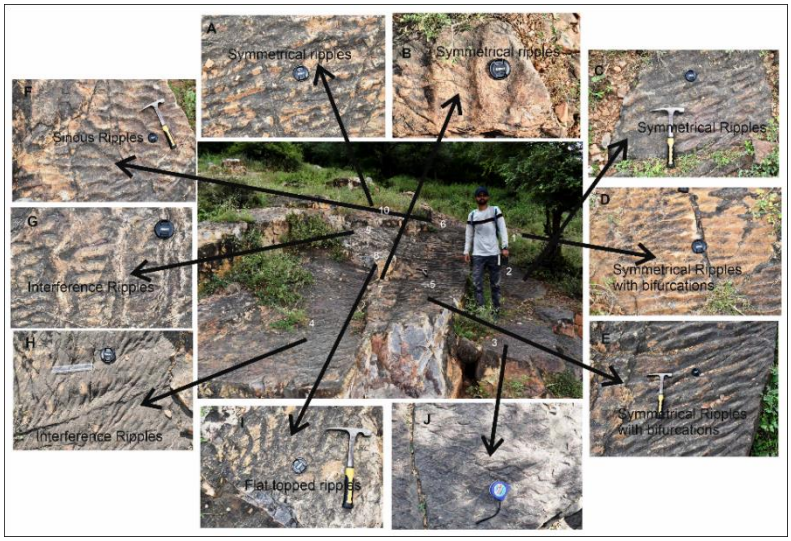

Figure 3 Field Photographs showing variety of ripple marks at site A (refer to Fig. 1): A, B & C – symmetrical ripples, D & E- symmetrical ripples with bifurcations, F- sinuous ripples, G & H- Interference ripples, I- flat-topped ripples

roundness and composition (Fig. 2). In general, grain size varies from 0.25 mm to 0.45 mm with an average 0.35 mm. The quartz grains, the most dominant minerals, are well sorted and sub-rounded, in addition <5 % phyllosilicates are also present. The monocrystalline quartz is dominant in comparison to polycrystalline quartz (Fig. 2).

RIPPLE MORPHOLOGY

The ripple morphometric data are provided in Table 2, wherein Wave length (S) is the horizontal distance from crest to crest between adjacent ripples, H is the vertical length (amplitude) from crest to trough. Vertical Form Index (VFI) or Ripple Index (RI) represents the ratio between wave length and amplitude (S/H), and Ripple Steepness (R.S.) is derived by the ratio of amplitude and wavelength (H/S). Orbital diameter (d_0) is the maximum distance of water particles move as wave passes. The orbital diameter is calculated by: d_0= S/ 0.65 (Miller and Komar, 1980) for symmetric orbital ripples near sediment- water interface. Tm is the maximum wave period that can yield bottom velocities above the threshold for initiation of movement for grain size

Figure 4 Field Photographs showing variety of ripple marks at site B (refer to Fig. 1): A– symmetrical ripples, B & C- symmetrical ripples with bifurcations, D-sinuous ripples and E- pointed crest and rounded trough ripples.

(D). It is calculated by 0.17 × (d_0^2/D)1/3 (in cm and seconds) (Dingler, 1979). The average values of these parameters are provided in the Table 2.

RIPPLE CLASSIFICATION

Ripples are classified on the basis of a combination of morphological parameters, such as the Ripple Wave length (S) and Amplitude (H). The ripples with amplitude <0.5 cm, considered as 'small ripples'. Ripples wavelength from 2.5 to 5 cm considered as 'medium ripples' and wave length > 5.0 cm considered as 'large ripples' (Aspleri et al., 1994). Ripples with wave length >25cm are named 'Very Large Ripples' or Mega Ripples. As per this criterion, out of total studied ripples, 59% of are classified as large, 24% as small, 12% as medium, and remaining 5% as very large ripples (Table 2).

The ripples are predominantly symmetric (straight crest) type (Fig. 3a, b and c; Figs. 4a, 5a and

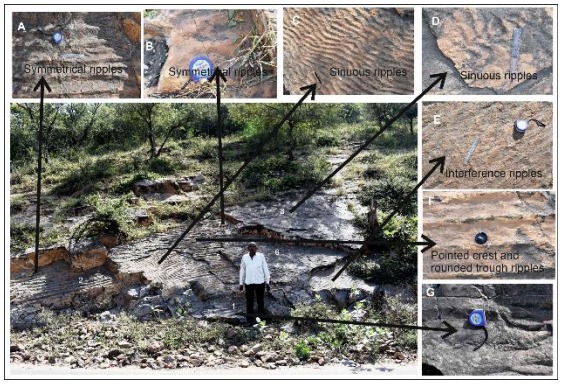

Figure 5 Field Photograph showing variety of ripple marks at site C (refer to Fig. 1): A & B – symmetrical ripples, C & D- sinuous ripples, E- Interference ripples, F- pointed crest and rounded trough ripples

Figure 6 Field Photograph showing variety of ripple marks at site D (refer to Fig. 1): A, B & C - symmetrical ripples, D- symmetrical ripples with bifurcations, E- Pointed crest and trough ripples, F- flat-topped ripples, G- pointed crest and rounded trough ripples

Figure 7 Field Photographs showing other types of ripple marks in the study area: A – Pointed crest and trough ripples, B- flat-topped ripples, C- catenary ripples, D & E- mega ripples, F- current ripples, G- criss-cross ripples, H- road side view of exposure

b; and 6 a, b, and c) and show further variations, such as bifurcation types (Figs. 3d and e, 4b and c, and 6d), sinuous (curved crest) ripples (Figs. 3f, 4d, 5c

and d), interference ripples (Figs. 3g and h and 5e), pointed crest and pointed trough ripples (Figs. 6e and 7a,), flat topped ripples (Figs 3i, 6f, and 7b), pointed crest with rounded trough ripples (Figs. 4e, 5f, and 6g), catenary ripples (Fig. 7c) and mega ripples (Fig. 7d and e). Apart from these types, asymmetric current ripples (Fig. 7f) and criss-cross ripples (Fig. 7g) are also present.

RIPPLE SHAPE

The shape of ripples can be explained with the help of ripple symmetry, ripple index and ripple steepness. The ripple index (RI) values (Table 2) range from 2.8 to 15.0 with an average 6.8, significantly below the values for wind ripples (VFI > 15; Tanner, 1967). The majority of ripples are symmetric, indicating either current or wave dominated environment. The ripples are straight, long-crested, two-dimensional forms and interference ripples are also common. The average ripple steepness values for small, medium, large and very large ripples are 0.14, 0.21, 0.18 and 0.13, respectively. Occasional criss-cross ripples, catenary ripples, current ripples and flat-topped ripples were also observed.

RIPPLE CREST LINE

The ripple crust line is an indicator of the paleocurrent direction as it is oriented parallel to the wave front. The orientation crest line of all studied ripple marks are ranges between 330° and 109° but maximum number of ripples are aligned between 6° and 45°N. Majority of small ripples range between 16° and 19°N and medium ripples between 6° and 20°N. Large ripple crest line is aligned mainly between 21° and 37°N (Fig. 8).

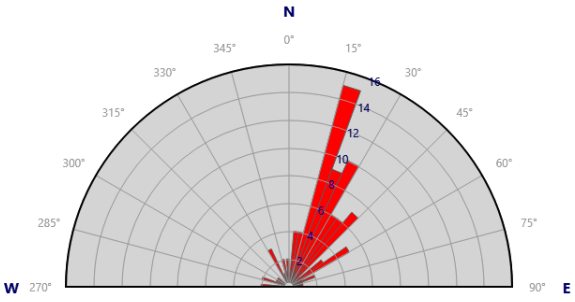

Figure 8 Rose diagram showing orientation of Ripples crest lines underling maximum ripples aligned in NE- SW direction.

VERTICAL DISTRIBUTION OF BEDS AND VARIATION IN RIPPLE MARKS

The vertical description of quartzite beds with ripple marks at four sites namely A, B, C and D (Fig. 9) is described as below:

Site A: This site comprises a total thickness of 112 cm with ten ripples including three small ripples, two interference ripples and five large ripples. The small ripples are aligned in 334° to 34° and large ripples in 26° to 69° direction. Their amplitude and wave length varies from 0.4 to 0.5 cm and 4 to 4.5 cm, respectively for small ripples and from 1.1 to 3.1cm and 6 cm to 19 cm, respectively for large ripples. The exposed thickness of lowest bed with small ripples is 35 cm, and it is overlain by large ripples (symmetrical) of 2 cm thickness. These are

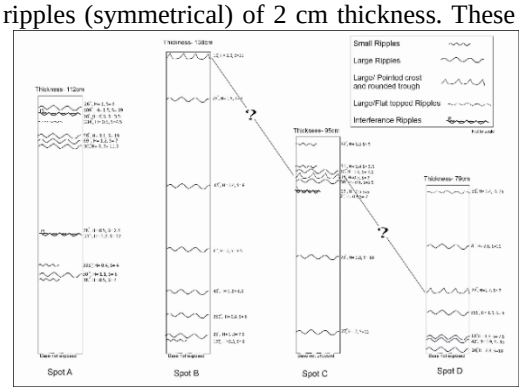

Figure 9 Vertical bed description for sites A, B, C & D, showing ripples types exposed on different beds.

further overlain by small ripples (symmetrical) with 5 cm thickness. The next bed is 15 cm thick and marked by interference ripples. These ripples are overlain by large (symmetrical) ripples contained within a 40 cm thick bed, followed upward by a 2 cm thick bed having large, sinuous ripples (sinuous). It is overlain by large ripples (symmetrical). Seven cm thickness was measured for next bed which contains flat-topped, small ripples. It is overlain by a second set of interference ripples contained in a 2 cm thick bed. The uppermost, 2 cm this bed, displays large ripples.

Site B: The complete column thickness of 138 cm contains eight ripples comprising one small ripple and seven large ripples. The large ripples are aligned in 350°N to 65° N direction, their amplitude ranges between 0.8 and 2.5 cm and wave length varies from 6 to 11 cm. The exposed thickness of lowermost small ripple (sinuous) is 7cm. It is overlain by 3 cm thick, large ripples (symmetrical with bifurcation). The subsequent bed with similar large ripples, is 8 cm thick, followed by a 10 cm thick one. Further up section, large ripples (symmetrical) are exposed on beds of 20 cm, 30 cm, and 40 cm thickness. The uppermost bed is 40 cm thick and contains large ripples (pointed crest with rounded trough).

Site C: This comprises a total thickness of 95 cm with nine ripples comprising three small and six large ripples. The small ripples are aligned in 2°N to 92°N direction, with amplitude between 0.4 and 0.5 cm, and wave length between 2.5 to 7 cm. The large ripples are aligned in 11°N to 50°N directions, with significant variable amplitude fluctuating between 0.6 and 1.8 cm, and wave length from 5.5 to 11 cm. The exposed thickness of lowest bed is 10 cm having large ripples. It is overlain by a 35 cm thick bed with large ripples (symmetrical). Further upward, the 30

cm thick bed has large are sinuous types with a thickness of 5 cm. It is overlain by a 1.5 cm thick bed with large ripples (pointed crest and rounded trough). It is overlain by large ripples of a 2 cm thick bed. The next bed with small ripples is also 1.5 cm thick with small ripples (symmetrical) and the uppermost small ripple (sinuous) bed has 10 cm thickness.

Site D: This section comprises seven large ripples in a 80 cm column thickness. These ripples are aligned in 355°N to 42° N direction and their amplitudes range between 1.5 and 2.8 cm, and wave length from 7 to 18 cm. The lowermost ripple (symmetrical) is contained in a 1 cm thick bed, which is overlain by a 8 cm thick bed with symmetrical ripples. The thickness of next bed is 2 cm, which in turn, is overlain by a 13 cm thick bed with large ripples (pointed crest and trough). it is overlain by a 10 cm thick bed with pointed crest and rounded trough ripples. The next 20 cm thick bed contains symmetrical ripples while the uppermost, 25 cm thick bed exposes flat topped large ripples.
A correlation among these sites is unclear, however, the pointed crest and rounded trough ripples are common at site B, C and D. These show a lateral continuity; however, a direct correlation seems unlikely due to lack of supporting evidence.

DISCUSSION

PALEODEPTH AND PALEO-WAVE CONDITIONS

Relevant morphological parameters, Wave height (H) and Water depth (h) were calculated by using the formula of Tanner (1971) below:

$$H = 38.52 + 1.89 \times S - 7.11 \times \ln D$$
$$\ln h = 14.64 + 0.61 \times S - 2.45 \times \ln D - 0.28 \times \lambda$$

Wherein, S is the ripple wave length, D is grain size, λ is water wavelength. The minimum water depth for wave propagation is 4.3 cm (Tricker, 1965). The water wavelength (λ) was estimated by the formula: $\Lambda = 33.77 + 1.72\ S - 7.22\ \text{In h}$ (Tanner 1971). Since sedimentary structures (ripple marks) are well preserved, we assume that the rock did not undergo significant recrystallization. Therefore, the grain size of quartz can be considered to represent original grain size. The quartz grain shows a correspondence with the size of ripples and progressively increased from small, medium to large - very large ripples. Very large ripples are comprised by largest grains. The estimated wave height for small ripples ranges from 1.59 cm (minimum) to 13.88 cm (maximum) with an average of 4.37 cm. Similarly, the medium ripples show an overlap and range between 2.54 and 8.21 cm with an average of 4.64 cm. In the case of large ripples, the wave height ranges from 1.60 to 44.12 cm with an average of 13.33 cm, while in case of very large ripples it ranges from 47.90 to 110.27 cm with an average of 70.58 cm.

Bartholdy et al. (2015) suggested that the logarithmic velocity profile, grain-size and flow depth have a direct impact on the formation of ripples. In the present study, water depth calculations shows, a range between 17.56 and 49.52 cm with an average value of 25.66 cm for small ripples, between 21.85 and 32.89 cm with an average of 25.57cm for medium ripples, from 20.41 to 439.16 cm with an average of 85.55 cm for large ripples and 576.90 cm to 51.99 m with an average of 11.6 m for very large ripples. The average wave height and water depth for all three types of ripples are 24.23 cm and 2.9 m respectively (Table 3).

Table-3 Average values of statistical parameters of ripples in Jamwa Ramgarh quartz arenite

Parameters	small (n=22)	Medium (n=11)	Large (n=55)	Very Large (n=6)	Total (n =94)
H	0.46	0.84	1.87	4.52	1.92
S	3.90	4.11	10.92	39.00	14.48
RI	8.64	5.11	6.16	8.73	7.16
RS	0.14	0.21	0.18	0.13	0.16
d_0	5.99	6.32	16.81	60.00	22.28
Tm	2.81	2.95	5.55	13.14	6.11

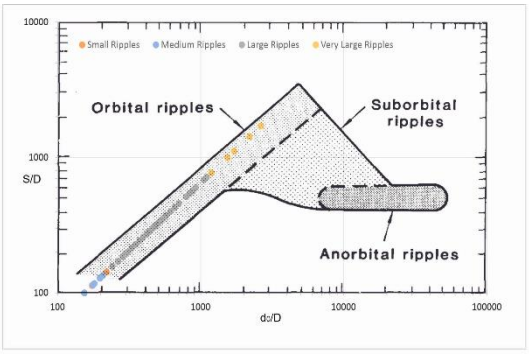

Figure 10 Plot of ratio of ripple wave length to grain size against ratio of orbital diameter to grain size (Clifton and Dingler, 1984) showing orbital ripple affinity for all ripples in the study area.

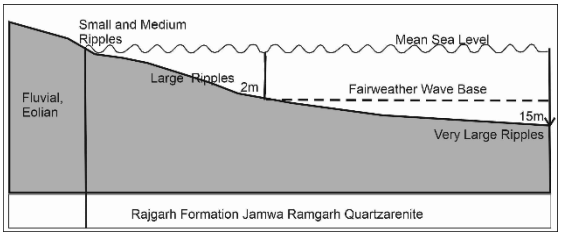

Figure 11 Plot depicting low energy coastal profile for the studied ripples.

On the basis of relationship between ripple wave length and orbital diameter, Clifton (1976) subdivided symmetrical ripples into three types i.e., orbital ripples, suborbital ripples and an-orbital ripples, The Jamwa Ramgarh ripple data were plotted to discriminate them (Fig. 10) and all the sample plot in the orbital ripple field. Their d_0/D ratios for small ripples ranges between 72 and 396 with an average of 173, from 132 to 264 with an average of 181 for medium ripples, from 110 to 1099 with an average of 480 for large ripples, and

from 1187 to 2637 with an average of 1714 for very large ripples. Due to the requirement of short oscillatory motion, the orbital ripples most commonly occur in very shallow water conditions, under short period waves (Pedocchi and García, 2009; Bartholdy et al., 2015). Pedocchi and García (2009) suggested that the sediment size has an important effect on the size and geometry of bed forms that can be generated by oscillatory flows. Alternatively, Aldridge et. al. (2015) recommended that the distribution of highest-level disturbance, where mega ripples formed, showed a complex relationship between water depth, tidal stress, wave fetch and grain size.

Table-4 Calculated wave parameters and water depth of Jamwa Ramgarh quartz arenite

Ripples	Wave Length (cm)	Wave Height H (cm)	Water Depth h (cm)
Small	3.90	4.38	25.60
Medium	4.11	4.64	25.57
Large	10.92	17.52	87.06
Very Large	39.00	70.58	11645.62
Average	14.48	24.28	2945.96

The wave ripple crest are reliable indicators of paleo-shoreline trend as the incoming waves of variable trend become realigned parallel to the shoreline. The position of symmetrical wave ripples with an average wave height of 24.2 cm and average water depth of 2.9 m can be classified as beach sand at shallow marine area. The large long period waves cannot be supported by such water depth. The wave period for small ripples ranges from 1.52 to 4.99 seconds with an average of 2.81 seconds, from 2.40 to 3.81 seconds with an average of 2.95 seconds for medium ripples, from 3.60 to 9.87 with an average 5.61 seconds for large ripples, and from 10.39 to 17.69 with an average of 13.14 seconds for very large ripples. The average wave period for all these ripples is 6.13 seconds. The large and very large ripples are formed in slightly deeper continental shelf area (Fig. 11). Allen (1984) described a close relationship of ripple morphology, water depth and wave velocity. In the Jamwa Ramgarh area, very large ripples can be associated with higher water depth, courser grain size, higher wave height and long wave periods.

The presence of criss-cross and interference ripples shows waves from different weather systems meet each other almost at the right angle. They indicate two dominant paleocurrent directions. Sinusoidal profile of many ripples indicates an environment with weak currents where water motion is dominated by wave oscillations (Boggs, 2006).

CONCLUSION:

1) On the basis of ripple wave length and amplitude, four types of ripples are observed in the study area i. e. small, medium, large and mega ripples.
2) The main direction of sediment transport was from north-northwest during the formation of ripples.
3) The total thickness of the quartzite containing ripples marks is consistently small and indicates an average water depth of less than 3 m.
4) The wave periods in case of small, medium and large ripples are generally short (approx. 6 seconds) to ensure bottom orbital velocities adequate for sediment movement.
5) The maximum distance water particle can move as wave passes, is approximately 17 cm.
6) The wave period for very large ripples is approx. 13 seconds and the maximum distance the water particle can move as wave passes is approx. 60 cm.
7) Continental shelf with variable depth is proposed for development of these wave ripples.

REFERENCES

Allen, J.R.L. (1984). Sedimentary Structures, Their Character and Physical Basis: vol. 1. Elsevier Scientific Publ. Co., Amsterdam, 593p.

Aldridge, J.N., Parker, E.R., Bricheno, L.M., Green, S.L. and Van der Molen, J. (2015). Assessment of the physical disturbance of the northern European Continental shelf seabed by waves and currents. Continental Shelf Research, vol. 108, pp. 121-140.

Aspler, L.B., Chiarenzelli, J.R. and Bursey, T.L. (1994). Ripple marks in quartz arenites of the Hurwitz Group, Northwest Territories, Canada; evidence for sedimentation in a vast, early Proterozoic, shallow, fresh-water lake. Journal of Sedimentary Research, vol. 64 (2a), pp. 282-298.

Baas, J.H. (1999). An empirical model for the development and equilibrium morphology of current ripples in fine sand. Sedimentology, vol. 46, pp. 123-138.

Baird, D.M. (1962). Ripple marks. Journal of Sedimentary Research, vol. 32(2), pp. 332-334.

Bartholdy, J., Ernstsen, V. B., Flemming, B. W., Winter, C., Bartholomä, A., and Kroon, A. (2015). On the formation of current ripples. Scientific Reports, vol. *5* (1), pp. 11390.

Bergman, C. (1979). Ripple marks in the Silurian Gotland Sweden. Geologiska Foreningen Stockholm Forrhandlingar.

Boggs, S. (2006). Principles of sedimentology and stratigraphy (Vol. 662). Upper Saddle River, NJ: Pearson Prentice Hall.

Bose, U., Mathur, A.K., Sahoo, K.C., Bhattacharya, S., Dutt Krishan Kumar, A.V., Sarkar, S. S., Choudhary, S. and Choudhary, I. (1996). Event stratigraphy and physicochemical characters of B.G.C and associated supracrustals in the south Mewar plains of Rajasthan. Journal of the Geological Society India, vol. 47, pp. 325-338.

Chang, T.S. and Flemming, B.W. (2013). Ripples in intertidal mud—a conceptual explanation. Geo-Marine Letters, vol. 33, pp. 449-461.

Cheng, C.H., De Smit, J.C., Fivash, G.S., Hulscher, S.J., Borsje, B.W. and Soetaert, K. (2021). Sediment shell-content diminishes current-driven sand ripple development and migration. Earth Surface Dynamics Discussions, vol. 9 (5), pp. 1335-1346.

Clifton, H.E. (1976). Wave-formed sedimentary structures—a conceptual model; In: R.A. Davis, R.L. Ethington (Editors), Beach and Nearshore Processes. Society of Economic Paleontology and Mineralogy, Special Publications, vol. 24, pp. 126-148.

Clifton, H.E. and Dingler J.R. (1984). Wave-formed structures and Paleoenvironmental Reconstruction. Marine Geology, v. 60, pp. 165-198.

DR map (2022). District Resource Map of Jaipur District, Geological Survey of India.

De Vleeschouwer, D., Leather, D. and Claeys, P. (2015). Ripple marks indicate mid-Deonian paleo-wind directions in the Orcadian Basin (Orkney Isles Scotland). Palaeogeography, Palaeoclimatology, Palaeoecology, vol. 426, pp. 68-74.

Deb, M. and Thorpe, R.I. (2004). Geochronological constraints in the Precambrian Geology of Rajasthan and their Metallogenic implications In: Deb M. Goodfellow WD (Eds) Sediment-hosted Lead–Zinc Sulphide Deposits. Narosa Publishing House New Delhi, pp. 246-263.

Dingler, J.R. (1979). The threshold of grain motion under oscillatory flow in a laboratory wave channel. Journal of Sedimentary Research, vol. 49(1), pp. 287-293.

Ewans, O.F. (1942). The relation between the size of wave formed ripple marks, depth of water, and the size of the generating waves. Journal of Sedimentary Petrology, vol. 12, pp. 31-35.

Gregory, L.C., Meert, J.G., Pradhan, V., Pandit, M.K., Tamrat, E. and Malone, S. J. (2006). A paleomagnetic and geochronologic study of the Majhgawan Kimberlite India: implications for the age of the Upper Vindhyan Supergroup. Precambrian Research, v. 149, pp. 65-75.

Gupta, P., Arora, Y.K., Mathur, R.K., Iqbaluddin, Prashad, B., Sahai, T.N. and Sharma, S.B. (1997). Lithostratigraphic map of the Aravalli region southern Rajasthan and northeastern Gujarat. Geological Survey of India Publications, Jaipur, vol. 123, pp. 262.

Harms, J.C. (1969). Hydraulic significance of some sand ripples. Geological Society of America Bulletin, vol. 80 (3), pp. 363-396.

Heron, A.M. (1953). Geology of central Rajasthan. Mem. Geol. Surv. India, v.79, 389p.

Kindle, E.M. and Bucher, W.H. (1926). Ripple mark and its interpretation. Treatise on Sedimentation, pp. 451-483.

Komar, P.D. (1976). Beach Processes and Sedimentation. Prentice-Hall Inc Englewood Cliffs New-Jersey 429p.

McKenzie, N.R., Hughes, N.C., Myrowc, P.M., Banerjee, D.M., Deb, M. and Planavskye, N. J. (2013). New age constraints for the Proterozoic Aravalli–Delhi successions of India and their implications. Precambrian Research, vol. 238, pp. 120-128.

Miller, M.C. and Komar, P.D. (1980). Oscillation sand ripples generated by laboratory apparatus. Journal of Sedimentary petrology, vol. 50, pp. 173-182.

Pedocchi, F. and García, M.H. (2009). Ripple morphology under oscillatory flow: 1. Prediction. Journal of Geophysical Research, Oceans, 114(C12).

Rasmussen, B., Bose, P.K., Sarkar, S., Banerjee, S., Fletcher, I.R. and McNaughton, N.J. (2002). 1.6 Ga U-Pb zircon age for the Chorhat Sandstone lower Vindhyan India: Possible implications for early evolution of animals. Geology, vol. 30, pp. 103-106.

Ray, J., Martin, M.W., Veizer, J. and Bowring, S.A. (2002). U–Pb zircon dating and Sr isotope systematics of the Vindhyan Supergroup India. Geology, vol. 30, pp. 131-134.

Romanovski, S.I. (1977). Sedimentologicheskie osnovy litologii [Sedimentological fundamentals of lithology] Nedra Leningrad 408p [in Russian].

Roy, A.B. (1988). Stratigraphic and tectonic framework of the Aravalli Mountain Range In Precambrian of the Aravalli Mountain Rajasthan India Mem. Geological Society of India, vol. 7, pp. 3-31.

Roy, A. B. and Kataria, P. (1999). Precambrian geology of the Aravalli Mountain and

neighbourhood: Analytical update of recent studies; Proc. Sem. Geology of Rajasthan: Status and Perspective, MLS University, Udaipur, pp.1-56.

Roy, A.B. and Kröner, A. (1996). Single zircon evaporation ages constraining the growth of the Archaean Aravalli craton northwestern Indian shield. Geological Magazine, vol. 133(3), pp. 333-342.

Roy, A.B. and Jakhar, S.R. (2002). Geology of Rajasthan (Northwest India) Precambrian to Recent; Scientific Publishers (India) Jodhpur, 421p.

Sinha Roy, S. (1984). Precambrian crustal interactions in Rajasthan NW India; Proceeding of Seminar on Crustal Evolution of Indian Shield and its Bearing on Metallogeny, pp. 84-91.

Sinha-Roy, S., Malhotra, G. and Mohanty, M. (1998). Geology of Rajasthan. Geol. Soc. India Bangalore 278p.

Sukanta, G., Atanu, M., Purnajit, B. and Syed, Z. (2017). Primary sedimentary structures and MISS in Gulcheru quartzite along SW part of Cuddapah Basin. Journal of the Geological Society of India, vol. 89, pp. 511-520.

Tanner, W.F. (1967). Ripple mark indices and their uses. Sedimentology, vol. 9, pp. 89-104.

Tanner, W.F. (1970). Triassic-Jurassic lakes in New Mexico. The Mountain Geologist.

Tanner, W.F. (1971). Numerical estimates of ancient waves water depth and fetch. Sedimentology, vol. 16, pp. 71-88.

Tanner, L.H. (1982). Description interpretation and geologic history of the Peru Sand outcrop in Catoosa Oklahoma, pp. 344-355.

Tricker, A.R. (1965). Bores Breakers Waves and Wakes; Elsevier New York NY 250 p.

Wang, W., Cawood, P.A., Pandit, M.K., Zhou, M.F. and Chen, W.T. (2017). Zircon U-Pb age and Hf isotope evidence for Eoarchean crustal remnant and crustal growth and reworking respond to supercontinental cycles in NW India. Journal of Geological Society, v. 174, pp. 759 -772.

Wiedenbeck, M., Goswami, J.N. and Roy, A.B. (1996). Stabilization of the Aravalli Craton of northwestern India at 2.5 Ga: an ion microprobe zircon study. Chemical Geology, v. 129 (3-4), pp. 325-340.

Received on: July 3, 2024
Revised accepted on: Sept 18, 2024

JOURNAL INDIAN ASSOCIATION OF SEDIMENTOLOGISTS ISSN NO 2582 – 2020
Vol. 41, Issue II, 2024, pp. 52 – 62
DOI: https://doi.org/10.51710/jias.v41iII.384

Tertiary Coal Deposits from the North-eastern Region of India – A review

Manabendra Nath
Department of Geology, Gurucharan College, Silchar-788004, Assam
Email: dr.manabendra.nath@gmail.com

ABSTRACT

This review paper aims to provide a comprehensive account of the Tertiary coal resources of north-eastern region of India. The coal belt of North-East India developed in two different geo-tectonic settings – one is the foreland basin (Assam, Arunachal Pradesh, Nagaland Oligocene coals) and the other platform areas (Meghalayan Eocene coals). The rank of eastern Himalayan coals varies from sub-bituminous to high volatile bituminous C. The carbon content of Oligocene coal is much higher and show caking characteristics. The coals of this part of India have low ash (<8%), low moisture (<5%), high volatile matter (>40%), high sulphur (>3%), high hydrogen content (>4%), low nitrogen (<1%) and oxygen (<12%). Petrographically they are rich in vitrinite, moderate Liptinite and low inertinite. High concentrations of trace elements (like Cu, Cr and Ni) and sulphur content indicate marine influence in the depositional basin. In the north-eastern coals the dominance of typical Tertiary angiosphermic floral assemblage is well indicated by the occurrence of single, double and triple celled telutospores.

Keywords: Sulphur deposits, petrography, coal, India

INTRODUCTION

Coal is a naturally occurring fossil fuel that contributes immensely to the energy and power sectors. This fossil fuel is abundant and most important in India and other parts of the world like China, USA, Australia and Indonesia. It contributes about 37% and 73% of the global and Indian electricity supply (Indian Bureau of Mines, 2019) (Fig.1a and b). Indian coal resources belong to two principal stratigraphic horizons viz Permian sediments deposited in intra-cratonic lower Gondwana basins and Tertiary coal in near-shore basins and shelf having mainly peri-cratonic set-up. Major coal resource occurs within the Gondwana basins that are preferentially located in the eastern and southeastern parts of the country in the states of Jharkhand, Bihar, West Bengal, Odissa, Madhya Pradesh, Andhra Pradesh and Maharashtra (Kumar, 2022). Only a small portion of the total coal resources constitute the Tertiary coal of northeastern states of Assam, Arunachal Pradesh, Nagaland and Meghalaya (Fig. 2) (Kumar, 2022). However, Tertiary coal contribute (0.5%) meagre amount to the total coal reserve of India (1655.54 M.T., G.S.I, 2022). However, these coal resources are still important because they are quite far distant from the principal coal-producing zones of the country (in the extra-peninsular part). Hence these resources have a crucial role in meeting the local and regional coal demands of the north-eastern states of India. The Tertiary coals invariably have low ash content but high sulphur intimately intermingled with the coal. Industrial use of these coals is thus restricted as the latter causes deleterious effects on the furnace. The Geological Survey of India has provided detailed the stratigraphic sequences, structural elements and tectonic settings of North–East India in the year 1974, 1981, 1989, 1994 and 2009. The coal

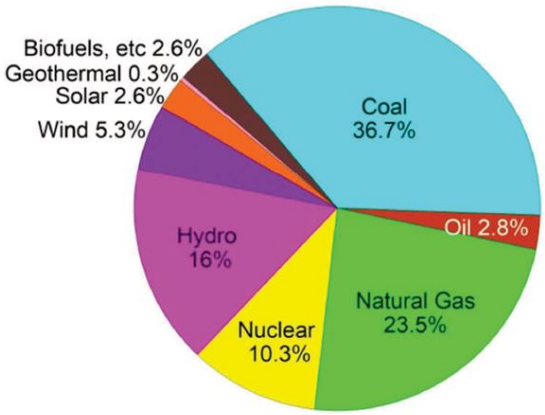

Fig. 1 (a): World Electricity Generation

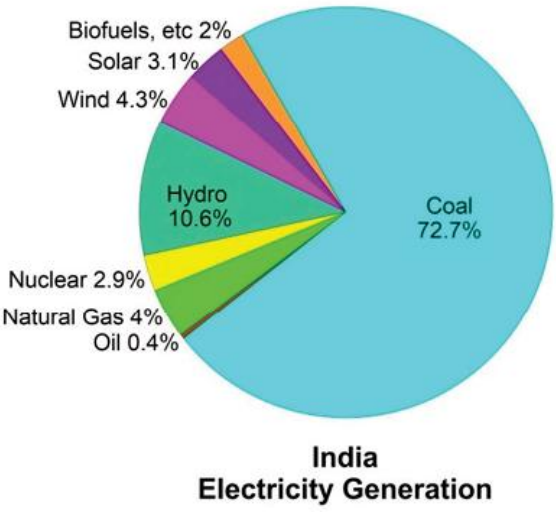

Fig. 1 (b): India Electricity Generation

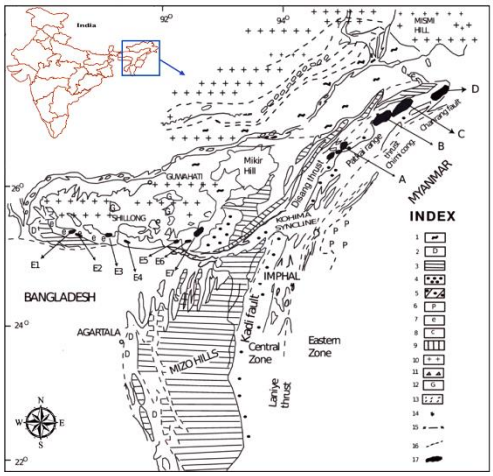

Fig. 2. Geological Map of Coalfields of North Eastern region of India modified after Singh and Singh 2022
1). Alluvium **2)**. Dihing and Dupi Tila Group **3).** Tipam and Surama Group **4).** Barail Group **5).** Undifferentiated Sandstone Group **6).** Pondaungs and Younger Sediments **7).** Jaintia and Disand Group **8).** Langpar and Mahadek Formation **9).** Lower Gondwana System **10).** Metamorphic and Igneous Rocks **11).** Granite **12).** Serpentine Intrusion Result **13).** Basalt **14).** Salt Springs **15).** Line Of Demarcation between High And Low Intensity Foldings **16).** Faults **17).** Coldfields [**A.)** Borjan Coalfield **B).** Dilli Jeypore Coldfield **C).** Makum Coldfield **D).** Namchik Namphuk Coalfield **E1).** West Daranggiri **E2).** Siju **E3).** Langrin **E4).** Mawlong-Shella **E5).** Cherrapunji **E6).** Laitryngew **E7).** Bapung)

resources of the North-Eastern Region of India have been studied by various authors from time to time concerning their geology, chemical and petrographic characteristics, trace elements, hydro-carbon generation potential and depositional set-up along with utilization potential (Ahmed, 1971; Ahmed and Bharali, 1983; Goswami, 1985; Singh, 1989; Mishra, 1991; Mishra, 1992; Chandra and Behera, 1992; Mukherjee et al., 1992; Ahmed and Rahim, 1996; Mishra and Ghosh, 1996; Rajanathnam et al., 1996; Ahmed and Phukan, 1999; Singh et al., 2000; Singh et al., 2003; Mukherjee and Srivastava, 2005; Singh et al., 2012; Singh et al., 2013; Nayek, 2013; Singh, 2015; Nath, 2017; Singh, 2018; Gogoi et al., 2020; Nath, 2021; Kumar et al., 2021; Nath et al., 2022; Adsul, 2024). Though the report of first occurrence of coal in North-East India made by Medlicott (1865) for Assam coals and Medlicott (1868) for Maghalaya coals followed by Mallet (1875), La Touche (1889), Bose (1904), Erans (1932), Fox (1934), Ghosh (1940; 1964), Goswami and Das (1965), Chakraborty and Bhatacharyya (1969), and Raja Rao (1981).

In this study, an attempt has been made to summarise and compile all the published papers in order to get an in-depth overview of the coal resources of the north-eastern part of India.

GEOLOGY OF THE PLATFORM AREAS

The Shillong Plateau, bordered by Brahmaputra lineament to the north, Dauki fault to the South, Naga-Disang thrust to the east and

Table 1. Geological succession of coalfields of Platform areas (Meghalaya) (modified after Raja Rao, 1981 and GSI, 2009)

Age	Group		Formation and member	Thickness (in m)	Lithology/Rock type	
Late Eocene	Jaintia Group		Kopoli	-	Ferruginous Sandstone, grey siltstone and shale	
Middle Eocene		SHELLA FORMATION	Sylhet limestone: Prang limestone/Siju limestone	60 – 150	Bluish massive to thinly bedded limestone with marly interbands	
Early Eocene			Nurpuh sandstone	15 – 26	Coarse to medium grained ferruginous sandstone with bands of sandy limestone	TURA SANDSTONE
Early Eocene			Umlatdoh limestone	70 – 110	Grey to pinkish grey limestone, sandy limestone and calcareous sandstone	
Early Eocene to Palaeocene			Lakadong sandstone	35 – 250	Predominantly buff coloured medium grained arkosic sandstone with thin grey and carbonaceous shale and coal seams	
Early Eocene to Paleocene			Lakadong limestone	25 – 60	Grey to brownish grey limestone, siliceous limestone	
Early Eocene to Paleocene			Therria sandstone	20 – 80	Buff colured medium to coarse grained arkosic sandstone with thin hands of yritic rich silty sandstone	
Late Cretaceous (Danian)			Langpar	10 – 50	Buff coloured calcareous-ferruginous sandstones, earthy limestones etc.	
Late Cretaceous (Maastrichtian)			Mahadek	160 – 335	Massive coarse grained glauconitic sandstones containing dark grey shales and calcareous horizons	
Jurassic to Early Cretaceous			Sylhet Trap	250 – 400	Aa and pahoehoe type basalts	

Dhubri-Yamuna lineament to the west, represents the Precambrian cratonic – the extension of which goes up to Shillong Plateau of NE India. The Plateau is tectonically sensitive and seismically very active due to continued north-north-eastward counter clockwise movement of the Indian plate producing severe compression tectonics. (*Harijan et al., 2003; Ramesh et al. 2005*)

The platform areas developed in the Shillong Plateau of Meghalaya, where Eocene-age coal deposits were deposited in the peripheral margins. During the cretaceous period, this shield got uplifted to form host structure and finally the plateau formed because of its peneplanation. Later on along the peripheral region of the Plateau, deposition of coal took place. The lateral variation of lithofacies occurred because of the sediments deposited on the shallow marine shelf, which extended as an embayment. The stratigraphic succession of the coalfields of Meghalaya is presented in Table-1 (after Raja Rao, 1981). The principal coal-bearing formation of Garo Hill is the Tura Formation of the Jaintia Group while in Khasi (both East and West) & Jaintia (East) Hills the coal-bearing horizon occurs in the Lakadong Sandstone Member of the Shella Formation of Jaintia Group which was developed because of intermittent transgression & regressions of during Eocene times. The oldest rock encountered in the platform area is the Sylhet trap which forms the basement of Cretaceous-Tertiary sedimentation.

GEOLOGY OF THE ZONE OF SCHUPPEN (FOREDEEP BASIN)

In pericratonic down warps in the 'belt of schuppen' over the northern flank of Naga-Patkai range the Oligocene coal deposits occur and spread over the states of Upper Assam, Arunachal Pradesh and Nagaland (Evan, 1932; Biswas et al., 1994; Mishra and Ghosh, 1996; Srivastava et al., 2004). Dasgupta and Biswas (2000) observed that shallow brackish water condition prevailed during the Oligocene period when the stratigraphic formation of Barail took place. Arranged in imbricately along the Naga Hills the belt of Schuppen has been characterised by a series of at least eight complex thrust faults. To the foreland ridges the Naga Hills have moved towards north-west by fault activity. Extending from Nagaland through Assam up to Arunachal Pradesh (with thick coal seams) developed large molasses basins during Oligocene-Miocene times. Large-scale, open, upright folds have occurred due to vertical block movements eventually forming the major thrust faults. In the flanks of trough of the Indo-Burmese range a thick sequence (2-6 km) of Tertiary sediments has accumulated which was deposited in deltaic facies. Makum and Namchik-Namphuk coalfield encloses the northern part of the belt where coal seams are thick (18 m in Makum coalfield) whereas the southern part of belt includes Dilli-Jeypore of Assam, Borjan and Tiru Valley of Nagaland and also includes some minor coalfields where the thickness of coal seams are of 1.5 m. The stratigraphic succession of coalfields of the foreland basin is shown in Table-2 (after Raja Rao, 1981). Here principal coal-bearing sequence is the Tikak Parbat Formation (alternate bands of sandstone, sandy shale and coal seam) of the Barail Group of the Oligocene age. The Barail group is underlain by Disang group. In the Barail group lower Naogaon formation also developed in Makum, Dilli-Joypore of Assam, Borjan, Tiru Valley of Nagaland and Namchik-Namphuk of Arunachal Pradesh. Above Barail Group lies Tipam Group. Tipam Group of rocks also developed in Dilli-Joypore, Namchik-Namphuk, Borjan and Tiru valley coalfields. Above Tipam lies Namang Formation and at the top is Dihing.

DISTRIBUTION PATTERN OF TERTIARY COALS

The Tertiary coal measures of the north-eastern region of India are unevenly distributed in the four states of Assam, Arunachal Pradesh, Nagaland and Meghalaya which enclose 67

Table 2. Geological succession of coalfields of zone of Schuppen (Assam, Arunachal Pradesh, Nagaland) (modified after Raja Rao, 1981)

Age	Group & Formation	Thickness	Rock Types
Pliocene	Dihing Group	1800 m	Mostly pebbly sandstone with thin greyish clay beds
..... Unconformity			
Mio-Pliocene	Namsang Formation	800 m	Fine to coarse grained sandstone with bands of clay
..... Unconformity			
Miocene	Tipam Group (i) Girujan Clay (ii) Tipam Sandstone	 1800 m 2300 m	 Mottled clay with greyish soft sandstone Ferruginous, fine to coarse grained micaceous to felspathic sandstone
..... Unconformity			
Oligocene	Barail Group (i) Tikak Parbat Formation (ii) Baragolai Formation (iii) Naogaon Formation	 600 m 3500 m 200 m	Greyish to yellowish sandstone, sandy shale, coal seams. Greyish to bluish grey or yellowish red mudstone, shale, sandstone, carbonaceous shale and thin coal seam Compact, fine grained, dark grey sandstone with bands of splintery shale
Eocene	Disang Group	3000 m	Splintery dark grey shales and thin sandstone interbands

individual minor to moderate coal deposits (Mishra and Ghosh, 1996). The coal belts in this region are sub-divided into two areas viz. (i) coalfields of upper Assam, Arunachal Pradesh, Nagaland and (ii) coalfields of central and lower Assam comprising the coal measures of Karbi-Anglong and Meghalaya.

Tertiary coal formed near marine milieu like estuarine, lagoonal or deltaic environments. The migration of marine pump related to transgressive and regressive events controlled the development of coal swamps and the formation of coal deposits. The coal belts of Garo, Khasi and Jaintia Hills of Meghalaya and Mikir Hills of Assam occur within the Early Eocene sediment package. They generally formed thin, splitting and pinching coal seams in the coastal parts of the shelf zone of the early Eocene sea, close to the peripheries of and over the Meghalaya-Assam crystalline massif. On the other hand, the coal deposits of Upper Assam, in Makum, Dilli-Jeypore coalfields and those of adjacent Nagaland and Arunachal Pradesh were formed within the Barail Group during the Oligocene in the peri-cratonic molassic basins. In the Assam shelf, the locally thick Barail coal seams are disposed of as lenses because of close interaction of fluvial, lagoonal and shallow marine environments. The molasse basin slowly and was flanked by the rising Indo-Burma ranges. The Barail sediments along this belt develop persistent thick coal seams. These were later unconformably superposed by the Neogene sediments and were subsequently affected by folding and thrusting. They occur now at the floor of several often-anastomosing thrust slices that cut through the overlying Neogene mollasse sequence within the "belt of schuppen".

The most important coalfields in these areas where exploitation or prospecting of coals carried out/going on are shown in Table 3 and Table 4.

CHARACTERISTICS OF TERTIARY COAL

The coals from the 'Zone of Schuppen' and 'Platform areas' are non-bonded and bright with humic components strongly decomposed Megascopically the north-eastern coals are soft, friable, dark black and highly vitrain-rich and exhibit sub-conchoidal to conchoidal fracture and on weathering they break parallel to bedding plane. The coals show greasy to vitreous lustre. These coals also show cleat. Pyrite is the dominant mineral in those coals as bleds, nodules, veins and specks. The coal seams of Meghalaya are relatively thin (0.3 – 2.0 m) because of the development of encroachment of fast shifting of distributary channels over swamp abating the development of peat (Raja Rao, 1981). The coal seams are sometimes characterised by pinching and swelling character.

Both Eocene and Oligocene coals are chemically almost the same but the only difference is that Eocene coals are slightly less mature (Mishra and Ghosh, 1996). Coals of both areas are low in moisture (<5%), low ash (<8%) but volatile matter is quite high (>40% average). Oligocene coals average carbon content (74% to 83%) is higher than the Eocene coals (67% to 78%). The north-eastern coals are generally non-caking based on carbon and volatile matter content. However, coals from Makum of upper Assam and Namchik-Namphuk of Arunachal Pradesh show strong swelling index ranging from 3 to 9 (Ghosh & Mishra, 1996). Coals of this region vary from sub-bituminous type C to high volatile bituminous type C in rank as per German (DIN) and North American clarification (Singh et al 2000, 2013) based on vitrinite reflectance and volatile matter. As per Seyler's diagram, the coals of Meghalaya fall within the 'Ortholignitous' to 'para-bituminous' rank (Singh, 2018).

The north-eastern coals have higher sulphur content (generally > 3%) which even reaches upto 7% (Nath, 2021). All forms of sulphur-sulphate, pyritic and organic sulphur are recognised where organic sulphur (>80%) predominates the other forms of sulphur. Chandra et. al. (1983) observed that coals of Meghalaya show an increasing sulphur content from bottom to the top of

Table 3. Coalfields of platform areas of Meghalaya of Northeastern region of India

A. East Jaintia Hills (latitude $25^0$10' – $25^0$28'N and longitude $92^0$08' – $92^0$33' 30" E)

1. Bapung
2. Sutunga
3. Jarain – Tkentalang
4. Lakadong
5. Mutang
6. Loksi
7. Umlatdoh
8. Musiang Lamare

B. Khasi Hills (latitudes 25^0 10' – 25^0 42' N and longitudes 91^0 40' – 91^0 55' E)

1. Langrin
2. Umrileng
3. Mawsynram
4. Mawlong – Shella – Isamati
5. Cherrapunji – Mawkma – Laitryngew
6. Mawpholong
7. Pynursla – Lyngkyrdn – Thangjinath
8. Lundidom
9. Laitduh
10. Mawbehlarkar

C. Garo Hills (latitudes 25^0 12' – 25^0 44' N and longitudes 89^0 58' – 90^0 58' E)

1. West Daranggiri
2. East Daranggiri
3. Siju
4. Karaibari
5. Rongrenggiri
6. Balphakram – Pendengru

the seam. They opined that pH values decreased with depth and alkalinity increased from the bottom to the top, thereby bringing highest sulphur content at the top of a sequence because the alkaline condition is conducive to sulphide deposition. Again Chandra et al. (1983) observed that a gradual increase in the total sulphur content from west to east in the coals of Meghalaya within the basin of deposition is due to the increasing marine influence of the peat forming swamps of Khasi and Jaintia Hills (i.e. Langrin, Bapung coalfields) in the eastern part of the Meghalaya as compared to the Garo Hills in the West (West Daranggiri, Siju coalfields). The total sulphur content of Tiru Valley of Nagaland even reaches upto 11% (Sing et al., 2012) which places them as super high organic sulphur (SHOS) (as per Chou classification, 2012, 1990). Many researchers like Ahmed et al. (1981, 1985, 1992, 1996), Gogoi et al. (2020) Nath (2021) have shed light on the distribution/abundance of sulphur of north-eastern coal. Saikia et al. (2014) studied the geochemistry and nano-mineralogical studies of medium sulphur coals of Assam whereas Choudhury et al. (2016) contributed on the multi-analytical study on sulphur components in some sulphur-rich Assam coals.

Table-4 Coalfields of Foredeep basins of northeastern region of India

Assam:

1. Makum coalfield (five coal seams recorded in this area. These are 5 ft. seams, 8 ft. seams, 20 ft. seams, 60 ft. seams and new seam. Only 20 ft. and 60 ft. seam is persistent throughout the area).
2. Dilli – Jeypore

Arunachal Pradesh:

(Eight persistent coal seams ranging in thickness from 1 to 17.4 m)

1. Namchik – Namphuk (latitudes 27^0 18' and 27^0 28' N and longitudes 95^0 58' and 96^0 14' E) – eastern part of the Tirap district and is the extension of Makum coalfield of Assam.

Nagaland:

1. Borjan (2 seams)
2. Tiru valley (1 seam)
3. Moulong Kimong (latitude $26^0$19'7'N; longitude 94^0 30'44''7'E)

These coals have relatively less oxygen (< 12% average) because of the replacement of oxygen by sulphur (Lahiri, 1965). The hydrogen content is high (>5%). The nitrogen content is quite low (< 2%) in all the coals of the belt.

Mukherjee et al. (1992) studied the geochemistry of trace elements of Tertiary coals of North-East India. The concentration of trace elements (in ppm) of west Daranggiri, Siju and Langrin coals of Meghalaya are Ge → 229 to 395, less than 5, Ni → 42 to 64, 20 to 40, 20 – 90, Co → 25 to 51, 15 to 25, less than 10 to 80, Cu → 23, 5 to 80, 25 to 800, Pb → 110 to 280, less than 5 to 50, less than 10 to 24, Mo → less than 5 to 13, less than 5, less than 5 to 15, Zr → 57 to 88, 60 to 70, 80 to 115, Mn → 290 to 483, 90 to 200, 180 to 400, Cr → 66 to 106, 40 to 150, 70 to 130, Ba → 147 to 162, 30 to 400, 60 to 118, Ga → 7 to 14, less than 10 to 15, less than 10 to 63, V → 25 to 66, 40 to 500, 30 to 200, Sr → 105 to 120, less than 10 to 150, 70 to 373 respectively. Here germanium (Ge) concentration is significantly higher (229 to 395) in West Daranggiri coals and lesser in Siju and Largin coals (less than 5). Maximum concentration of Mn in all the coalfields suggest possible association of organic matter. The high Cu, Ni and V concentration in Langrin coals show affinity with organic matter. Upward increase (from bottom to top seam) of elements such as Pb, Mn and V further suggest the conformity of increase of sulphur content from bottom to top seam as per Chandra et al. (1983) because the alkaline condition is favourable to the deposition of sulphide. Again Chandra et.al (1983)'s observation of the increase of sulphur content from the western to the eastern part of Meghalaya is corroborated by the accumulation trend of Cu (80 to 800 ppm), Zr (88 to 115 ppm), Sr (150 to 373 ppm) which also suggest marine environment contributed to the deposition of Lithophile (Zr) and Chalcophile (Cu and Zn) elements.

In case of Assam Oligocene coals the concentration of trace elements in ppm of Makum and Dilli – Jeypore coalfields are Ge → 69 to 72, 40 to 60, Ni → 504 to 754, 120 to 450, Co → 18 to 77, 150 to 450, Cu → 948 to 1264, 150 to 400, Zr → 126 to 174, 80 to 250, Mn → not detected, negligible, Cr → 1169 to 1641, 300 to 1000, Ba → 783 to 1110, 400 to 700, V → 209 to 533, 200 to 600, Y → 22, less than 20 to 50, La → nil, less than 30, Nb → not detected, 150 to 450, Pb → 82 to 198, 30 to 110 (Mukerjee et al., 1992).

Here Mn is negligible and not even detected in Makum coal and Ge is also very less in both coals. Nb concentration is higher in Dilli-Jeypore coals and not detected in Makum coals. The high concentration of Cu, Ni, Cr, V strongly suggest their association with the organic fraction of the coal and also indicate marine influence in the depositional basin because these elements are more abundant in marine water (Nichols, 1968). Also, this

high value indicates that Oligocene Assam coals are significantly different from those of Eocene Meghalayan coals.

The reflectance of Oligocene and Eocene coal varies from 0.53% to 0.74% and 0.37% to 0.67% respectively, indicating that Oligocene coals are of deeper burial (Ghosh and Mishra, 1996).

Petrological studies made by various workers like Lahiri and Bhattacharya (1961), Ahmed and Bharali (1983), Goswami (1985), Ahmed and Rahim (1996), Singh (1989), Mishra (1992), Chandra and Behra (1992), Mishra and Ghosh (1996), Rajaratham et al. (1996), Singh and Singh (2000), Pareek (2004), Singh et al. (2012), Singh et al. (2013). Sharma et al. (2016), Gogoi et al. (2020), Nath et al. (2021), Kumar et al. (2022), Nath (2022), and Adsul et al. (2022) on the north-eastern coal show that they are rich in vitrinite with moderately high concentration of Liptinite and low inertinite. The mineral matter content is also quite high. Singh et al. (2006) also suggested a proposal for the distribution of pyrite of Tertiary coals of Northeast India.

The details of micro-petrographic characteristic of both Oligocene and Oligocene coal are given below:

COAL FROM THE SCHUPPEN ZONE NORTH-EAST INDIA

Singh et al. (2013, 2012) studied the coal deposits of Makum, Dilli Jeypore of upper Assam, Nanchik – Namphuk of Arunachal Pradesh, Borjan and Tiru Valley of Nagaland. Makum coals are rich in vitrinite which ranges from 81.7 to 94.7 vol. % (84.6 to 96.6 vol. % mmf basis) while Liptinite and inertinite content varies from 2.6 to 14.4 vol. % (2.7 to 14.9 vol. % mmf basis), 0.4 to 2.2 vol. % (0.4 to 3.3 vol. % mmf basis). In Dilli-Jeypore coal vitrinite, Liptinite and inertinite ranges from 71.4 to 95.2 vol. % (81.7 to 95.8 vol. % mmf basis), 2.9 to 12.7 vol. % (3.1 to 15.7 vol. % mmf basis), 0.1 to 3.1 vol. % (0.1 to 3.3 vol. % mmf basis), respectively. In Namchik-Namphuk coals vitrinite, Liptinite, inertinite varies from 41.3 to 77.3 vol. % (68.8 to 84.4 vol. % mmf basis), 13.9 – 32.9 vol. % (15.9 – 35.4 vol. % mmf basis), nil to 1.4 vol. % (nil to 1.5 vol. % mmf basis). In Borjan coals vitrinite, Liptinite, inertinite content spreads from 53.2 to 81.4 vol. % *0.6 to 89.7 vol. % mmf basis), 8.5 to 16.1 vol. % (9.3 to 21.8 vol. % mmf basis), nil to 1.3 vol. % (nil to 1.6 vol. % mmf basis). In Tiru Valley coals the macerals are varies from 95 to 99 vol. %, 1 to 3 vol. %, nil to 2 vol. %.

In vitrinite group the identified macerals are collotelinite, gelinite, corpogelinite, collodetrinite, dark-vitrinite and phlobaphinite in all coals of foreland basins. Amongst them collotelinite predominates the other form while telinite is rare but occurs with well-preserved cell structure in all the coals while gelinite is absent in Arunachal and Nagaland coals, collodetrinite absent in Arunachal Pradesh coals. Vitrodetrinite, pseudovitrinite and phlobaphinite are absent in upper Assam coals and phlobaphinite is absent only in Arunachal Pradesh coals.

In Liptinite group identified macerals are sporinite, cutinite, resinite, suberinite, alginite, butuminite, fluorinite, exsudatinite, liptodetrinite. Resinite is the most dominant Liptinite maceral in these coals.

Inertinite macerals are fusinite, semi-fusinite, macrinite, funginite, interto detrinite. Fusinite, semifusinite with well preserved and less preserved cell structure found only in Dilli-Jeypore coals of upper Assam. Macrinite occurs as fine particulate matter in the form of lenses found only in upper Assam coals. Funginite is the most common maceral in these coals. Inertodetrinite derived from crushing of teleutospores are only seen in Dilli-Joypore coals.

Observed mineral matter varies from 0.9 – 9.2 vol. % (3.26 vol. % average), 0.7 – 13.5 vol. %. (3.88 vol. % average), 4.8 – 38.8 vol% (18.5 vol. % average), 9.2 to 37.9 vol. % (23.55 average), 1-86% (19.55 vol. % average) in upper Assam, Arunachal Pradesh and Nagaland coal deposits. Observed mineral matter in these coals are clay, carbonate and sulphides of which clay dominance the other. As ground mass both clay mineral and carbonates occur and also as fissure, crack, cleat filings, strings and fissure fillings. Pyrite is classified here as framboidal, disseminate, cavity and fisher filling, massive, discrete grain of which framboidal is the dominant form. Vitrite is the dominant microlithotype in these coals.

Further Singh et al (2012) observed that high GI and TIP values suggest peat growth under telmatic conditions with prolonged wet conditions and high tree density. Highly gelified peat results from high GI indicates a continuous influx of calcium-rich waters in the swamp. The value of GWI and VI also indicates that the peat formed in bog forest under mesotrophic to ombotrophic hydrological conditions.

COALS OF MEGHALAYA (PLATFORM BASIN), NORTH EAST INDIA

Singh et.al (2000) studied in detail the coal deposits of the three Hills of Meghalaya (Garo, Khasi and Jaintia). The analysed major coalfields are west Daraggiri, Siju of Garo Hills, Langrin, Mawlang – Shella of Khasi Hills while minor coal fields include Cherrapungi, Laitryangew (Khasi Hills) and Bapung (Jaintia Hills)

GARO HILLS

Daranggiri coals are rich in vitrinite which, ranging from 20.9 to 69.6 vol. % (56.8 to 86.6 vol. % mmf basis). Collotellinite is the dominant maceral in this group while telinite is absent in this coal while

other macerals are gelinite, corpogelinite, collodetrinite, dark vitrinite and vitro-detrinite. The frequency distribution of Liptinite and inertinite macerals are 9.1 – 22.2 vol. % (13.0 to 36.7 vol. % mmf basis), 0.2 – 4.6 vol. % (0.4 to 7.4 vol. % mmf basis). The identified macerals are sporinite, cutinite, resinite, suberinite, alginite, bituminite, fluorinite, exsudatinite, liptodetrinite (tiptinites) where resinite is the dominant one. Inertinite includes fusinite, semifusinite and inertodetrinite while sclerotinite and macrinite are not observed here. Mineral matter (MM) varies from 7.7 to 66.5 vol. % (46.8 vol. % mean values). Among MM, clay minerals dominate the other sulphide and carbonate minerals. Both clay & carbonate minerals occur as ground mass plus cracks, cleats, fishers, cell fillings. The dominant sulphide mineral is pyrite.

The Siju coals the vitrinite, Liptinite, inertinite and mineral matter varies from 29.2 to 58.2 vol. % (59.9 to 80.6 vol. % mmf basis), 7.5 – 27.2 vol% (14.2 to 35.2 vol. % mmf basis), 1.2 – 6.6 vol. % (1.9 to 9.4 vol. % mmf basis), 23.4 – 50.2 vol% (37.3 vol. % average). All the macerals like Daranggiri coals are present here.

KHASI HILLS

The frequency distribution of maceral and mineral matter composition of Langrin, Mawlong-Shella,Cherrapunji and Laitryngew coals are vitrinite – 19.6 to 78.0 vol% (45.0 to 87.5 vol. % mmf basis), 48.5 to 97.9 (65.7 to 2.9 vol. % mmf basis), 56.9 to 71.8 (68.3 to 79.5 vol. % mmf basis), 51.7 to 83.1 (62.4 to 86.3 vol. % mmf basis), Liptinite – 6.2 to 27.5 (11.8 to 53.1 vol. % mmf basis), 5.4 to 24.8 (5.5 to 32.4 vol. % mmf basis), 9.1 to 23.0 (9.1 to 23.0 vol. % mmf basis), 8.8 to 27.5 (9.1 to 31.7 vol. % mmf basis), interdinite – nil to 13.1 (0.0 to 13.8 vol. % mmf basis), nil to 3.7 (0.0 to 4.1 vol. % mmf basis), 2.2 to 5.9 (2.2 to 5.9 vol. % mmf basis), 1.3 to 5.7 (1.4 to 6.6 vol. % mmf basis) and mineral matter – 2.8 to 67.6 vol% (34.7 vol. % mean values), 1.9 to 27.8 vol% (15.2 vol. % mean values), 10.0 to 26.9 vol% (16.4 vol. % mean values), 3.6 to 30.8 vol. % (17.4 vol. % mean values). The identified macerals of vitrinite group are collotelinite (dominant) followed by gelinite, corpogelinite, collodetrinite, pseudoritrinite, dark vitrinite, vitrodetrinite. Telinite is rare while gelinite is absent in Laitrygew coal. In Liptinite group the macerls found are sporinite, cutinite, resinite, suberinite, alginite, liptodetrinite (structured) bituminite, fluorinate and exsudatinite (secondary). Amongst Liptinite resinite is the dominant maceral which occurs in oral to spherical or elliptical shape. Cutinite occurs as thread-like bodies. Inertinite group includes fusinite, semifusinite, sclerotinite, macrinite, inertodetrinite. Fusinite is characterized by well-preserved cell structure and sometimes showing bogan structure. Rounded to oval bodies of macrinite have been observed only in Langrin coal. In these coals, visible mineral matters are clay, carbonate and sulphide while clay is the dominant mineral. Clay minerals occurs as groundmass alongwith fissure, crack, cleat and cell infillings of fusinite, semifusinite and sclerotinite. Carbonate minerals also appear as ground mass, as stringers, as fissure fillings. The sulphide in the form of pyrite occurs as disseminated, blebs, discrete grains, framboidal bodies, massive replacement and fissure fillings.

JAINTIA HILLS

The frequency distribution of maceral and mineral matter composition (in vol%) of Bapung coals (which includes Sutunga, Jarain, Musiang, Lamare, Loksi, Khliehriat) are vitrinite – 49.4 to 68.4 vol. % (71.2 to 81.1 vol. % mmf basis), Liptinite – 10.9 to 23.5 vol. % (17.8 to 27.5 vol. % mmf basis), inertinite – 0.3 to 1.2 vol. % (10.3 to 1.7 vol. % mmf basis), mineral matter – 14.6 to 38.6 vol. % (23.6 vol% mean values). Here all the maceral groups are observed with collotellinite being the dominant maceral in the vitrinite group. Collodetrinite in the vitrinite group, bituminite and fluorinite in Liptinite group, fusinite, semifusimite, selerotinite, macrinite, inertodetrinite are absent here. Nayak (2013) studied the mineral matter and nature of pyrite of these coals and observed that the minerals in these coals are sulphide (pyrite, marcacite), sulphates, oxides, hydroxides, phosphate, carbonate, silicates and kaolinitic clay. The disulphides occur in 2 modes like pyrite and occasionally marcasite and in various forms like framboids, colloidal precipitate, colloform banded, fine dissemination, discreate grains, dendritic (feathery), recrystallized, nuggests, discoidal, massive, cavity-fracture and cleat-fillings. In the early stages of coalification framboidal pyrite has formed primarily due to biological activities of sulphur reducing bacteria. He found from sulphur isotopic values that pyrites are of biogenic origin.

In Meghalayan coals common occurrence of one, two and three-celled teleutospore in collotelinite corroborates the view that these coals have evolved from angiospermic floral assemblages. Further Singh et al. (2000), plotted microlithotypes in the double diamond diagram of Hacquebard and Donaldson (1969) suggesting that these coals have evolved from wet forest moor, reed moor and open moor facies. The Khasi and Jaintia Hills coals plot in the forest moor facies of the telmatic to limnotelmatic zones, while the coals of Garo Hills plot mainly in the open moor and need moor facies of the telmatic and limmic zones. To corroborate this by plotting in the Diessel (1986) facies model of GI and TIP, these coals show high GI and high TPI values that evolved under telmatic conditions with high tree density under prolonged wet conditions. Also, abundance of microlithotype strongly suggests that during pet formation wet condition prevails. A

constant influx of calcium-rich water into the coal swamps occur because of high GI. The decomposition of organic matter & formation of humates accelerate because of the high concentration of calcium ions. Marine-influenced coals have this typical property. Further Singh et.al opined that terpene type primary resins (in high concentration) of very large dimensions suggest abundant growth of conifers in the basin & temperate climatic conditions during the evolution of these coals.

Singh et al. (2001) observed that north-eastern coals are oil-prone where H/C>0.8. Also, Gogoi et al. (2008, 2020), Nath (2022, 2023) based on geochemical and rock eval investigation indicate they contain type II kerogen and grade to mixed kerogen (type II/III), with mainly gaseous hydrocarbons potential and few amounts of liquid hydrocarbon generation. The source rock is good for hydrocarbon generation in these coals.

POTENTIAL UTILIZATION OF TERTIARY COALS

The Tertiary coals of North-Eastern states are generally very low in ash which can be used as blends and per hydrous in nature. Besides their normal use as fuels for general industries they are ideally suitable for direct hydrogenation for the production of synthetic oil on which the coals of upper Assam have a major role. In spite of their high sulphur content, these coals are profitably used (10% even more) as blends in metallurgical coke making and for the production of Ferro-Silicon. Due to high percentage of sulphur these coals also best utilized for cement manufacturing (presently going on in Meghalayan cement industries). Most of these coals are used in brick industries, domestic fuel and also exported to Bangladesh. The high volatile matter concentration and hydrogen content make its suitable for liquefaction and garification. (Singh, 2018) which was initiated by CSIR, Jorhat where it showed that 80-90% of the coal can be liquefied despite the hurdles of sulphur (Lahiri, 1965). High sulphur Tertiary coal has wide scope of utilisation in fertiliser industry. They are good source rock for hydrocarbon generation (Gogoi et al., 2008; Gogoi et al., 2020; Nath et al., 2023). The desulphurization of this coal with bacterial biomass was initiated recently and if it comes out successful then these coals will be a real asset for the people of north-eastern India. Though desulphurization techniques of (Sakia et al., 2014) showed that the organic sulphur content of coal could be removed which generally intermingled with coal.

Among the Tertiary coal deposits, the Makum coals of Assam, Namchik-Namphuk coals of Arunachal Pradesh and Bapung and Langrin coals of Meghalaya are the most potential.

CONCLUSIONS

1. The coals of Meghalaya (Eocene age) formed in platform areas whereas coals of Assam, Arunachal Pradesh and Nagaland (Oligocene age) formed in foredeep basins in the eastern part of Himalaya.
2. The north-eastern coals have low moisture, low ash, high volatile matter, high sulphur (mostly organic), high carbon, high hydrogen, low nitrogen and low oxygen chemically whereas petrographically they have high vitrinite, moderately high content of Liptinite and low inertinite. The mineral matter represented by clay minerals, sulphides and carbonates are also quite high.
3. In the Eocene and Oligocene coals of north-eastern India, the concentration and distribution of trace elements (Ge, Ni, Co, Cu, Pb, Mo, Mn, etc.) indicate marine conditions/or inclusion which is corroborated with high content of sulphur.
4. Coals of this region range from sub-bituminous type C to high volatile bituminous type C in rank.
5. Meghalaya (Platform basin) coal-bearing sequence indicates intermittent transgression and regression during Eocene. Further occurrence of single, double and three-celled teleutospores suggests mangrove-rich angiosperm that grew in tropical humid climate and the presence of large resins suggests growth of conifers. In the eastern Himalayan foreland coal basin due to the regression of sea prograding delta emerged and subsequently grew of angiospermic flora in dominance, which occurred in the form of coal-bearing sequences. In mesotrophic to ombrotropic hydrological conditions bog forest developed here.
6. The high sulphur content (>3% and reaching up to 12%) of north-eastern coal suggest for further research regarding desulphurization whereby it can be utilized in a better way for industrial purpose in near future.

DECLARATION OF CONFLICTING INTEREST

The author declares no competing interest

REFERENCES

Adsul, T., Beirne, M.D., Fike, D.A., Ghosh, S., Werne, J.P., Gilhooly III, W.P., Hackley P.C., Hatcherian, J.J., Philip, B., Hazra, B., Bhattacharyya, S., Konar, R. and Varma A.K. (2024). Decoding paleomire conditions of Paleogene superhigh-organic-sulfur coals, Int. Journal of Coal Geology, https://doi.org/10.1016/j.coal.2024.104559

Ahmed, M. (1971). Petrochemical study of coal, Laitryngew, Khasi & Jaintia Hills, Meghalaya. Journal of the Geological Society of Assam, v. 1, pp. 15-20.

Ahmed, M. and Bora, J.P. (1981). Geochemistry of Tertiary coal Bapung coalfield, Jaintia Hills, Meghalaya, Journal Assam Sc. Soc. v. 24 (2), pp. 9-10.

Ahmed, M. and Bharali, D. (1983). Petrographic characters of Tertiary coals, Nagalbibra, West Daranggiri Coalfield, Meghalaya: Proc. 5th Geophytology Conference, Lucknow, pp. 242-245

Ahmed, M. and Rahim, A. (1996). Abundance of sulphur in Eocene coals beds from northeast India. Internat Journal of Coal Geology, v. 30, pp. 315-318.

Ahmed, M. and Phukan, S. (1999). Trace element characterization of Eocene Coal, West Daranggiri coalfield, Garo Hills, Meghalaya, Pro. of the 10th Int. Conf. on coal Science, vol. 1, pp. 69-72.

Baruah, B.P., Sharma, A and Saikia, B. (2013). Petrological Investigation of some perhydrons Indian coals. Journal of the Geological Society of India, v. 81, pp. 713-718.

Chakraborty, S.N. and Bhattacharyya, U. (1969). Report on geology and coal resources of central part of the Mawlong-Shella Coalfield, United Khasi and Jaintia Hills, Meghalaya, Geol. Surv. India. unpublished report.

Chandra, D., Mazumder, K. and Basumallick, S. (1983). Distribution of Sulphur in the Tertiary coals of Meghalaya, India. International Journal of Coal Geology, v. 3, pp. 63-75.

Chou, C.L. (1990). Geochemistry of sulphur in coal. ACS Symposium Series Number 429, Geochemistry of Sulphur in Fossil Fuels, pp. 30-52.

Chanda, D. Behera, P. (1992). Abnormalities in the chemical properties of Tertiary coals of Meghalaya, India. Minetech, v. 13, pp. 18-22.

Chandra, D. and Behera, P. (1992). Abnormalities in the chemical properties of Tertiary coals of Meghalaya, India. Minetch, v. 13, pp. 18-22

Chou, C.L. (2012). Sulfur in coals: A review of geochemistry and origins. International Journal of Coal Geology, v. 100, pp. 1-13.

Choudhury, R., Gupta, U.N., Waanders, F.B. and Saikia, B.K. (2016). A multi-analytical study on the sulphur components in some high sulphur Indian Tertiary coals. Arabian Journal of Geosciences, v. 9(2), pp. 1-13. doi: 10. 1007/s12517-015-2178-8.

Diesel, C.F.K. (1986). On the correlation between coal facies and depositional environments. Proceeding 20th Symposium of Department Geology, University of New Castle, New South Wales, pp. 19-22.

Dasgupta, A.B. and Biswas, A.K. (2000). Geology of Assam. Geological Society of India, pp. 1-167.

Evans P. (1932). Tertiary Succession in Assam. Transactions Mining and Geological Institute of India, v.27, pp. 155-260.

Evans, P. (1932). Explanatory notes to accompany a table showing the Tertiary succession in Assam, Trans. Miner. Geol. Met. Institute of India, v. 27, pp. 168-248.

Fox, C.S. (1934). Garo Hills Coalfields, Assam. Records of the Geological Survey of India, v. 71 (Pt.1), pp. 35-37.

Geological Survey of India (GSI) (1974) Geology and mineral resources of the states of India. Geological Society of India, Miscellaneous Publication 30 (IV), pp. 1-78.

Geological Survey of India (GSI) (1981). Coalfields of India, Bulletin Series A, No. 45.I, Coalfields of northeastern India, Geological Society of India, pp. 1-75

Geological Survey of India (GSI) (1982). Himalayan Geology Seminar, New Delhi Misc Publ No. 41, Pt. III, Sec. IIA, Geol Surv India, Calcutta, 449p.

Geological Survey of India (GSI) (1989). Key papers presented in group discussion on Tertiary stratigraphy of northeastern India held at Shillong, April, 1985. Geological Society of India, Special Publication, v. 23, pp. 1-43.

Geological Survey of India (GSI) (1994). An inventory of the coal resources in different coalfields of India as on 1.1.94. Geol. Soc. India. Calcutta, Geological Society of India, note 8.

Geological Survey of India (GSI) (2009). Geology and mineral resources of Assam. Miscellaneous Publication No. 30, Part IV, Vol. 2.

Geological Survey of India (G.S.I) (2022): Indian coal & lignite resources. Natural Energy Resources Mission-II, B, pp 1-3.

Ghosh, A.M.N. (1940). Stratigraphical position of the Cherra sandstone. Assam. Records of the Geological Survey of India, v. 75, pp. 1-19.

Ghosh, T.K. (1964). On Tertiary coal from Daranggiri, Assam. Geological Society of India, v. 36, pp. 91-94.

Goswami, A.C. and Das, M.K. (1965). Detailed mapping of the Cherrapunji Plateau. United Khasi and Jaintia Hills district Assam. Geological Survey of India, unpublished report.

Goswami, D.N.D. (1985). Macerals and low temperature tar of the Tertiary coals of Assam, Meghalaya, and Nagaland. Geosciences Journal, v. 6 (1), pp. 95-102.

Goswamy, D.N.D. (1985). Macerals and low temperature tar of the Tertiary coals of Assam, Meghalaya, and Nagaland. Geosciences Journal, v. 6, p. 95-102.

Gogoi, K., Dutta, M. and Das, P. (2008). Source rock potential for hydrocarbon generation of Makum coals, upper Assam, Indi. Cement science, v. 95 (2), pp. 233-239.

Gogoi, M., Kuma, T.S. and Phukan, S. (2020). Organic Geochemistry, petrography, depositional environment and hydrocarbon potential of Eocene coal deposits of West Daranggiri coalfield. Journal of the Geological Society of India, v. 95, pp. 84-94.

Hacquebard, P.A. and Donaldson, J.R. (1969). Carboniferous coal deposition associated with flood plain and limnic environments in Nova Scotia. In: Dapples, E.C., Hopkins, M.E. (Eds.), Environment of Coal Deposition. Geological Society of America Special Paper, v. 114, pp. 143-191.

Harijan, N., Sen, A.K., Sarkar, S., Das, J.D. and Kanungo, D.P. (2003). Geomorphotectonics around the Sung valley carbonatite complex, Shillong plateau, NE India: Remote sensing and GIS approach. Journal of the Geological Society of India, v. 62(1), pp. 103-109.

Indian Bureau of Mines (2019). Indian Minerals yearbook. 2019 (Part III: Mineral Reviews) 58th Edn.

Kumar, A. (2022). Tertiary coal and Lignite deposits of India and their source rock potential: A Review on the contribution of the Indian Coal Petrologists. Journal of the Geological Society of India, v. 98, pp. 1745-1753.

Kumar, A., Nath, M. and Singh, A.K. (2021b). Source Rock Characterization for Hydrocarbon Generative Potential and Thermal Maturity of Sutunga Coals, (East Jaintial Hill) Meghalaya, India: Petrographic and Geochemical Approach. Journal of the Geological Society of India, v. 97(6), pp. 643-648.

La Touche, T.H.D. (1889). Report on Cherrapunji Coalfields. Geological Survey of India Records, v. 22 (Pt. 3), pp. 167-171.

Lahiri, A. (1965). Utilisation of Assam coals, Fuel Res. Institute News, v. 15, pp. 129-130.

Lahiri, K.C. and Bhattacharya, R.R. (1961). Petrographic studies of some Indian coals, Pt. I Petrographic techniques for the examination of Indian Coals. Journal of Mines Metals and Fuels, v. 9(9), pp. 1-3 & 18.

Medlicott H.B. (1865). The coal of Assam, results of a brief visit to the coalfields that province in 1865; with Geological note on Assam and the Hills to the south of it. Memoir of the Geological Survey of India 4(3), 388-442.

Medlicott, H.B. (1868). Coals in Garo Hills. Geological Survey of India, Records, v. 1 (Pt 1), pp. 1-22.

Mishra, B.K. (1991). Genesis of Indian Tertiary coals and lignites: a bio-petrological and palaeobotanical view point. Palaeobotanist, v. 40, pp. 490-513.

Mishra, B.K. (1992). Optical properties of some Tertiary coals from northeastern India: their depositional environment and hydrocarbon potential. International Journal of Coal Geology, v. 20, pp. 115-144.

Mukherjee, K.N., Dutta, N.R., Chandra, D. and Singh, M.P. (1992). Geochemistry of trace elements of Tertiary coal of India, International Journal of Coal Geology, v. 20, pp. 99-117.

Mishra, H.K. and Ghosh, R.K. (1996). Geology, petrology and utilisation potential of some Tertiary coals of northeastern region of India. International Journal of Coal Geology, v. 30, pp. 65-100

Mukherjee S. Srivastava SK (2005) Trace elements in high-sulfur Assam coals from the Makum coalfield in the Northeastern Region of India. Energy Fuel 19: 882-891

Nath, M. (2017). Trace element characterization of Eocene coal, Bapung coalfield, Jaintia Hills, Meghalaya, North-East India, Journal of applied geochemistry, vol. 19, No.2, pp. 200-202

Nath, M. (2021). High sulphur Tertiary coals of North East India: implications for paleoenvironment and paleoclimate. Arabian Journal of Geosciences, v. 14, pp. 1-13

Nath, M. (2021). Sulphur study of the Tertiary coals from Jaintia Hills, Meghalaya, NE India: Implication for palaeoenvironment, utilisation prospects and environmental impacts. Journal of the Indian Association of Sedimentologists, v. 38, issue 2 pp. 115-121.

Nath, M. and Kumar, A. (2022). A study of geochemical and petrographic characteristics of Eocene coal from Bapung coalfield, East Jaintia Hills, Meghalaya, North-East India. Arabian Journal of Geosciences, v. 15, pp. 1-11.

Nath, M. and Sen, S. (2022). Abundance of sulphur in Tertiary coals of North-East India and its paleo-environmental implications. Journal of the Indian Association of Sedimentologists, v. 39, issue 1, pp. 64-73.

Nath, M. and Sen, S. (2022). Petrographic characterization and evolution of Eocene coal from Bapung coalfield, East Jaintia Hills, Meghalaya, North-East India. Journal of the Indian Association of Sedimentologists, v. 39, issue 1, pp. 74-75.

Nath, M, Gopinathan, P., Santosh, M.S., Subramani, T., Ramakrishna, V., Khan, A.A. and Ravikumar, C.R. (2023). Exploring the potential of sulphur forms in Northeastern Indian coals: Implications in environmental remediation and heavy metal sensing. Chemosphere, v. 338, 139471, pp. 1-16.

Nath, M, Panwar D.S., Chaurasia, R.C., Akanksha, Kaur, J. and Kohli, D. (2023). New insight into geochemical characterization of Paleogene coals from Jarain coal field, Meghalaya, NE India: Hydrocarbon potential and organic petrographic analysis. Geo Energy Science & Engineering, pp. 1-14.

Nath, M, Panwar, D.S., Chaurasia, R.C. and A. Kanksha (2023). Hydrocarbon generative potential and thermal maturity of newly discovered coal seams from Bapung coalfield, Meghalay, India: Rock-eval pyrolysis and organic petrographic analysis. Journal of Sedimentary Environments, v. 8(3), pp. 1-13.

Nayak, B (2013). Mineral matter and the nature of pyrite in some high-sulfur Tertiary coals of Meghalaya, North-east India. Journal of the Geological Society of India, v. 1, pp. 203-214.

Nichols, G.D. (1968). in 'Coal & coal-bearing strata' (Eds : Murchison, D & Westoll, T.S.), Oliver & Boyd, Edinburgh & London, 418.

Pareek, H.S. (2004) Progress of coal Petrology in India. Memoirs Geological Society of India, no. 57, p. 161.

Raja Rao, C.S. (1981). Coalfields of India, coalfields of northeastern India. Geological Survey of India, Bulletin Series, v. A 45, pp. 1-76.

Rajarathnam, S., Chandra, D. and Handique, G.K. (1996) An overview of chemical properties of marine influenced Oligocene coal from the northeastern part of the Assam-Arakan Basin, India. International Journal of Coal Geology, v. 29, pp. 337-361.

Ramesh, D.S., Ravi Kumar, Uma Devi, and Raju, P.S. (2005). Morpho-geometry and upper mantle images of NE India. Geophysics Research Letters, v. 32, pp. L14301-04.

Singh, M.P. (1989). On the origin of fusain in the Tertiary coals of Meghalaya. Journal of the Geological Society of India, v. 33, pp. 99-103.

Singh, M.P. and Singh, A.K. (2000). Petrographic characteristics and depositional conditions of Eocene coals of platform basins, Meghalaya, India. International Journal of Coal Geology, v. 42, pp. 315-356

Singh, M.P. and Singh, A.K. (2001). Source rock characteristics and maturation of Tertiary coals, Northeast India. Journal of the Geological Society of India, v. 57 (4), pp. 353-368

Singh, M.P. and Singh, A.K. (2003). Hydrocarbon Emigration through Microfracturing in Vitrinite: An Example from the Oligocene Coals of Borjan Coalfield, Nagaland. Journal of the Geological Society of India, v. 61(2), pp. 170-176.

Srivastava S.K., Pandey N. and Srivastava V. (2004). Tectono-Sedimentary evolution of Disang – Barail Transition, northwest Kohima, Nagaland. India. Himalayan Geology, v. 25(2), pp. 121-128.

Singh, M.P. and Singh, A.K. (2006). Morphology, maceral association and distribution of pyrite in the Tertiary coals of northeast India: a proposal for the classification of high sulphur coals. Journal of the Geological Society of India, v. 67(6), pp. 783-802.

Singh, Prakash K., Singh, M.P., Singh A.K. and Naik, A.S. (2012). Petrographic and geochemical characterization of coals from Tiru valley Nagaland, NE India. Energy, Exploration and Exploitation, v. 30, pp. 171-192.

Singh A.K., Singh, M.P. and Singh Prakash, K. (2013). Petrological investigations of Oligocene coals from foreland basin of northeast India. Energy, Exploration and Exploitation, v. 31(6), pp. 909-936.

Saikia B.K., Ward, C.R. Oliveira, M.L.S., Hower, J.C. Baruah, B.P., Braga. M. and Silva, L.F. (2014). Geochemistry and nano-mineralogy of two medium sulphur northeast Indian coals. International Journal of Coal Geology, v. 121. pp. 26-34.

Singh A.K. (2015). Petrological investigation of Eocene coals, Garo Hills. Meghalaya, India. Arabian Journal Geosciences, v. 8, pp. 10705-10714.

Sharma, A, Saikia, B.K., Phukan, S. and Baruah, B.P. (2016). Petrographical & Thermo-chemical investigation of some North-East Indian High Sulphur Coals. Journal of the Geological Society of India, v. 88, pp. 609-619.

Singh, A.K. (2018). Classification and potential utilization of Eocene coals of Meghalaya, North East India. Journal of the Geological Society of India, v. 91, pp. 181-187.

Received on: July 9, 2024
Revised accepted on: Sept 28, 2024